

JAAN LAUR

Variability survey of massive stars
in Milky Way star clusters



JAAN LAUR

Variability survey of massive stars
in Milky Way star clusters



UNIVERSITY OF TARTU
Press

This study was carried out at the University of Tartu and Tartu Observatory, Estonia.

The Dissertation was admitted on 30.05.2017, in partial fulfilment of the requirements for the degree of Doctor of Philosophy in physics (astrophysics), and allowed for defence by the Council of the Institute of Physics, University of Tartu.

Supervisors: Dr. Indrek Kolka,
Tartu Observatory,
Estonia

Dr. Laurits Leedjärv,
Tartu Observatory,
Estonia

Opponents: Prof. Dr hab. Andrzej Niedzielski,
Toruń Centre for Astronomy,
Nicolaus Copernicus University,
Poland

Dr. Michaela Kraus,
Astronomical Institute,
Academy of Sciences of the Czech Republic ,
Czech Republic

Defence: 29.08.2017, University of Tartu, Estonia

This work has been partially supported by Graduate School of Functional materials and technologies receiving funding from the European Regional Development Fund in University of Tartu, Estonia.



European Union
European Regional
Development Fund



Investing
in your future

ISSN 1406-0302
ISBN 978-9949-77-495-1 (print)
ISBN 978-9949-77-496-8 (pdf)

Copyright: Jaan Laur, 2017

University of Tartu Press
www.tyk.ee

CONTENTS

List of original publications	7
Introduction	8
1 Massive stars	10
1.1 Overview of massive stars	10
1.2 Asteroseismic observations of massive stars	12
2 Campaign overview	16
2.1 Observations	16
2.2 Data reduction	21
2.2.1 Correcting for the scattered light	24
2.3 Calibrated data	27
3 Catalogue of variable stars	32
3.1 Detection of variability	32
3.1.1 Frequency analysis	33
3.2 Description of the catalogue	36
3.3 Classification of variable stars	40
3.3.1 Eclipsing binaries	41
3.3.2 β Cephei stars	42
3.3.3 SPB stars	43
3.3.4 Be stars	44
3.3.5 α Cygni stars	45
3.3.6 Wolf-Rayet stars	45
3.3.7 Late-type stars	46
3.3.8 Cepheids	47
3.3.9 Other variables	49
3.3.10 Further discussion	49
3.4 Cluster membership analysis	51
4 Period change of selected massive binaries	55
4.1 Compiled data	57
4.2 Bayesian approach for parameter estimation	62
4.3 Parameters for selected massive binaries	64
4.3.1 Schulte 5	71
4.3.2 A36	73
4.3.3 B17	74

4.3.4	MT059	75
4.3.5	MT696	76
4.3.6	MT720	78
4.3.7	Schulte 3	79
5	Summary	81
6	Kokkuvõte (Summary in Estonian)	83
	Bibliography	86
	Acknowledgements	97
	Attached original publications	99
	Curriculum vitae	107
	Elulookirjeldus	110
	Appendix	113

LIST OF ORIGINAL PUBLICATIONS

This thesis is based on the following publications:

- I **J. Laur**, T. Tuvikene, T. Eenmäe, I. Kolka, L. Leedjärv 2012, "Variability survey of massive stars in OB-associations: preliminary results on the Cygnus region", *Baltic Astronomy* 21, 531
- II **J. Laur**, E. Tempel, T. Tuvikene, T. Eenmäe, I. Kolka 2015, "Period change of massive binaries from combined photometric and spectroscopic data in Cygnus OB2", *Astronomy and Astrophysics* 581, A37
- III **J. Laur**, I. Kolka, T. Eenmäe, T. Tuvikene, L. Leedjärv 2017, "Variability survey of brightest stars in selected OB associations", *Astronomy and Astrophysics* 598, A108

Author's contribution to the publications

Author's research has given an essential contribution to all these publications. The author's contribution to the original publications is indicated below. The Roman numerals correspond to those in the list of publications.

Publication I. The author gathered and reduced most of the observational data as well as did the analysis and prepared the original draft.

Publications II. The author gathered and reduced most of the observational data, did all of the modelling and analysis (except for the Bayesian parameter estimation which was done by Elmo Tempel) and wrote the paper.

Publications III. The author gathered and reduced most of the observational data, did all the analysis and wrote the paper.

INTRODUCTION

"At first sight it would seem that the deep interior of the Sun and stars is less accessible to scientific investigation than any other region of the Universe. Our telescopes may probe farther and farther into the depths of space; but how can we ever obtain certain knowledge of that which is hidden behind substantial barriers? What appliance can pierce through the outer layers of a star and test the conditions within?"
– Sir Arthur Stanley Eddington in his book *The Internal Constitution of the Stars* (1926).

Astronomy developed a millennia before physics, chemistry and biology because of the limited amount of data made it a much more approachable field of study. In ancient times, there were only seven moving objects in the sky – the Sun, the Moon and five planets as "wandering stars". All the other stars formed a spinning fixed system. Although, at first glance, the number of stars in the night sky seems immeasurable, there are only around 3000 stars in the sky that are visible to the human eye at any time. Hipparchus, the Father of the magnitude system, measured the positions of all the 1025 stars that he could see from his Rhodes vantage point and ranked them based on their apparent brightness. His naked eye measurements were made much easier by the fact that stars were not a boring grid of uniform points but instead are grouped into memorable shapes called constellations. As every constellation looks different, it was a natural conclusion that there had to be a greater reasoning behind this. Different civilizations had distinctive folklore behind every constellation, but they all agreed that reading the night sky meant reading the will of the Gods. So stellar astronomy was born out of the necessity to understand what omens the sky foretold for the people.

The general acceptance of the Copernicus' heliocentric cosmic model opened up a new study of the stars – measuring their distances using the parallax method. During a six-month journey, the Earth moves from one side of the solar system to the other. This movement makes nearby stars move with respect to the more distant ones and from that, the distance to the nearby stars could be calculated.

It turned out that stars are further away than predicted and it wasn't before the 19th century, when the telescopes became powerful enough, that these distances were actually measured. The study of stellar distances helped build a cosmic distance ladder that opened up a whole new picture of the world. For example, the constellations that were all known to be a close group of stars, were actually just a projection in the sky where the stars themselves were sometimes very far apart. Also, the brightness of all the stars that were visible by the naked eye appeared to differ no more than 1000

times from each other, yet the absolute luminosity of the star is actually also dependent on the distance the star is at. So, after the real distances to the stars became clearer, the brightness scale had to be extended enormously as there were massive stars million times brighter than the Sun and dwarf stars thousand times fainter than the Sun. Cepheid stars were even used as standard candles to measure the distances of nearby galaxies and find out the shocking truth that the Universe is constantly expanding.

The discovery and mapping of spectral lines in the spectrum of the Sun together with the development of laboratory spectroscopy started the boom of stellar spectroscopy in the early 19th century. These observations revealed another aspect of the nature of stars – not all of them were identical balls of fire, but differed in both chemical composition and temperature. This resulted in a classification of observable stars under the Morgan–Keenan system, a sequence from the hottest to the coolest star. By adding a luminosity class, the stars seem to lie in specific regions on the Hertzsprung–Russell diagram and these regions are now used to describe stellar evolution from the birth of a star to its ultimate demise. In addition, the knowledge of chemical composition of stars led to the discovery that all the heavy elements in the Universe are generated by stars and then distributed through supernova explosions. So every one of us are made of actual stardust.

During the second half of the 20th century, cosmology and extragalactic research was put in the forefront of astronomy due to the discovery of dark matter and cosmic background radiation. As telescopes became better, observational cosmology became a viable new horizon for the first time in history and gradually less observing time was made available for studying stars in the Milky Way. But a number of open questions about massive stars remained: how are massive stars born, how do they evolve and most importantly, what lies inside them? This last question is also what Sir Arthur Stanley Eddington, in his quote, thought to be the biggest inquiry in stellar physics that might never be answered.

This all changed in the last decades with the introduction of asteroseismology, a study of stellar interiors that requires a time resolved monitoring of a star. A number of space missions have been launched to accommodate the need to constantly monitor a star with required precision. In addition, the increasing availability of small-scale telescopes combined with the need for more observational data has helped make stellar astronomy popular again. Although, only a small number of massive stars have been asteroseismically studied, we already have an impressive understanding of the interiors of massive stars. And this is just the beginning!

The aim of this work is to expand on the number of known asteroseismically classified variable stars in order to build a better catalogue for future space missions in the field of asteroseismology and massive star studies.

CHAPTER 1

MASSIVE STARS

1.1 Overview of massive stars

Massive stars are stars with initial masses above 8 times that of the Sun and according to some estimates can reach as high as 300 solar masses (M_{\odot}) (Vanbeveren et al. 1998; Maeder 2009; Grunhut et al. 2012; Vink 2015). They represent the most massive and luminous stellar components of the Universe, eventually leading to catastrophic supernova (SN) explosions. Even though massive stars are much less numerous than low-mass stars, they contribute significantly to the overall luminosity of other galaxies (Hirschi & et al. 2006). Massive stars provide feedback in the form of ultraviolet (UV) radiation, stellar winds, and SN, which affect the evolution of disc galaxies by mixing and driving turbulence of interstellar gas and by triggering star formation. Their UV radiation is the most observable tracer of star formation and is used to calculate the star formation rates (Kennicutt & Evans 2012). Massive stars are one of the main sites for nucleosynthesis that take place during both pre-SN burnings as well as during explosive burnings. Unlike lower mass stars, they go beyond the core carbon-burning phase, and produce many of the elements heavier than oxygen. They enrich the interstellar medium with these heavy elements and drive the chemical evolution of galaxies and the metallicity evolution of the universe. Therefore, knowing the evolution of massive stars gives us insight into the evolution of galaxies.

One of the open questions about massive stars is how can such high mass stars form by accretion as molecular cloud fragmentation, radiation pressure, photoionization, and stellar winds all disrupt the accretion of gas to the protostar (Vink 2015). Collapsing gravitationally unstable cloud tends to form objects with masses comparable to the Jeans mass of the cloud, yet massive stars with far larger masses exist. Radiation pressure in massive stars should expel circumstellar material and prevent stars from growing to masses substantially larger than $\sim 20 M_{\odot}$ (Larson & Starrfield 1971). Massive stars also produce huge Lyman continuum luminosities which can ionise the gas in a star-forming region, choking off accretion and limiting the star-formation efficiency of giant molecular clouds (Krumholz et al. 2006). A final challenge for the formation of massive stars is radiatively-driven stellar winds that start to play a big role for stars greater than $\sim 40 M_{\odot}$ (Vink et al. 2001). Alternatively, massive star formation via mergers has been proposed, but only few models have been made thus far (Glebbeek et al. 2013; Suzuki et al. 2007).

After ending their protostar phase and reaching the main sequence on the Hertzsprung-Russell (HR) diagram, massive stars, when compared to the Sun, fin-

ish their core hydrogen burning much sooner and thus evolve very rapidly. These relatively short lifetimes of massive stars are mostly influenced by their mass-loss rates (Langer 2012). For most of their lives, massive stars above $\sim 20 M_{\odot}$ shed mass in fast stellar winds that can be a significant fraction of their total mass. This mass loss determines the evolution of their temperature, luminosity and the type (Ib,c or II) of supernova explosion in the final evolutionary phases. Massive stars end their life as the remnants of these core-collapse supernovae, transforming into either a neutron star or a black hole. The evolution of a modelled massive star depends critically on the adopted stellar wind mass-loss rates during the core hydrogen burning phase, the hydrogen shell burning phase and the core helium burning phase. The uncertainties in determining the mass-loss rates for massive stars are still large even in the local Universe where we have excellent multiwavelength observations (Smith 2014).

By now, it is considered that most of the massive stars are actually multiple-star systems, where the mass loss plays an even greater role through mass exchange from the donor star. Sana et al. (2012) studied a sample of massive O stars and found that over 70% of them exchange mass with a companion. The speckle interferometric survey of Galactic massive stars (Mason et al. 2009) expanded upon a decade-old survey and noted that 75% of the massive stars in clusters and 59% in the field have either a spectroscopic or a visual companion. However, these observed binary fractions are only a lower limit, because they must be corrected for the spectroscopic binary systems that are missed due to low inclination, for the periods that are too long compared to the observational cadence, or for the low-mass companions that are more difficult to detect. When corrected to the observational bias, the upper limit for binarity fraction in bound systems can reach as high as $\sim 90 \pm 10\%$ (Kiminki & Kobulnicky 2012; Sana et al. 2012; Kobulnicky & Fryer 2007). Although photometric monitoring campaigns typically only detect binarity for system geometries that are close to edge on, each new eclipsing binary discovered among massive stars helps to constrain the binarity fraction.

The spatial concentration of massive stars is highest in young open clusters and OB associations. For example, $\sim 70\%$ of Galactic O-type stars are found in young clusters or loose OB associations (Portegies Zwart et al. 2010), making these systems ideal targets for massive-star studies. The scarcity of open clusters and associations older than 1 Gyr is attributed to encounters with giant molecular clouds, supported by the observed median cluster age in the solar neighbourhood of around 250 Myr (Kharchenko et al. 2005). This cluster age segregation means that different clusters contain massive stars in various evolutionary phases. In this way, a targeted photometric monitoring of clusters and associations to get a high yield of massive stars will also provide an opportunity to study the possible relationship between the age and variability characteristics of selected objects.

The detailed stellar evolution theory of massive stars is currently an open question, as physical phenomena like magnetic fields, core convective overshooting, internal stellar rotation and angular momentum distribution inside stars are poorly understood. There have been parametrised descriptions of those phenomena in corresponding models but they remain uncalibrated with high-precision observational data (Aerts et al. 2013). Observationally, we know of many different transition phases in the life of massive stars: luminous blue variables, B[e] supergiants, blue supergiants, red supergiants, yellow hypergiants, Wolf-Rayet stars, but it is unclear how massive stars evolve beyond the core-hydrogen burning from one phase to the other on their evolutionary path. The answers to these questions may lie in the field of asteroseismology.

1.2 Asteroseismic observations of massive stars

Asteroseismology is the study of oscillations in stars (Aerts et al. 2013; Chaplin & Miglio 2013; Handler 2013). By using the oscillations as seismic waves, one can determine the interior structure of a star, which is otherwise not possible from overall properties like stellar brightness or surface temperature. Stars in different evolutionary phases excite various oscillation modes as the stellar interior undergoes changes and different driving mechanisms (ϵ mechanism (Rosseland & Randers 1938), κ mechanism (Baker & Kippenhahn 1962), convective driving (Brickhill 1991), stochastic excitation (Willette 1994)) take over. Thus studying the oscillations of stars at different evolutionary phases, one can test theories of stellar structure, stellar dynamics and evolution, and constrain the physics of stellar interiors.

All pulsating stars are asteroseismically active. By measuring the time-dependant light output of a pulsating star, one can calculate the oscillation frequency spectrum to extract asteroseismic parameters (identified modes, small and large frequency separations, damping rate of solar-like oscillations (Tassoul 1980; Gough 2003)). These parameters can then be used to model the interior of the star, from the varying speed of sound and rotation to the mean stellar density (Gough 2002; Goupil et al. 2004; Guzik 2011).

Helioseismology (Kosovichev 2011) specialises in the interior structure and dynamics of the Sun, the first asteroseismic target that has been studied since 1960 (Leighton et al. 1962) and numerically modelled since 1989 (Stein & Nordlund 1989). Similarly to the Sun, solar-like oscillations have been found in numerous other F-, G- and K-type main-sequence to giant stars (White et al. 2011) and using the global asteroseismic parameters, unification with the evolutionary models have begun (Verner et al. 2011; Huber et al. 2012). But our knowledge of the interior of stars heavier than the Sun is relatively poor as massive stars have large convective and

Table 1.1: Asteroseismic campaigns.

Name	Location	Magnitude range <i>V</i> mag	Sampling data point/night	Light curve length days
Hipparcos	space	-1–14	0.08	1280
CoRoT	space	11–16	160	80
MOST	space	<6	1500	20–60
BRITE	space	<6	800	180
Kepler	space	12–22	50 & 1440	1500
NSVS	ground	8–15.5	0.3–1.5	365
ASAS	ground	8–14	0.3	3000

rotational motions in their core that leads to the mixing of chemical species, yet the modelling of this rotational mixing is still rather crude (Rauer et al. 2014). Therefore, investigation of stellar evolution for massive stars requires a larger number of stars to sample all relevant stellar parameters.

To obtain asteroseismic parameters from the frequency spectrum, the observations have to sample the full pulsation periods. Furthermore, the quality of the data is improved by the number of times these periods are sampled. But the pulsation periods for massive stars are on widely varying time-scales. β Cephei stars are in the order of hours, slowly pulsating B (SPB) stars are in the order of days whereas Mira and semi-regular (SR) stars are in the order of hundreds of days (Handler 2013). Thus, one needs sufficiently dense and long time-series to study massive stars over the whole HR diagram. As it is not feasible for a single mission to cover it all, multiple observation campaigns optimised for different time-scales are needed.

Some of the biggest asteroseismic campaigns are in Table 1.1 where both the length and the cadence of an average data product are listed. Magnitude range is the upper and lower magnitude limit of a campaign where most of the observed stars are expected to lie. These limits are dictated by the exposure times of a campaign, leaving targets either under or overexposed. The table was compiled from various mission archives and overviews.

Concerning photometric monitoring, the space missions like CoRoT (Convection Rotation and planetary Transits), Kepler and Canadian MOST (Microvariability and Oscillations of STars) and BRITE (Bright Target Explorer) have observed hundreds of OB main-sequence stars during the last decade and the pulsational modelling of a few tens of objects has greatly contributed to the asteroseismic description of their internal structure (Bedding 2014). But this is still an exploratory phase, and observations for ensembles of massive stars with known metallicity and age are needed (Aerts 2015).

The case of evolved OB stars is even more challenging, mainly due to the very small number of objects monitored from space up to now. In general, space missions have a very high observing cadence, due to their continuous monitoring of selected objects, but lack the quantity of monitored objects for exactly the same reason. There are the all-sky scanning space missions of Hipparcos and the ongoing Gaia telescopes that have a lot of observed objects, but their data lack the required cadence for asteroseismic analysis. An additional obstacle is the relatively short campaign lengths ranging from weeks (MOST) to months (BRITE; CoRoT; Kepler 2) which is not sufficient to investigate longer oscillation periods reaching up to several months in the case of OB supergiants (e.g. Moravveji et al. 2012). The long-term high-duty-cycle monitoring is also useful for main-sequence variables (β Cep and SPB stars) to check the possible long-term frequency or amplitude variability.

As a rule, ground-based photometric observations can not achieve the required precision of 0.1 to 0.5 mmag that is needed for proper asteroseismic analysis (Aerts et al. 2013). However, ground-based multicolour light curves (giving a precision of a few mmag) can be used to detect the pulsation modes with suitably high amplitudes (Saesen et al. 2013). For the less-studied supergiants, this approach would be especially profitable as they are the brightest objects in the near sky. In addition, ground-based campaigns serve as support for asteroseismic space missions by observing and compiling potential candidate catalogues that would be infeasible for space telescopes due to the sheer number of variable stars.

The All-Sky Automated Survey¹ (ASAS) is a fully automated survey consisting of two observing stations on both hemispheres, one in Las Campanas Observatory in Chile (1997) and the other on Haleakala in Hawaii (2006) (Pojmanski 1997; Paczyński 2000; Pigulski et al. 2009). Both are equipped with two wide-field instruments, observing simultaneously in *V* and *I* band with magnitude range of 8 to 14 magnitudes. ASAS-3 database boasts full coverage south of DEC=+28 degrees where every object is observed once in 1-3 days. Due to almost nightly sky coverage, ASAS have numerous discoveries of (dwarf) novae and new variable stars (five part series ending with Pojmanski et al. 2005) with the emphasis on eclipsing binaries (Paczynski et al. 2006a). In total, ASAS-3 photometric catalogue contains over 15 million light curves that is unrivalled by any space mission.

Northern Sky Variability Survey² (NSVS) was a similar automated survey of the sky north of DEC=-38 degrees with daily time sampling and one year of baseline from April 1999 to March 2000 (Woźniak et al. 2004). The survey was conducted from Los Alamos, New Mexico, in the course of the first generation Robotic Optical Transient Search Experiment (ROTSE-I) where the sky was covered in an unfiltered

¹<http://www.astrow.edu.pl/asas/?page=main>

²<http://skydot.lanl.gov/nsvs/nsvs.php>

optical region, ranging from 8 to 15.5 magnitudes. NSVS catalogue has been used to identify new variable stars using machine learning algorithms (Hoffman et al. 2008, 2009; Shin et al. 2012) and is used as a basis for further observations of specific targets (Schmidt 2013). NSVS photometric catalogue contains around 14 million light curves.

The use of automated small ground telescopes has resulted in many variable-star all-sky surveys. These surveys have revealed numerous new discoveries of variable stars (Norton et al. 2007; Nedoroščík et al. 2015) from eclipsing binaries to stars with as yet undefined variability types. But the need to cover nearly all of the observable sky takes its toll on the time resolution of the light curves for a given star, and therefore smaller-scope campaigns are needed to improve the observational time coverage for specific fields. As the all-sky surveys are usually conducted using wide-field cameras, stars in crowded fields can not be resolved due to large pixel scales of these cameras (~ 15 arcsec per pixel for ASAS and NSVS). In addition, the brightest stars in the sky are often overexposed in those surveys and consequently understudied (bright limit for ASAS and NSVS is $V \approx 8$ mag).

It is not feasible to observe bright objects in large sky areas (e.g. clusters and associations) with high cadence using large-aperture telescopes because of their low availability and typically limited field of view. But a number of small telescopes dedicated to astrophotographers exist that are suitable for bright-star observations with relatively large field of view and photometric filters. Commercially available telescopes (e.g. iTelescope.net or slooh.com) give us access to astronomical sites with better astroclimates and minimal effort of maintaining the equipment.

In order to study massive stars in different evolutionary phases, we observed a number of open clusters and OB associations in the northern sky over a 3-year period using a small commercial telescope. Finding new variable stars builds the foundation for stellar modelling by adding new test objects that can be used to narrow down asteroseismic constraints. The goal of this thesis is to expand the variable-star knowledge in our selected fields by extracting the variability types from the light curve information and perform a frequency analysis on the periodic variable stars. In addition, we study the period change in selected massive binary systems to extract mass-loss rates.

In Chapter 2 we give an overview of the conducted campaign and describe our data reduction procedures. Chapter 3 contains the description of the resulting variable star catalogue along with our classification methods and cluster membership analysis. Finally, Chapter 4 is dedicated to the period change analysis of selected binaries in the Cygnus OB2 region with the overview of the Bayesian method used to derive the orbital parameters. We also do binary modelling and derive stellar parameters and mass-loss rates.

CHAPTER 2

CAMPAIGN OVERVIEW

2.1 Observations

We obtained our photometric data set using the commercial iTelescope.net 0.25-m Takahashi Epsilon telescope (T4), located in Mayhill, New Mexico, USA. We opted for a commercial telescope platform due to their hosting locations, which have superior astroclimate when compared to Estonia. The New Mexico site is located 15 miles from Apache Point Observatory at an elevation of 2225 meters where the weather is much more suited for good time domain astronomy. This was especially important if we wanted to achieve a good time resolution for our observations as in Estonia there are usually less than 100 nights with sufficient photometric quality per year¹.

In addition, the remote access to the platform allowed us to use multiple telescopes in three separate continents – Australia, Europe and North America. Although this work is concentrated on the observations made with the T4 telescope in New Mexico, the whole project also made use of other telescopes to study the short period SX Phoenicis star CY Aqr (Wiedemair et al. 2016) and the northern ecliptic pole for Gaia Data Processing and Analysis Consortium. The latter was supplementary to the Gaia southern ecliptic pole Specific Objects Study (SOS) (Clementini et al. 2016).

An overview of the T4 telescope is given in Table 2.1. During the start of the campaign we did some test runs with 6 different telescopes in total. The T4 telescope (called GRAS-004 then) was most suited for our campaign due to the combination of available Johnson-Cousins *BVI* filters and its relatively big 60.5×40.8 arcmin field of view (FOV).

The telescope itself was remotely controllable through a web interface either by a hands-on approach or automatic scripts. Access to the telescope was granted through a scheduling system which, unfortunately, meant that on some nights observations had to be cancelled due to the system being overbooked. On the other hand, it made it possible to queue the whole observation night beforehand, even months in advance. Although the primary web interface had only a handful of basic imaging options available, the scripting of observing plans was done using a robust ACP environment that gave the user access to many more customisation options. This way, one could make a plan for the night and let it run automatically at set times without the need to interfere.

Our photometric data set was obtained from the summer of 2011 till the end of

¹<http://hermes.aai.ee/kliima/>

Table 2.1: Overview of the T4 telescope.

CCD	SBIG ST-10XME
QE	85% Peak
Full Well	$\sim 100,000e^-$ NABG
Dark Current	$\sim 1e^-/\text{pixel}/\text{sec}$ at 0°
Pixel Size	$6.8\mu\text{m}$ square
Resolution	1.64 arcsec/pixel
Sensor	Frontlit
Cooling	Set to -15c default
Array	2184 x 1472 (3.2 Megapixels)
FOV	60.5×40.8 arcmin
Filters	Photometric BVRI & Ha, SII & OIII & Clear by Custom Scientific
OTA	Takahashi Epsilon 250
Optical Design	Hyperbolic Flat-Field Astrograph
Aperture	250mm

2013. The T4 telescope was decommissioned at the beginning of 2014 in favour of a similar telescope that was installed a year prior. We give an overview of the campaign in Table 2.2 where we count the number of nights that specific fields were observed as well as the used passbands. For the preliminary results of the observations in the Cygnus region during the 2011 season, see Paper I.

The time resolution was one of the priorities of the campaign and therefore observations were carried out as frequently as possible. During the campaign, the telescope was used in total on 488 nights out of 996, having an uptime of 49%. We started the campaign with only three test fields and then expanded the campaign twice, once in the latter part of the first year and again at the start of the second year. The usual observing night was carried out by observing every available field once per night with occasional nights dedicated to specific fields with multiple observations.

A single observation consisted of three consecutive exposures in a set of *VI* or *BVI* passbands with exposure times optimised for the brightest sources in each field. For some fields, we opted for two different exposure times in order not to saturate the brightest stars and, at the same time, to monitor some of the fainter massive stars in that field. Analysis of our data set was mostly done using the *V* passband. *B* passband exposures were only obtained for two of the fields, so we could not use it for consistency reasons, whereas *I* passband exposures were optimised for the red supergiants, leaving most of the hotter sources underexposed and thus having larger scatter than in *V* passband.

Table 2.2: Overview of the campaign.

Field	RA Hms	DEC Deg	2011	2012	2013	Passband
			Number of nights			
Berkeley 87	20:23:23	+37:14:50	83	138	128	<i>VI</i>
NGC 6913	20:24:00	+38:15:43	77	134	110	<i>VI</i>
Cyg OB2	20:32:41	+41:22:00	80	138	126	<i>BVI</i>
Berkeley 86	20:18:57	+38:44:43	0	104	108	<i>VI</i>
P Cygni	20:18:56	+38:02:09	0	104	108	<i>VI</i>
NGC 7510	23:14:30	+60:30:30	36	101	72	<i>VI</i>
NGC 7654	23:25:24	+61:23:40	52	101	72	<i>VI</i>
PZ Cas	23:45:52	+61:56:00	35	101	72	<i>VI</i>
NGC 581	01:35:18	+60:49:30	28	79	39	<i>VI</i>
NGC 663	01:45:37	+61:12:00	28	79	39	<i>VI</i>
NGC 869/884	02:20:07	+57:07:55	31	79	39	<i>VI</i>
NGC 957	02:30:17	+57:39:30	6	79	39	<i>VI</i>
IC 1805	02:33:00	+61:33:00	6	79	38	<i>VI</i>
EO Per	02:53:45	+57:36:00	6	79	37	<i>VI</i>
Gem OB1	06:11:00	+23:02:00	17	65	56	<i>BVI</i>

After the decommissioning of the T4 telescope in 2013, we continued the observations for another year with the successor of T4, an 0.25-m Takahashi Epsilon telescope T5. They were both the same aperture size telescopes and had the same camera with identical FOV. They also had a similar photometric Johnson-Cousins *BVI* filter system albeit with a differently shaped transmission bands. Due to these differences in filter systems, the two data sets were shifted depending on the stellar colour indexes of the observed stars. To correct this, we should have constructed transformation equations to convert between the two filter sets (Park et al. 2016), taking also into account the colour of the comparison stars. In addition, as the T5 telescope was used on far fewer nights than T4, the inclusion of these observations were left for future works.

Simultaneous observations in some of the fields were also carried out by Tõnis Eenmäe during 2013–2014 using the Tartu Observatory 0.31-m RAITS telescope, located in Tõravere, Estonia. RAITS was equipped with an Apogee Alta U42 CCD camera and Astrodon Johnson-Cousins *BVRI* filters. The FOV was 37×37 arcmin that has about a quarter less total area than the 60.5×40.8 arcmin FOV from the T4 telescope. The data were acquired in total from 103 observing nights during two seasons in 2013 and 2014. These observations were used together with T4 observa-

tions in the period change analysis of eclipsing binary systems in Cygnus OB2 field (Chapter 4).

In addition to the photometric observations, the classification of selected brighter variable stars without known spectral types was carried out using the 1.5-m telescope AZT-12 at Tartu Observatory, Estonia. Spectral data were collected using a long slit spectrograph ASP-32 with 600 lines/mm grating, yielding $R \approx 1550$ and covering wavelength range $\lambda \approx 3680$ to 5830 \AA .

In total, we observed 22 northern open clusters and associations in four different constellations across 15 fields. The fields were chosen for their number of bright OB stars and the age difference of the clusters. The observations were not centred on the clusters but instead the field of view was set to maximise the number of massive stars in each field based on the catalogue of supergiants and O stars by Humphreys (1978).

Table 2.3 lists all of the associations and open clusters within our observed fields. The ages of the clusters have been gathered from literature with the references given in parentheses. In addition to smaller works, two larger catalogues were used for the cluster age determination. The first is by Kharchenko et al. (2013) who compiled a catalogue of over 470 million stars and used a homogeneous method for determining cluster parameters for 3006 open clusters. These are published as the Milky Way Star Clusters Catalogue (MWSC). The other compilation of cluster literature data is the DAML02 (Dias et al. 2002) database, containing cluster parameters for more than 2167 open clusters.

Cluster age determination is usually done by main-sequence turn-off point fitting (Kharchenko et al. 2013; Monteiro et al. 2010). This method relies on the assumption that all stars in a cluster are formed almost simultaneously from the same cloud of interstellar gas and thus the stars in the cluster are all of the same age and at the same distance from us. In addition, the chemical composition of all the stars is assumed to be very similar because the cloud of gas from which the stars are formed is expected to be fully mixed. The speed of stellar evolution is dependant on the initial stellar mass meaning that the more massive the star, the faster it evolves away from the zero age main sequence. As all the stars in the cluster are representative of the cluster age, the turn-off point on the HR diagram (the leftmost point on the zero age main sequence) identifies the cluster age.

The main problem with the determination of cluster ages is that modelled theoretical HR diagrams for different cluster ages (called isochrones) cannot always be unambiguously fitted to the cluster main sequence on colour-magnitude diagrams (Dambis et al. 2017). This is especially important as one has to account for the reddening and cluster metallicity when fitting isochrones (Oliveira et al. 2013). Depending on the adapted values, the resulting cluster age can differ by a large margin. This can be seen from the large scatter in cluster ages in Table 2.3. On a side note, the

Table 2.3: Observed clusters.

Field	Cluster	Cluster age					
		Myr					
Berkeley 87	Berkeley 87	2.5 ^(a)	14 ^(b)	13 ^(c)	14 ^(d)		
	MWSC 3336	30 ^(c)					
NGC 6913	NGC 6913	5 ^(b)	32 ^(c)	13 ^(d)	5 ^(e)	1.75 ^(f)	
Cyg OB2	Cygnus OB2	5 ^(c)	1 ^(g)	1 – 7 ^(h)			
	FSR 0236	158 ^(b)	158 ^(c)				
Berkeley 86	Berkeley 86	3 ^(a)	13 ^(b)	6 ^(e)			
P Cygni	IC 4996	7 ^(b)	14 ^(c)	9 ^(d)	10 ⁽ⁱ⁾		
	Dolidze 42	35 ^(b)	33 ^(c)	35 ^(d)			
	Berkeley 85	1000 ^(b)	1160 ^(c)	1000 ⁽ⁱ⁾			
NGC 7510	NGC 7510	22 ^(b)	50 ^(c)	38 ^(d)	10 ^(j)	6 ^(k)	
	Markarian 50	12 ^(b)	13 ^(c)	12 ^(d)	7.5 ^(l)		
	FSR 0422	461 ^(b)	461 ^(c)				
NGC 7654	NGC 7654	158 ^(b)	79 ^(c)	58 ^(d)	10 ⁽ⁱ⁾	100 ^(m)	
	Czernik 43	40 ^(b)	58 ^(c)	50 ^(d)			
PZ Cas	Stock 17	6 ^(b)	10 ^(c)	4 – 25 ⁽ⁿ⁾			
NGC 581	NGC 581	22 ^(b)	28 ^(c)	16 ^(o)			
NGC 663	NGC 663	25 ^(b)	32 ^(c)	20 ^(p)	13 ^(q)	20 – 25 ^(r)	
NGC 869/884	NGC 869	12 ^(b)	19 ^(c)	11 ^(s)	13.5 ^(t)		
	NGC 884	13 ^(b)	16 ^(c)	11 ^(s)	14 ^(t)		
	NGC 957	NGC 957	10 ^(b)	18 ^(c)	11 ^(d)	10 ^(u)	
IC 1805	IC 1805	3 ^(b)	18 ^(c)	7 ^(d)	1 – 7 ^(s)	1 – 3 ^(v)	
EO Per	–						
Gem OB1	Gemini OB1	9 ^(r)					

References. (a) Massey et al. (2001); (b) Dias et al. (2002) ^a; (c) MWSC Kharchenko et al. (2013) ^b; (d) WEBDA ^c; (e) Straižys et al. (2014); (f) Joshi et al. (1983); (g) Massey et al. (1995); (h) Wright et al. (2014); (i) Maciejewski & Niedzielski (2007); (j) Barbon & Hassan (1996); (k) Piskunov et al. (2004); (l) Baume et al. (2004); (m) Choi et al. (1999); (n) Pandey (1986); (o) Sanner et al. (1999); (p) Georgy et al. (2014); (q) Pandey et al. (2005); (r) Pigulski et al. (2001); (s) Tetzlaff et al. (2010) ^d; (t) Currie et al. (2010); (u) Yadav et al. (2008); (v) Wolff et al. (2011).

^a<http://www.wilton.unifei.edu.br/ocdb/>

^b<https://heasarc.gsfc.nasa.gov/W3Browse/all/mwsc.html>

^c<http://www.univie.ac.at/webda/navigation.html>

^d<http://mnras.oxfordjournals.org/content/402/4/2369/T14.expansion.html>

age discrepancy of NGC 7654 is thought to be caused by multiple and independent star formation periods as there seems to be an older cluster behind a group of younger stars (Pandey et al. 2001).

2.2 Data reduction

Data reduction was carried out using the PHOTWORK software (Tuvikene 2012) based on the IDL Astronomy User’s Library². PHOTWORK was developed for reducing and storing photometric observations from multisite campaigns. It incorporates the standard photometric reduction pipelines for bias, dark frame and flat-field corrections, as well as aperture photometry magnitude extraction, star catalogue matching and database storing.

Bias frames were obtained in between field switching on every observation run. Usually three to six bias frames were obtained per night and combined into a nightly master bias frame.

Dark frames were obtained for most of the different exposure times used in our observations. We reacquired dark frames every couple of months to update the master dark frames used in the reduction. For the exposure times with no corresponding dark frames, we used an interpolated master dark frame.

Flat-field frames were supplied by the service provider for between one and ten nights per month, with three to six flat frames per respective night. Master flats were constructed individually for each observing night using raw flats from closest nights where flat frames were available. We excluded frames that exhibited systematic differences over 5% from the median flat of neighbouring nights. Typically between six and twelve frames from between two and four nights were combined to an individual master flat. During periods with very few provided flats, we constructed master flats from frames of a single night with minimal time separation from the observations.

The aperture photometry extraction was done with 10 different aperture sizes that were all scaled by the full width at half maximum (FWHM) of stars in any given frame. The used aperture sizes were between 0.8 and $3.5 \times$ FWHM with the main used aperture radius being $1.8 \times$ FWHM. The other radii were used to check any dependencies on the size of the aperture. For further analysis, we only used instrumental magnitudes with uncertainties less than 0.1 mag.

Additionally, SExtractor³ source extraction software (Bertin & Arnouts 1996) along with PSFEx (PSF Extractor) software (Bertin 2011) were used for Point Spread Function (PSF) photometry extraction. This was necessary to disentangle the light curves of stars where the signal of a source in a given aperture was contaminated by

²<http://idlastro.gsfc.nasa.gov/>

³<https://www.astromatic.net/software/sextractor>

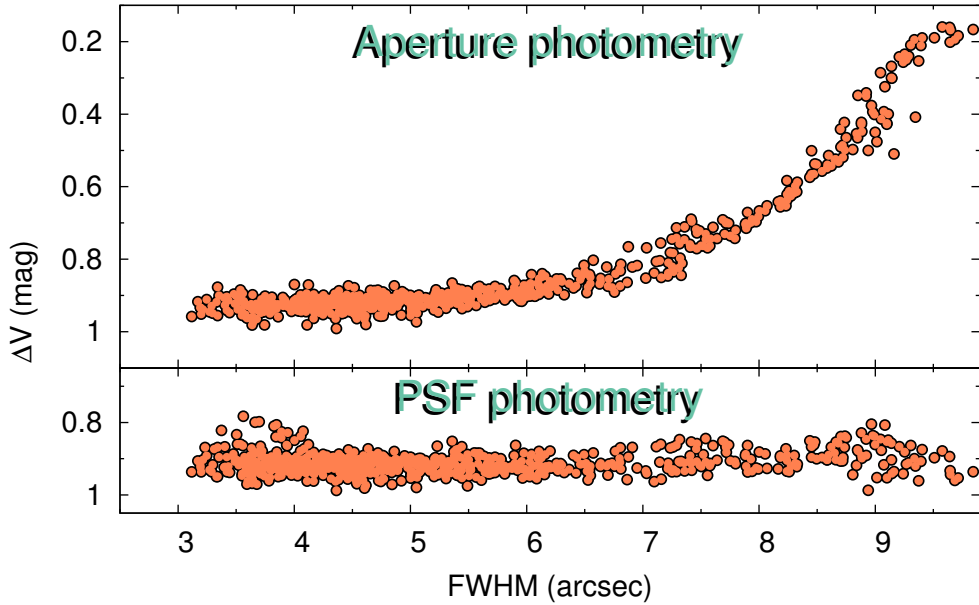


Figure 2.1: FWHM-magnitude plot for detecting nearby contaminating stars in a given aperture. The upper panel shows the brightness correlation measured in an aperture radius of $1.8 \times \text{FWHM}$. The lower panel is obtained by using PSF photometry on the same star and the graph shows no relation between the FWHM values and the acquired brightness values.

neighbouring stars. We determined this contamination from FWHM-magnitude plots by a detection of a strong correlation between the FWHM and magnitude values. This correlation indicates a nearby star that affects the total extracted magnitude when the aperture size changes with the FWHM value. PSF photometry was used for every object that was identified to have this problem.

Figure 2.1 shows FWHM-magnitude plots for a star V619 Per. The upper panel is a typical result from aperture photometry when the target has a closeby star. As the physical size of the aperture is scaled with the FWHM values, neighbouring stars start to enter the aperture radius on higher FWHM values. In case of V619 Per, the brightness starts to rise from the FWHM value of 5 arcsec and reaches a plateau around 10 arcsec. This means that between those values, the aperture contains more and more of the closeby star until the whole star is encompassed, increasing the brightness from ~ 0.9 mag to ~ 0.2 mag. As can be seen from the lower panel, PSF photometry disentangles V619 Per brightness from the neighbouring star and the true light curve can be extracted.

The PSF photometry extraction pipeline was developed using Python scripting and MySQL database system. The aperture and PSF photometry databases were then combined for simultaneous photometry analysis. In general, the aperture photometry had a smaller scatter for brighter sources, while PSF photometry was better for fainter and crowded stars.

We used Bouguer's extinction plots to flag data points affected by bad weather (Sterken & Manfroid 1992). This is done by constructing an instrumental magnitude - airmass plot and identifying measurements deviating from a fitted magnitude to airmass slope. We flagged data points for which the brightness drop due to extra atmospheric extinction exceeded 0.8 magnitudes from the fitted slope. This indicates that the bigger than average extinction in the atmosphere was most probably due to clouds.

The extracted sources were then matched with our internal star catalogue that was combined from Two Micron All Sky Survey (2MASS)⁴ and USNO CCD Astrograph Catalog (UCAC-3)⁵ source lists. This was done by transforming the image coordinates into sky coordinates using a FITS World Coordinate System (WCS) (Greisen & Calabretta 2002) and matching every extracted source with its closest counterpart from the star catalogue within 5 arcsec radius. Every star was attributed an internal ID number that increases with the decreasing of UCAC fit model magnitude (f.mag) from UCAC-3 catalogue. These ID numbers can be seen in Table 3.1 and in the Appendix at the end of this thesis.

Due to telescope control software issues, telescope centring on the target was inconsistent. There was a software bug in the system so that when the auto-focus routine failed, the telescope would do a correct auto-centring routine and slew to the target but would then slew for an additional time for every consecutive exposure in that field. These issues caused the frames to be at offset with respect to the targeted field. In the worst case, that offset was up to 1/4 of frame size, excluding about one third of the target stars. However, as most of the time the auto-focus was successful, this problem affected only a limited number of exposures.

To analyse the data, we used multiple comparison stars that were chosen to be, preferably, close to the centre of the frame to minimise systematic errors across the frame. They were also chosen to be usable in both the *V* and *I* passbands. The final comparison stars were selected by studying star pairs that matched the aforementioned criteria and provided minimal scatter in the combined light curve. We used between two and five comparison stars per field. This combination of comparison stars gives us a relative photometric precision of better than 0.01 mag.

⁴<http://irsa.ipac.caltech.edu/Missions/2mass.html>

⁵<http://www.usno.navy.mil/USNO/astrometry/optical-IR-prod/ucac>

In addition, all of the collected spectral data were reduced using IRAF⁶ tasks. First, a zero-level correction was applied along with the pixel-to-pixel non-uniformity corrections using incandescent lamp flat-field data. Then, for the wavelength calibration, a dispersion relation was established using a ThAr spectral lamp. Finally, to correct for the instrumental sensitivity effects, target spectra were corrected using one or more spectrophotometric standard stars from CALSPEC⁷ database (Bohlin 2014) that were observed on the same nights as the targets. For classification purposes, a digital spectral classification atlas⁸ by R. O. Gray for late-type stars and synthetic spectra for B-type stars⁹ (Gummersbach & Kaufer 1996) were used.

2.2.1 Correcting for the scattered light

Extra corrections to the photometric data had to be made due to the scattered light contamination in the flat-field frames. Scattered light that reaches the focal plane of the camera causes illumination gradients in flat-field frames and using these frames in the data reduction yields position-dependent systematic uncertainties in the resulting photometry (Manfroid 1995). The T4 telescope had a German equatorial mount and due to the aforementioned scattered light problem, the data show systematic effects depending on the telescope being on the east or west side of the pier. Changing of this pierside is caused by the target crossing the meridian and requiring a meridian flip, 180° telescope rotation, to be commenced. This means that the side of the pier is dependant on the object either being rising or setting at the time of the observation. As the observations were targeted to have low airmass values, the number of observations on the rising and setting branch were distributed quite equally during a season and thus make the systematic uncertainties noticeable.

To correct for these effects we constructed correction surfaces for the full frame. Based on the systematics in the light curves, we divided the data of the brightest constant stars from all the fields into distinct time intervals and then measured the offset of the mean magnitudes relative to the mean magnitude of the first time interval. In this way, we found a global difference surface over the whole frame for each of these time intervals in every filter. In total, we constructed correction surfaces for 14 time intervals that were separated based on the combination from the pierside position and other systematics in the data. We generated two different types of correction surfaces using either a median smoothing or a polynomial fitting. The analysis of light curves was done using a combination of both corrections.

An example spline fitted correction surface is given in Fig. 2.2. The shape of the

⁶<http://iraf.noao.edu/>

⁷<http://www.stsci.edu/hst/observatory/crds/calspec.html>

⁸http://ned.ipac.caltech.edu/level5/Gray/Gray_contents.html

⁹<https://www.lsw.uni-heidelberg.de/projects/hot-stars/websynspec.php>

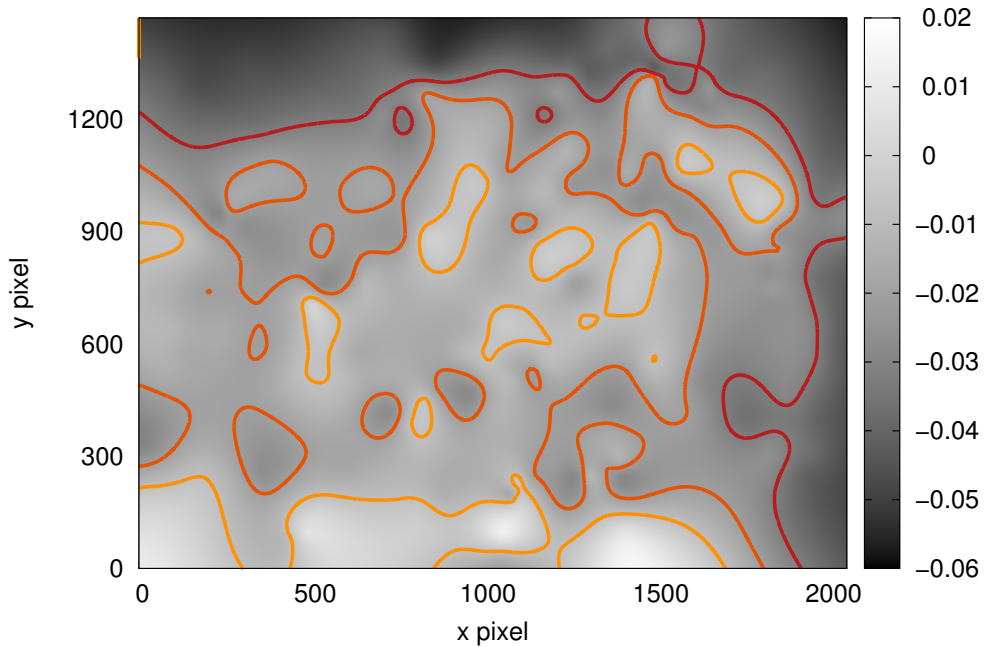


Figure 2.2: Full frame contour plot of a correction surface for a chosen time interval. The fifty shades of gray indicate the per pixel difference between the first and chosen time interval in magnitudes. The orange contours mark the -0.02, -0.01 and 0 levels with increasing brightness.

surface is rather complex and also differs between time intervals. Although, there is an indication of a gradient across the lower-left to top-right corner, no global parametric correction could be found that would satisfactorily describe the systematic errors.

In general, the amount of flat fielding error increases with the distance from the centre of the frame. So the reason to select comparison stars as close to the frame centre as possible was to minimise these correction uncertainties from comparison stars themselves. The correction was applied to both the programme star and the comparison stars. The mean correction value is 0.017 magnitudes. The nightly mean precision of brightest stars is better than the mean correction value (cf. Fig. 2.7) and as a result, the total signal-to-noise ratio of the data can be improved by implementing this correction.

In addition to the pierside position switches, separate time interval was selected between Julian dates (JD) 2456189 and 2456243. This was done because after the T4

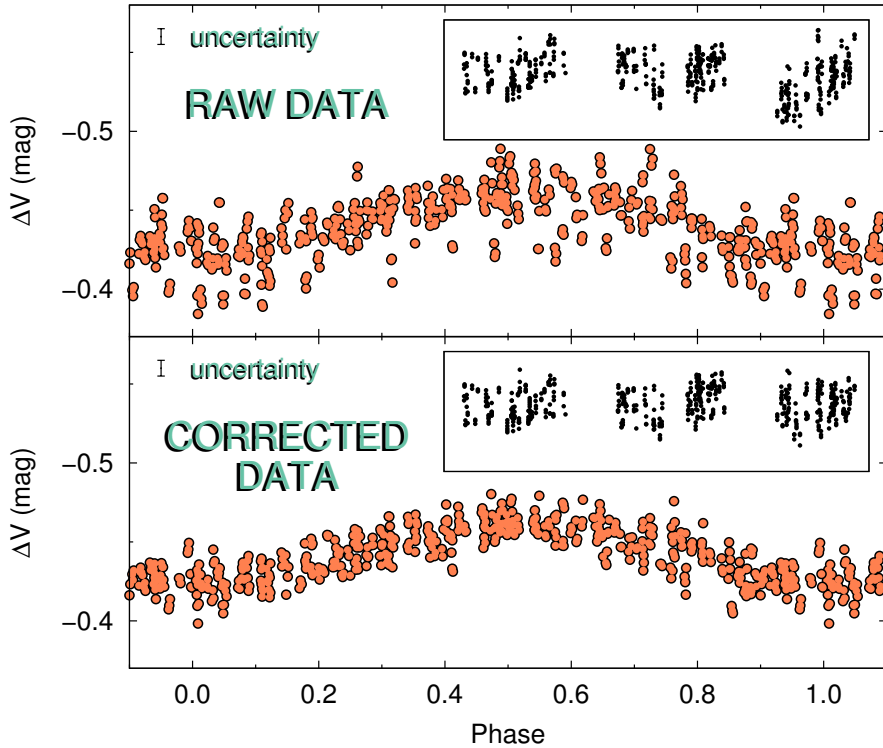


Figure 2.3: Example light curve correction for SPB star BD+59 2692. The light curve is folded with a period of 1.3032 days. The upper panel is the raw data and the lower panel is the final data obtained after using the correction surfaces. The main panels show a folded phase-curve and the small panels show light curves in time domain before and after correction.

telescope was upgraded to a new camera, the newly installed system was mounted incorrectly and caused the whole field to be rotated about 30 degrees. Also, the period between JD 2456350 and 2456413 needed to be corrected as there were erroneous flat-field frames supplied.

An example correction of a light curve is given in Fig. 2.3. The raw data (upper panel) show offsets in the light curve (inset panels) that are corrected (lower panel) based on the surfaces combined from constant stars. The need for the correction is more evident in the phased light curves (big panels) where the scatter of a phase curve can be seen reduced after applying the correction.

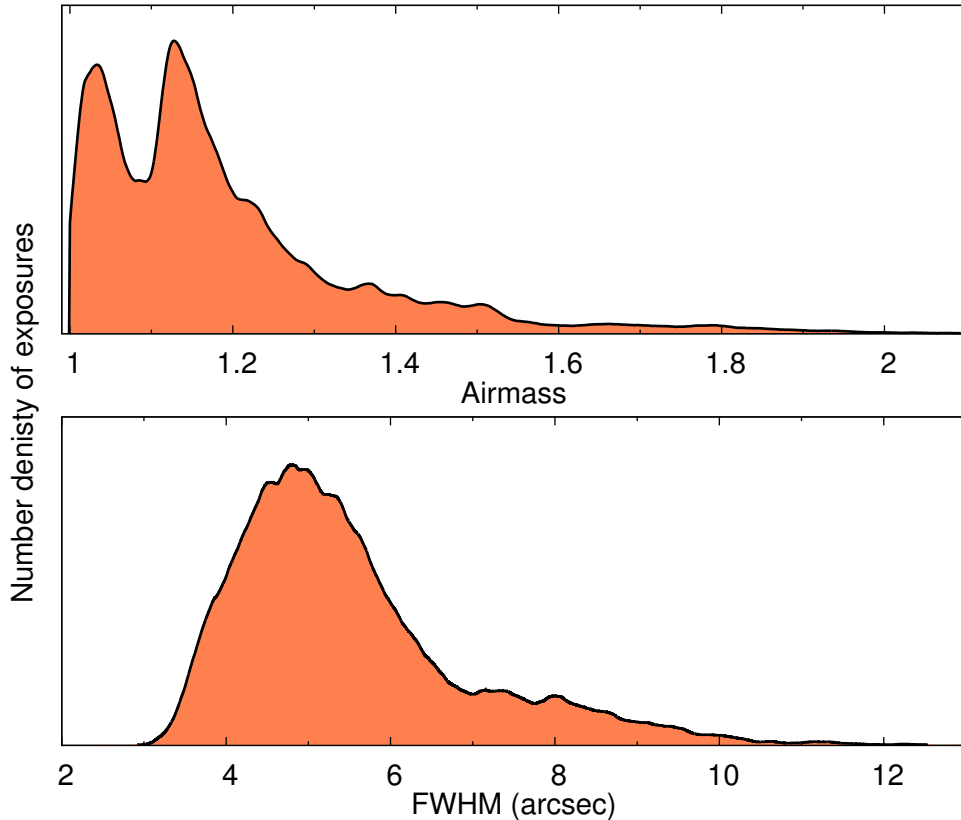


Figure 2.4: Airmass value (upper panel) and FWHM value (lower panel) distributions over the whole campaign.

2.3 Calibrated data

In total, 28 082 CCD frames were obtained and calibrated, of which 1942 were obtained in *B*, 13 428 in *V* and 12 712 in *I* passband.

We give the airmass distribution in the upper panel of Fig. 2.4. As the observation plans for the campaign were sequenced to observe every field preferably at lower airmasses, the airmass values are mainly in the range of 1 to 1.5. The two peaks of airmass values are due to two distinct maximum altitude ranges for our selected fields (mainly in Cygnus and Cassiopeia constellations) as seen from the New Mexico site.

The FWHM values on the lower panel in Fig. 2.4 were obtained from the CCD frames by analysing the brightest stars. From the weather data provided by the New

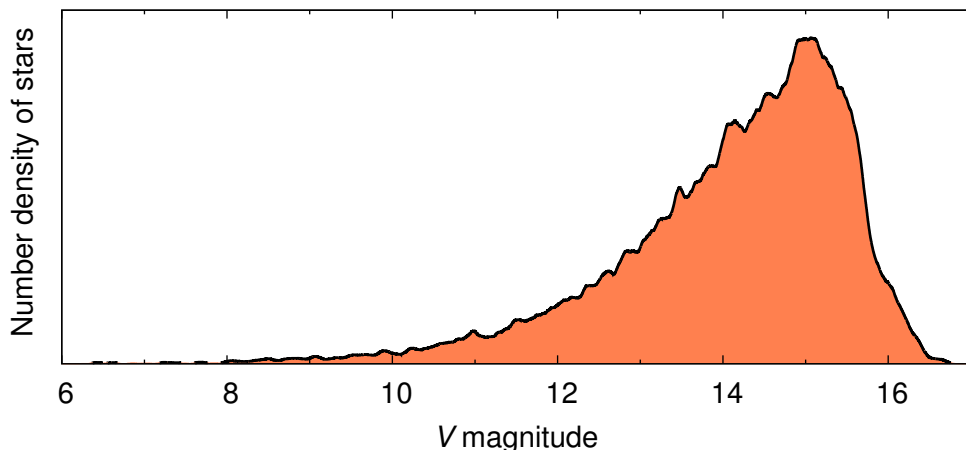


Figure 2.5: V magnitude distribution of all the detected sources in our data set.

Mexico Skies¹⁰, the yearly average atmospheric seeing value at the New Mexico site is around 1.7 arcsec. As FWHM is also worsened by the poor tracking and focusing of the telescope, the final values varied from 3 to 14 arcsec with the median value of 5.2 arcsec. Our obtained FWHM was good for observing bright stars, as we were able to use longer exposure times without overexposing our target stars and suppress scintillation noise at the same time. Although larger FWHM lowers the signal-to-noise ratio of faint stars and affects our limiting magnitude, the focus was on the brightest cluster members and the trade-off was deemed acceptable. We limited our analysis to using FWHM values of less than 10 arcsec, as the data become much worse at high values.

In total, we obtained light curves for 25 395 sources – these are sources with more than two extracted V magnitude measurements. As objects with fewer than 100 data points were deemed under sampled for our variability detection method, only the remaining 17 497 objects that had more than 100 measurements in V passband were used in the subsequent variability analysis. This hard cut-off level was chosen empirically from the average number of 674 frames per field.

Fig. 2.5 shows the V magnitude distribution of our observed stars. The measured stellar brightnesses were not transformed into standard photometric system. Instead we used an instrumental system that was shifted close to Johnson-Cousins system by using known standard magnitudes from the APASS¹¹ DR9 catalogue. The fall-off in the number of stars with the apparent magnitudes fainter than 15 mag is due to the

¹⁰<http://www.nmskies.com/weather.php>

¹¹<https://www.aavso.org/apass>

Table 2.4: Photometric quality of the V passband exposures.

Field	Exp. (s)	N	V range (mag)	Lim. (mag)	σ (mag)	N_{90}
Berkeley 87	60	1509	6–16.5	14.0	0.046	254
NGC 6913	60	1650	8–16.5	14.0	0.047	265
Cyg OB2	60	1392	6–16.5	14.0	0.045	284
Berkeley 86	5 + 20	2033	8–15.5	12.0	0.044	102
P Cygni	10	1311	7–15	12.5	0.047	98
NGC 7510	90	2146	8–17	14.0	0.044	456
NGC 7654	10 + 40	2777	6–16	12.5	0.046	143
PZ Cas	30	1946	6–16	13.5	0.047	225
NGC 581	8	850	7–14.5	12.0	0.041	95
NGC 663	40	1841	6–16	13.5	0.043	288
NGC 869/884	8 + 40	3321	6–16	12.5	0.049	269
NGC 957	20	1103	7–15	13.0	0.045	102
IC 1805	20	794	7–15	13.0	0.042	101
EO Per	120	1138	8–17	14.5	0.041	172
Gem OB1	4	456	6–14	11.5	0.038	43

Notes. Limiting V magnitude (Lim.) is shown on Fig. 2.6 and represents the cutoff where stars have been detected on more than 90% of the frames. The number of stars that have been detected >90% (N_{90}) is the total number of good quality sources in each field.

short exposure times and larger FWHM values.

The V passband data are summarised in Table 2.4. We list the V passband exposure times in column 2 (Exp.) and the total number of detected objects in column 3 (N). The given V magnitude range in column 4 are the extrema brightness values of detected objects in that field and indicate the brightness distribution of detected objects. The limiting V magnitude (Lim.) values in column 5 are given as the limit where fainter stars are detected on less than 90% of the frames (cf. Fig. 2.6). Stars that are detected on over 90% of the frames are defined as stars with good photometric quality and the number of them is given in column 7 (N_{90}). These are stars for which the detection on our frames was not affected by the airmass or seeing values. The total number of N_{90} stars is around 2900. The quick dropoff in detection for fainter stars is to be expected due to variable FWHM values and strict photometric detection limit.

Column 6 in Table 2.4 lists the typical photometric internal root-mean-square (RMS) noise (σ) of the constant stars to quantify our photometric precision at the limiting V magnitude (Lim.). The RMS noise is defined in Kjeldsen & Frandsen

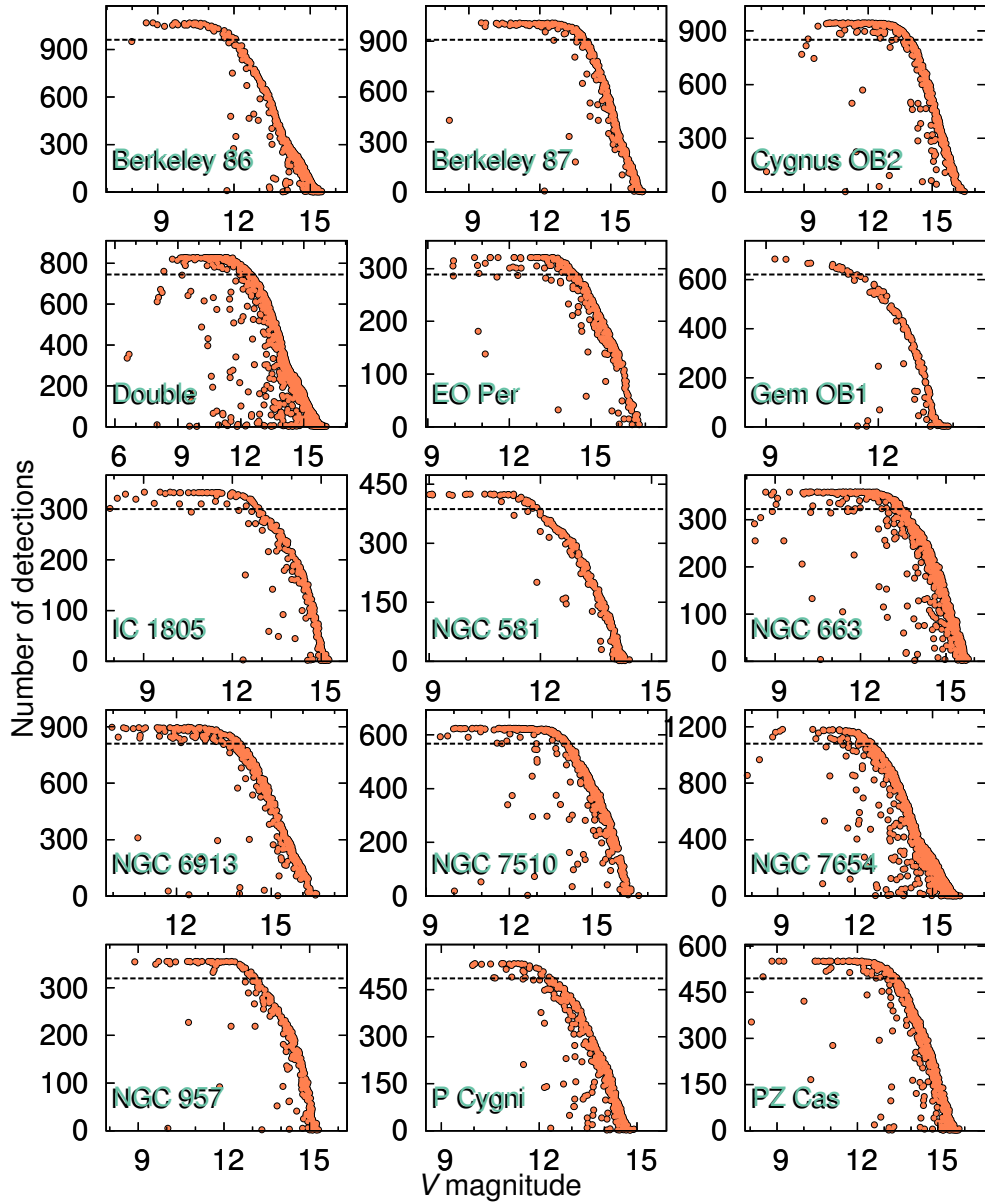


Figure 2.6: Number of detections per star as a function of V magnitude for each of the fields. The dashed line represents the 90% detection limit. We obtained the limiting V magnitudes from the graphs by assessing the intersection of the 90% line with the spine of the data. Stars above the 90% line are considered as stars with good photometric quality.

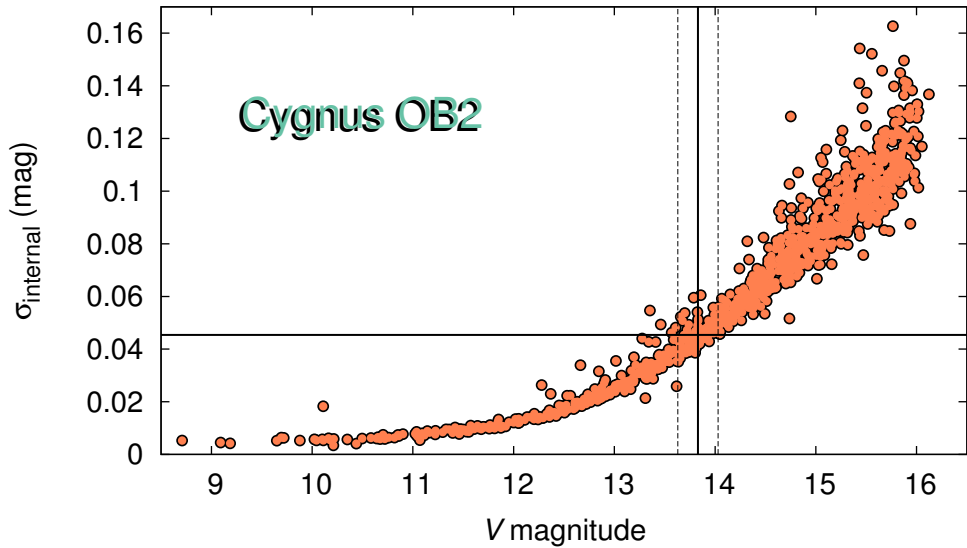


Figure 2.7: Internal RMS noise as a function of magnitude in Cygnus OB2 field. The solid vertical line is the calculated limiting V magnitude and the dashed vertical lines show the bin in which the median precision (horizontal line) is measured.

(1992) as:

$$\sigma_{internal} = \sqrt{\frac{\sum_{i=1}^{N-1} (m_i - m_{i+1})^2}{2(N-1)}}, \quad (2.1)$$

where m_i and m_{i+1} are consecutive magnitudes measured during the same night and N is the total number of measurements. As a typical observing night consisted of three measurement in a single field, the internal noise value represents an average brightness standard deviation per night.

The precision in column 6 is given as an intersection on a σ -magnitude diagram between the internal noise and the limiting V magnitude value. A representative σ -magnitude diagram of Cygnus OB2 field is shown in Fig. 2.7. The resulting precision at limiting magnitude was obtained as a median internal noise from stars in a 0.4 magnitude bin around the limiting V magnitude value (between the two dashed vertical lines).

CHAPTER 3

CATALOGUE OF VARIABLE STARS

3.1 Detection of variability

Variable stars were initially selected on the basis of a variability index (Kjeldsen & Frandsen 1992). This variability index is defined as a ratio between the standard deviation of the full light curve and the internal RMS noise (Eq. 2.1). For a constant star, the value would be close to unity whereas stars with values above 1.5 are considered photometrically variable objects. The variability index is useful for a wide variety of observations, as the internal RMS noise takes into account all instrumental uncertainties and the resulting value is therefore independent of the total scatter of the data, effectively measuring only the signal-to-noise ratio of variability.

Throughout the variability determination, we use measurements in the *V* pass-band because of the better scatter values for most of the sources. As the variability index is a measure of the signal-to-noise ratio of variability, we calculated the value of the variability index for most of our objects. We only omitted stars that had fewer than 100 measurements from the selection to exclude very faint stars and spurious detections. For every star, we calculated the variability index based on three different data sets. Two of these data sets were acquired by applying the two flat-field correction surfaces described in Section 2.2 and the third was the raw light curve. The final selection was based on the lowest variability index value of those data sets to minimise erroneous variability detections.

Every star with variability index over 1.5 was then visually inspected for any erroneous detections. A number of faint stars in crowded fields had to be discarded as they were too close to bright stars to disentangle even with PSF photometry. Some light curves of stars that lied closer to the frame edges were rechecked with a different set of close-by comparison stars. This was done to minimise global systematic effects in the light curve and remove spurious variability detection for stars with variability index only slightly above 1.5. We also excluded some stars from the very edge of the frame as they were measured only when the telescope pointing was off-centre.

We then flagged our selected variable stars, based on the presence or absence of systematic effects, under different flags. As the aforementioned problems requiring the flat-field correction were too severe in some cases, we had to flag a number of stars unusable when a clear separation between the data from the east and west side of the pier was seen. Additional flagging was done based on the photometry extraction method used. We used aperture photometry for brighter sources and PSF photometry for fainter and crowded stars.

To analyse the light curve shapes of different type of variable stars, we used a Python library called Feature Analysis for Time Series (FATS). It extracts up to 64 different features from an unequally sampled time series that are described in Nun et al. (2015). These features can be used in a machine learning algorithms (Mackenzie et al. 2016; Pichara et al. 2016; Kim et al. 2014) to classify previously unclassified stars using a known training set. We used some of these features as supplementary information to describe our data set.

3.1.1 Frequency analysis

To search for periodic variables and eclipsing binaries from our data set, we used the discrete Fourier transform code SigSpec (Reegen 2007). It calculates a significance value describing the probability that an amplitude is not caused by noise. E.g., a significance value equal to 5 indicates that the considered amplitude level may only be due to noise in one out of 10^5 cases. SigSpec derives the resulting frequencies by iteratively prewhitening the frequency power spectrum using the most significant signal components from each run. We confirmed the dominant frequencies by visually identifying an amplitude of at least twice of the folded phase curve scatter.

Our typical spectral window is given in the upper panel of Figure 3.1. A spectral window is a Fourier' transform of observational sampling, showing possible aliasing problems and helping with the prewhitening of the power spectrum. As our observations were carried out periodically around the same time each night, the spectral window displays strong daily sidelobe aliases occurring at intervals of $\pm 1 d^{-1}$. In addition, smaller one year aliases from seasonal observations can be seen near the daily sidelobes, occurring at intervals of $\pm 0.00274 d^{-1}$.

In the case of suspected eclipsing binaries, we also used the phase dispersion minimisation (PDM) method (Stellingwerf 1978). The result of a PDM run is a power spectrum where minima values correspond to minimal dispersion of a phase folded light curve. It is calculated by dividing the phase curve into set number of bins and finding the average dispersion within these bins. As the sizes of the bins can be variable, this method is useful for data sets with gaps, non-sinusoidal variations, poor time coverage or other problems that make Fourier techniques less reliable. We used PDM to improve the period estimation of eclipsing binaries, as it accounts better for the different shapes of phase folded binary light curves.

Figure 3.1 gives the SigSpec output for the eclipsing binary A36 (V2550 Cyg in Table 3.1). The upper panel shows the aforementioned spectral window. The middle panel shows the raw frequency power spectrum where the primary frequency corresponds to half the period of the binary. The nearby frequency of $1 - 0.427 = 0.573 d^{-1}$ is a spurious period due to aliasing (Deeming 1975). This is a typical result for an eclipsing binary light curve analysis, as the full phase curve (lower panel in

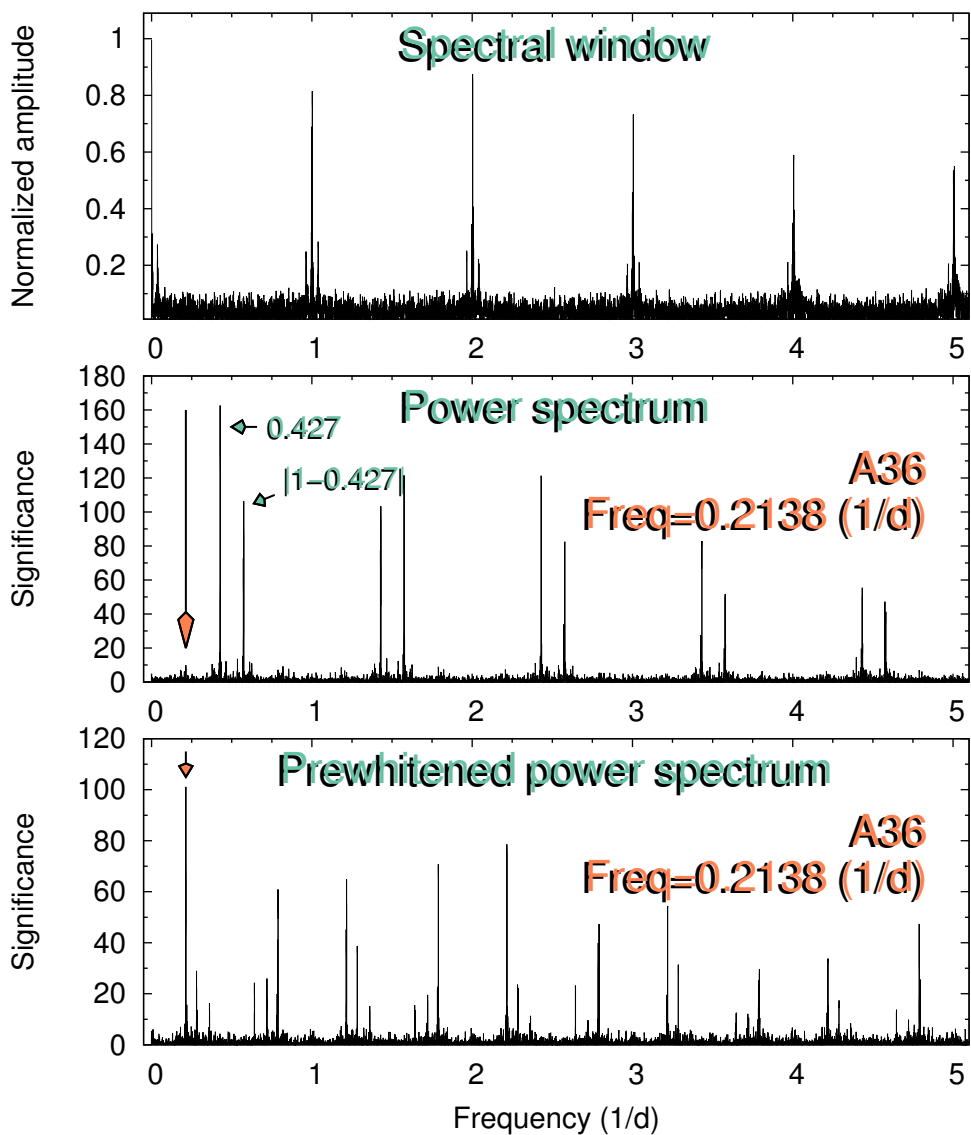


Figure 3.1: SigSpec output for eclipsing binary A36. The upper panel shows our spectral window. The middle panel is the raw frequency power spectrum with a primary peak and its first alias shown with green labels. The lower panel is the frequency power spectrum after prewhitening. Orange arrow shows the true frequency of the binary.

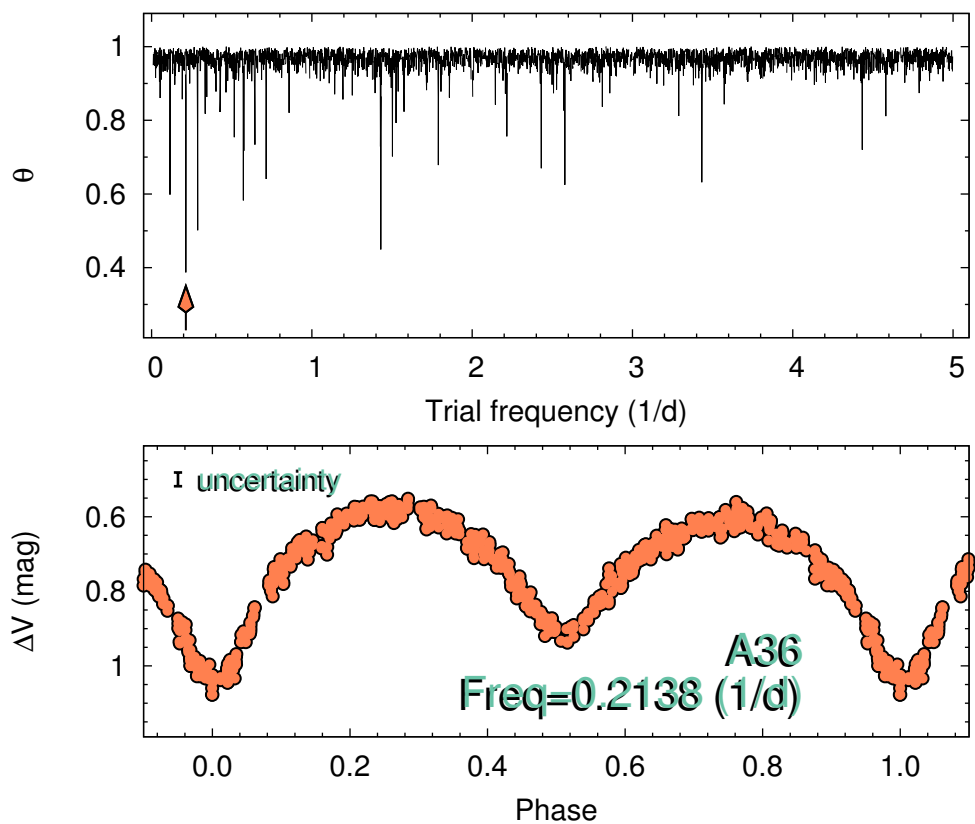


Figure 3.2: Phase dispersion minimisation method output for eclipsing binary A36. The upper panel shows the frequency spectrum and the lower panel shows the final binary phase curve. Orange arrow shows the true frequency of the binary.

Fig. 3.2) comprises of two sine waves of uneven amplitudes. The result would be indistinguishable from a pulsating star when relying on the SigSpec result alone.

Figure 3.2 shows the output from PDM algorithm for the same eclipsing binary A36. From the upper panel, it can be seen that the real frequency is dominating in the raw frequency power spectrum. This is due to the PDM ability to distinguish between the unequal minima in the phase curve.

3.2 Description of the catalogue

In total we found 354 variable stars in the observed fields. We list these objects in the Appendix distributed into different tables that are separated by variability type. The published catalogue along with all the light curves is available at the Strasbourg Astronomical Data Center (CDS)¹.

Table 3.1 is an excerpt from the full table (Table 1 at CDS and Appendix) of all the eclipsing binaries we found. The table lists our field names and internal ID-s of the stars. This was added to help identify the stars in our finding charts that are available in Appendix B from paper III. The designations are based on the SIMBAD database and, in case the star was absent there, 2MASS designations were used. Given coordinates are based on 2MASS All-Sky Point Source Catalog².

¹<http://cdsarc.u-strasbg.fr/viz-bin/qcat?J/A+A/598/A108>

²<http://irsa.ipac.caltech.edu/cgi-bin/Gator/nph-scan?submit=Select&projshort=2MASS>

Table 3.1: Observed eclipsing binaries.

Field	ID	Designation	RA J2000	DEC J2000	Cluster membership	Spectral type	V (mag)	Amp. (mag)	Period (days)	VSX info	VSX per. (days)
Berkeley 86	3	V444 Cyg	20:19:32.4	+38:43:54	–	WN5+O6II-V	7.973	0.336	4.2130	EA/WR	4.2124
Berkeley 86	22	HD 228989	20:20:21.4	+38:42:00	–	O8.5V:+O9.7V:	9.686	0.091	1.7734	–	–
Berkeley 86	52	LS II +38 43	20:19:36.8	+38:35:21	Berkeley 86	B1V	10.676	0.148	1.9102	–	–
Berkeley 86	289	V435 Cyg	20:16:27.0	+38:45:41	–	B3V(e)	12.749	0.659	6.7758	EA/SD	6.7719
Berkeley 86	381	2MASS J20190590+3853009	20:19:05.9	+38:53:01	–	–	12.808	0.569	4.3262	–	–
Berkeley 87	18	BD+36 4063	20:25:40.6	+37:22:27	–	ON9.7Ib	9.656	0.187	4.8121	E/GS	4.8126
Berkeley 87	50	TYC 2697-130-1	20:25:30.6	+37:25:48	–	F5V*	10.736	0.169	0.7726	EA	0.7726
Berkeley 87	87	V2538 Cyg	20:23:33.5	+37:25:45	–	BIIII-V*	12.003	0.496	3.1620	EB	3.1616
Berkeley 87	131	TYC 2697-883-1	20:25:38.3	+37:03:11	–	–	12.188	0.183	1.8632	–	–
Berkeley 87	203	2MASS J20222399+3658020	20:22:24.0	+36:58:02	Berkeley 87	–	12.940	0.198	20.3009	–	–
Berkeley 87	251	2MASS J20215480+3654426	20:21:54.8	+36:54:43	–	–	13.324	0.376	6.4827	–	–
Berkeley 87	288	NSVS 5733998	20:25:15.8	+37:33:18	–	–	13.139	0.635	1.6691	E	0.8340
Berkeley 87	414	2MASS J20241336+3704436	20:24:13.4	+37:04:44	–	–	13.830	0.668	0.2540	VAR	0.2540
Cygnus OB2	5	BD+40 4220	20:32:22.4	+41:18:19	Cygnus OB2	O7I+O6I+O9V	9.185	0.292	6.5980	EB/D/GS	6.5978
Cygnus OB2	18	BD+40 4212	20:31:37.5	+41:13:21	Cygnus OB2	O6IV+O9III	10.214	0.190	4.7460	EA	4.7463
Cygnus OB2	42	Schulte 1	20:31:10.5	+41:31:54	Cygnus OB2	O8V	11.072	0.089	4.8523	–	–
Cygnus OB2	48	V2550 Cyg	20:34:58.8	+41:36:17	FSR 0236	B0Ib+B0III	11.418	0.447	4.6760	EA	4.6760
Cygnus OB2	117	Schulte 27	20:33:59.5	+41:17:35	Cygnus OB2	O9.5V+B0V	12.203	0.612	1.4692	EW/KE	1.4600
Cygnus OB2	158	V1827 Cyg	20:30:27.3	+41:13:25	FSR 0236	O7I+O9I	13.053	0.509	4.0218	EB	4.0217
Cygnus OB2	187	V2186 Cyg	20:33:10.5	+41:22:22	Cygnus OB2	B0V+B3V	12.958	0.161	2.9787	EA	2.9788
Cygnus OB2	224	[MT91] 720	20:34:06.0	+41:08:09	–	B0.5V+B1.5V	13.415	0.241	4.3620	–	–
Cygnus OB2	362	[MT91] 36	20:30:56.1	+41:28:54	–	–	13.691	0.592	0.6856	EA	0.6858

Notes. Full Table 3.1 is available in Appendix and at the CDS (Table 1). Similar tables are available for other variable stars. A portion of the table is given here to show the general style and form of the resulting data.

Table 3.2: Spectral classifications based on our observations.

Designation	Previous sp. type	Determined sp. type
V1319 Cyg	–	K0I
TYC 2697-130-1	–	F5V
V2538 Cyg	–	B1III-V
TYC 2684-1267-1	–	K5V
J02163833+5705124	M2 ⁽¹⁾	M2:
BD+56 596	B ⁽²⁾	B0II-III
BD+56 733	OB+e: ⁽³⁾	B1II-III
TYC 3709-420-1	–	A1V
V472 Cas	–	M4:
BD+60 358	B5 ⁽⁴⁾	B1Ve

References. (1) Lee et al. (1943); (2) Skiff (2014); (3) Hardorp et al. (1959); (4) SIMBAD.

The spectral types listed in Table 3.1 are combined from multiple sources. The main contributor was the SIMBAD³ database, as it is the largest stellar database online. In addition, we used a number of additional smaller compilations to improve the selection. The Tycho-2 spectral type catalogues (Fabricius et al. 2002; Wright et al. 2003) are separate compilations that match Tycho-2 catalogue to various classification works and consist of around 300 000 classifications each. Around 800 000 spectral type determinations have been compiled by Skiff (2014) including first time results from many large-scale objective-prism spectral surveys. Currie et al. (2010) have spectroscopically observed and classified most of the stars in the Double cluster (NGC 869/884) with ~11 000 spectra. Wright et al. (2015) have compiled spectral classification data for all the massive stars in Cygnus OB2 region from 19 sources with the majority of the classifications coming from Massey & Thompson (1991) and Kiminki et al. (2007). Spectral types with lower case letters are obtained from photometric observations in the Vilnius 7-colour system (Milašius et al. 2013).

Based on our spectral observations from Tartu Observatory, we obtained spectral classifications for ten variable stars of which six had no previous classifications. These classified variable stars are listed in Table 3.2 and marked with an asterisk (*) behind the classification in Table 3.1.

From our spectra, BD+60 358 is a B1Ve type star as both $H\beta$ and Fe lines are in emission. V472 Cas is an M4 or later type star and based on the Ca I 4227 line, its luminosity class is from V to III. V2538 Cyg is a previously known eclipsing binary star (Nicholson & Scottish 2006) and the lines from its companion are also visible in

³<http://simbad.u-strasbg.fr/simbad/>

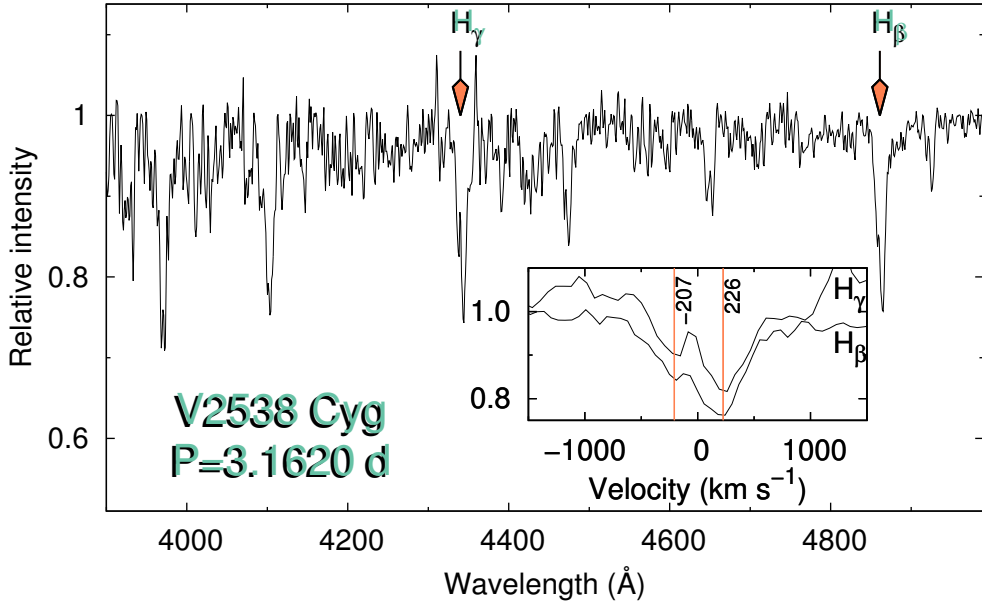


Figure 3.3: Spectrum of the double line B1III-V binary V2538 Cyg. The spectrum was obtained at phase 0.225 with 1.5 meter telescope AZT-12 at Tartu Observatory. Double lines are visible in all hydrogen and helium lines and the component velocities are shown in the inset panel.

our spectra, making it an SB2-type spectroscopic binary with a B1III-V type primary and a B-type secondary component (cf. Fig 3.3). The spectrum for V2538 Cyg was taken at a phase of 0.225 and the component radial velocities of -207 and $+226$ km s^{-1} were estimated by Gaussian fitting the line components.

To calculate the cluster membership fraction among the variable stars, we used the Milky Way Star Clusters Catalogue (MWSC) project (Kharchenko et al. 2013) which incorporates cluster membership probabilities around open clusters. They give three different probabilities based on proper motion and photometric $J-K$ and $J-H$ colour. These probabilities were determined from the location of the stars with respect to the reference sequences of either the average cluster proper motion in kinematic diagrams or the isochrones in photometric diagrams. They find about 400 000 stars to be cluster members having kinematic and photometric membership probabilities higher than 60%. We adopt their membership probabilities (kinematic probability ($P_{\text{kin}} > 50\%$) and photometric probabilities ($P_{\text{JKs+PJH}} > 100\%$) to determine the cluster membership of our variable stars. Column 5 in Table 3.1 list the name of the cluster that an object is a probable member of.

In Table 3.1 we compare our variable stars with previously known variability information on these objects. For this comparison we use the International Variable Star Index (VSX)⁴ database run by the American Association of Variable Star Observers (AAVSO) to identify possible first discoveries of variability. VSX is an initiative to catalogue all known variable stars and by now it incorporates variable star information from various variable star surveys as well as peer reviewed user submitted data. It encompasses variable star information from Combined General Catalog of Variable Stars (GCVS 4.2, 2004 Ed.), Northern Sky Variability Survey (NSVS), the 3rd All Sky Automated Survey (ASAS-3), various volumes of the Information Bulletin on Variable Stars (IBVS), Optical Gravitational Lensing Experiment (OGLE-II), Robotic Optical Transient Search Experiment (ROTSE-I) and additional peer reviewed user submitted data. Due to the extensive compilation of different sources, the VSX database includes information on 398 915 (as of June 2017) variable stars. In the VSX "info" and "period" columns, we label stars that have no entry in the VSX database with "-" and those matches in the VSX catalogue with no variability classification with "?". Table 11 in the Appendix is a compilation of all the variable stars that are not listed in the VSX database.

In Table 3.1, we give an amplitude value as a modified FATS amplitude. The amplitude value in the Table is defined as the difference between the median of the maximum 5% and the median of the minimum 5% magnitudes.

In Table 3.1, we report only the periods corresponding to the dominant frequencies. We list β Cep and slowly pulsating B (SPB) stars with multiple frequencies in Table 3.4. A frequency power spectrum peak is commonly called significant when the signal-to-noise ratio of an amplitude is $S/N > 4$ (Breger et al. 1993) which corresponds to a significance value of 5.46 in SigSpec. Following the more conservative approach by Chapellier et al. (2011), we list only the frequencies with significance value over 20 because the periodograms below this began to show a forest of peaks.

3.3 Classification of variable stars

Table 3.3 summarises our observed variable stars. The classification of variability was based on the period of variability as well as position on the HR diagram. An illustrative pulsation HR diagram can be seen on Fig 1.12 in Aerts et al. (2010) and a similar depiction of pulsating variables is available in Becker (1998). As we observed only the brighter objects in each field, the variability types we found are also from the upper part of the HR diagram, containing mostly α Cygni, β Cephei, Be, SPB, Cepheid, semi-regular (SR) and Mira type variables. Variables with no identified periods and unknown spectral types were left unclassified.

⁴<https://www.aavso.org/vsx>

Table 3.3: The observed variable stars by variability type.

Variability type	No. of stars observed	No. in clusters	Cluster membership	No. of new discoveries
EB	80	18	23%	47
β Cep	13	3	23%	11
SPB	16	3	19%	15
Be	62	4	6%	29
α Cyg	30	8	27%	9
WR	3	0	0%	1
Cepheid	7	0	0%	2
γ Dor	1	0	0%	0
SR	63	8	13%	33
unclassified	80	9	11%	74

The full tables listing all the members of each type are available in the Appendix and at the the CDS. In addition, CDS hosts light curves for all of our variable stars (column named "LC"). These light curves are automatically converted into phase curves using our given dominant period value. The full light curve is visible by setting the period value back to zero. In the following subsections, we give links to other specific phase curves from other works that can be used to visually compare the validity of our period determination.

3.3.1 Eclipsing binaries

Eclipsing binaries are systems of two stellar components that, due to high inclination angle of the orbital plane, periodically eclipse each other, exhibiting light variations with eclipse minima. As binary systems are born during the fragmentation of the molecular cloud, the spectral classes of the components vary depending on their initial mass and their evolution due to mass transfer in the system (Smith 2014). The typical orbital periods range from 0.22 (Rucinski 2007) to over 1000 days (Paczyński et al. 2006b).

Ellipsoidal variables (Morris 1985) are close binary stars that are non-spherical due to tidal interactions and exhibit sinusoidal phase curves due to the changes in the cross-sectional area that is visible to the observer. In addition, some cases of overcontact binaries exhibit similar sinusoidal phase curves. The phase curves of these binary stars are identical to pulsating variables and we only classified stars with light curves that show unequal minima or maxima as eclipsing binaries, as this indicates tidal distortion effects or an uneven surface distribution of chemical elements (Kourniotis

Table 3.4: β Cephei and SPB stars with multiple frequencies.

Type	Designation	Frequency d^{-1}	Period d	Amplitude mag	Sig.
β Cep	LS II +36 70	4.63301	0.2158	0.0164	89
		4.77155	0.2096	0.0074	44
		4.52160	0.2212	0.0059	30
		4.14302	0.2414	0.0059	22
β Cep	V665 Per	4.12750	0.2423	0.0241	51
		3.98230	0.2511	0.0117	42
β Cep	J23175230+6025022	6.05643	0.1651	0.0244	43
		6.29459	0.1589	0.0147	23
β Cep	LS III +60 58	4.67678	0.2138	0.0141	67
		4.51472	0.2215	0.0052	20
SPB	HD 229253	0.636170	1.5719	0.0050	36
		0.289096	3.4590	0.0042	26
SPB	TYC 2684-312-1	1.16245	0.8603	0.0130	41
		0.812356	1.2310	0.0108	28
SPB	[MT91] 626	0.900873	1.1100	0.0174	36
		0.905040	1.1049	0.0152	35

Notes. Sig. - Significance from SigSpec

et al. 2014). Other periodic stars were left classified as pulsating variables.

We classified eclipsing binaries based on their previous classifications from VSX or, in case of new discoveries, based on their non-sinusoidal phase curves. In total, we found 80 eclipsing binary stars (Table 1 at CDS) in all of the fields, for 69 of which we identified their orbital periods. The remaining 11 were named binary candidates as their light curves include some eclipse-like drops, but no period could be extracted due to the limited data. According to VSX, 47 eclipsing binaries are new discoveries with no known period and variability designation.

3.3.2 β Cephei stars

β Cephei stars are pulsating early-to-mid B-type dwarfs to giants with periods ranging between two and eight hours. They are defined in Stankov & Handler (2005) as massive non-supergiant variable stars whose light, radial velocity and/or line profile variations are caused by low-order pressure and gravity mode pulsations. These surface pulsations are induced by the heat mechanism that enhance the stellar opacity due to iron group elements. The total number of known β Cephei stars is around 200

(Pigulski & Pojmański 2008).

We find 13 β Cephei candidates (Table 2 at CDS) of which two have been previously listed in the VSX database and eight have a known spectral type. We report four β Cephei stars that have multiple frequencies over the significance value of 20 (Table 3.4). An example of β Cep type is given in the lower panel of Figure 3.4.

As 13 is almost 7% of the number of known β Cephei stars, we resorted to naming them candidates. Our observations are made in a three successive exposures per night and thus we have not observed any of the periods in one full sequence. This complicates the analysis as our observations are undersampled for β Cephei stars. Nevertheless, our time series are long enough to determine constant short periods with sufficient amplitudes that have a significance value over 20.

The only β Cephei star in our selection with a previously determined period is V665 Per. Gomez-Forrellad (2000) reported two periods of 0.19493 and 0.24233 days. Their first period can be found in our data with significance value of eight. Their second period is closest to our dominant period of 0.242277 d but we would like to point out that our data do not support their period of 0.24233 d. This difference in periods can be interpreted by a period decrease of around five seconds in 15 years ($\dot{P}/P = -0.24 \text{ Myr}^{-1}$). This period change rate could be used to constrain evolutionary models for β Cephei stars by assuming different amounts of initial rotation and convective core overshoot and comparing the theoretical rate of period change to the measured one as done in Neilson & Ignace (2015).

3.3.3 SPB stars

Slowly pulsating B (SPB) type stars, like β Cephei, are driven by the heat mechanism of the iron group but instead of low order p modes, in SPB stars the high order g modes are excited, making their periods longer (Aerts et al. 2010). SPBs consist of mid-to-late B-type dwarf to giant stars with periods roughly between 0.8 and 3 days.

We find 16 possible SPBs (Table 3 at CDS) based on their periods, of which 12 have a spectral classification in the literature. We report three SPB stars with two frequencies over significance value of 20 (Table 3.4).

Our only matching SPB in the VSX database, V359 Per, is listed there as a β Cep star. The previous determination is done by the IOMC pipeline (Alfonso-Garzón et al. 2012) and they find a period of 0.275 d⁵. This period is not supported by visual inspection of the IOMC phase curve nor by our data. We find a different period of 1.2309 d, which is more in line with the star being an SPB type (cf. Fig. 3.4).

⁵<http://sdc.cab.inta-csic.es/omc/var/3694000069.html>

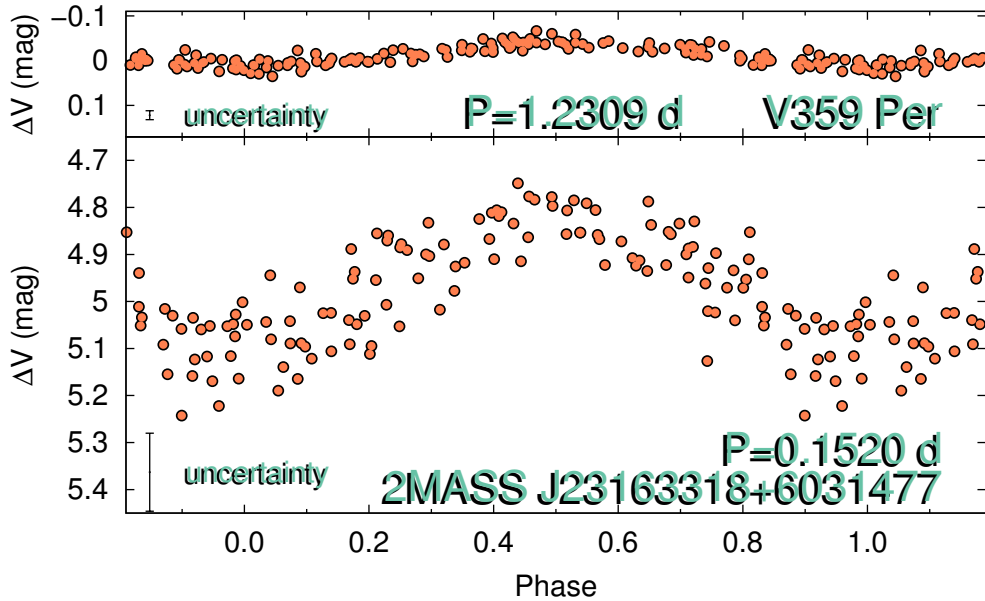


Figure 3.4: Example light curves of an SPB (upper panel) and a β Cep type (lower panel) variable stars. Data is comprised of nightly mean magnitudes. V359 Per is one of the brightest pulsating variable while 2MASS J23163318+6031477 is the faintest periodic star in our survey. The y-axis is on scale for both stars to show the difference in pulsational amplitude.

3.3.4 Be stars

While some Be stars show oscillations that are in accordance with either β Cep or SPB stars (Walker et al. 2005; Balona 1995), Be stars are known to infrequently exhibit photometric outburst behaviour linked to the dispersion of the circumstellar disk (Rivinius et al. 2013).

As Be stars are classified from their spectra, we have compiled here every variable B star that has shown some kind of emission in the past. In total, we find 62 Be stars (Table 8 at CDS) in our selection to be variable. Two of them, TYC 4279-2067-1 and V356 Per, exhibit additional β Cep-like pulsations with periods of 0.582 d and 0.342 d, respectively. V356 Per is previously classified by IOMC pipeline as a β Cep candidate⁶. They also find a period of 0.30595 d which is not supported by our data. Instead, we find a period of 0.342 d with a phase curve that is more sinusoidal than the IOMC data.

⁶<http://sdc.cab.inta-csic.es/omc/var/3694000050.html>

Be stars with photometric outbursts are indicated as "Y" in the outburst column in Table 8 at CDS. Outbursts can be caused by a heating front that propagates across the disk and, after reaching the critical density, pushes the disk into a hot state with high mass transfer and high accretion luminosity. (Mennickent et al. 2002) distinguish four types of photometric behaviour with type 1 being caused by accretion of matter with lower mass transfer rates and type 2 by a sustained period of a high mass-transfer rate. 27 of our Be stars exhibit outbursts with sudden rises and declines (type 1) during the three seasons. The highest amplitude outburst of 0.87 mag was seen in EO Per during the 2012 season. In addition, VES 203 exhibits behaviour of sudden brightness jumps (type 2) where the brightness dropped 0.2 mag for 100 days in the beginning of 2012 season and then stayed at a lower level for the remainder of the campaign. An example of a Be type star with outbursts is given in the upper panel of Figure 3.5.

3.3.5 α Cygni stars

α Cygni variables are non-radially pulsating supergiants of B–A spectral types with irregular variability caused by the superposition of many oscillations with close periods (Aerts et al. 2010; Saio et al. 2013). The typical observed timescales range from 1 to 50 days (Eyer & Mowlavi 2008).

We classified all of our variable B-to-early-A type supergiants (luminosity class I and II) as α Cygni variables. In total, we find 30 α Cygni variables (Table 7 at CDS) and for three of them, HD 229059, HD 14143 and V757 Per, we find pulsation periods. HD 14143 and V757 Per have previous period determinations of 0.0892 (Koen & Eyer 2002) and 0.1643 (De Cat et al. 2007) days, accordingly, although we found different period values with 0.5321 and 0.2453 days. Altogether, VSX lists periods for six of our determined α Cygni variables although none of those periods can be seen in our data. We may not have observed the same periods in our data because the variability of α Cygni type stars may be cyclic in nature, caused by interior mixing processes and atmospheric instabilities (Aerts et al. 2010).

3.3.6 Wolf-Rayet stars

Wolf-Rayet (WR) stars are supernovae progenitors which have lost most of their original massive envelope due to radiation driven winds. Almost all WR stars show no strict periodicities and the origin of their variability remains poorly understood (Aerts et al. 2010).

According to the spectral classification, we find three variable WR stars (Table 6 at CDS): WR 141, WR 158 and V444 Cyg. WR 141 and WR 158 exhibit irregular variability with amplitudes of 0.108 and 0.073 mag, respectively. WR 158 is

previously known spectroscopically variable star (St-Louis et al. 2009). WR 141 is previously classified as an SB2 binary (Marchenko et al. 1998) with an O5V–III companion and an orbital period of 21.698 d. Only from the first season of our observations do we find some signal with a period of 21.7 d, whereas there is no signal from the other seasons. This might be due to the flickering nature of WR 141 (Khalack 1996). V444 Cyg is a previously known eclipsing binary (Cherepashchuk & Khal-iullin 1973) with a WR component. Its orbital period from IOMC data is 4.213 d⁷ which can be confirmed with our data.

3.3.7 Late-type stars

Variable stars situated on the red side of the classical instability strip and with long periods ($P > 80$ days) are classified as Mira or SRa type variables if they are periodic and SRb type if they possess alternating intervals of periodic and slow irregular changes in their light curves (Aerts et al. 2010; Eyer et al. 2012). F–K spectral type weak-lined giants and supergiants are classified as SRd type variables. As we monitored our fields for three seasons our time series are not long enough to comfortably determine very long periods and therefore we classified all of the late-type stars into one group.

There are 46 variable stars in our fields with late-type spectral classification. Based on our measured $V-I$ colours and the shape of the light curves, we find additional 17 late-type candidates (Table 9 at CDS) with $V-I$ over 1.8 based on the effective temperature and colour tables from Currie et al. (2010). Due to the varying degree of reddening in young clusters, some of the candidates may be included because of the reddening difference between the comparison stars and target stars. We tried to account for that by calculating the differential reddening of the comparison stars by colour transforming the known APASS and 2MASS colours in the field. An example of a SRb type star is given in the lower panel of Figure 3.5.

From the total of 63 late-type variables, 30 are listed in the VSX database with 16 of them having a determined period. We find semi-regular periods for 19 stars only three of which are close to the previously determined periods. Some periods were obtained after de-trending the light curve with a wide median-filter to smooth out the slow irregular changes in semi-regular stars. As the periods are semi-regular and vary in time, the discrepancy between our newly determined and the previously determined periods is understandable.

⁷<http://sdc.cab.inta-csic.es/omc/var/3151000080.html>

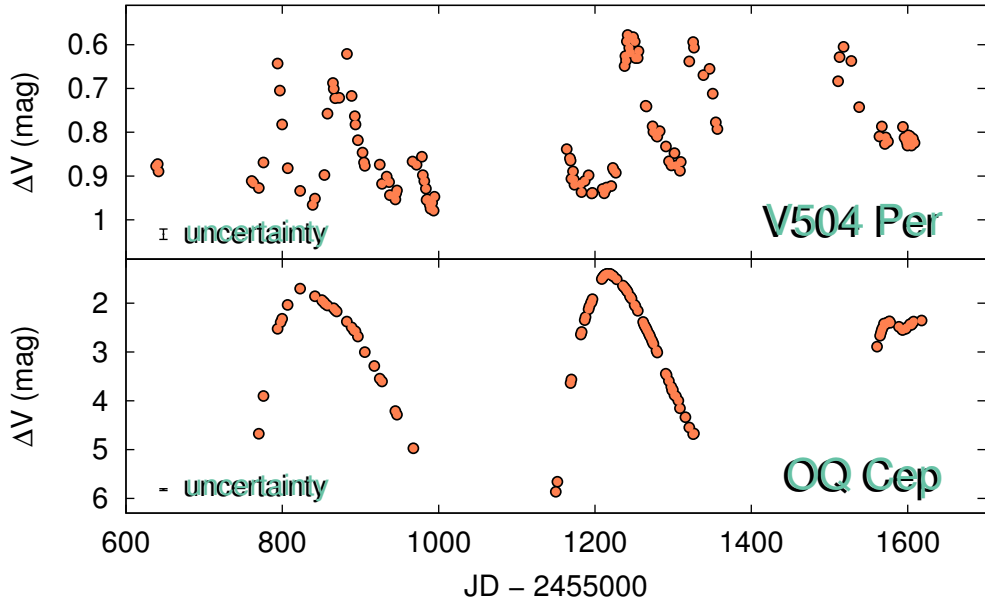


Figure 3.5: Example light curves of a Be (upper panel) and an SRb type (lower panel) variable stars. Data is comprised of nightly mean magnitudes. V504 Per shows multiple outbursts during the three seasons. OQ Cep has the highest variability amplitude in our survey even with the unobserved minima.

3.3.8 Cepheids

Stars with stellar masses above $5 M_{\odot}$ are observed as Cepheids after they start helium burning in their core and descend the giant branch (Aerts et al. 2010). Cepheids lie in the instability strip and are governed by the period-luminosity relationship. They are radially pulsating F–K type giants and supergiants and their luminosity classes change roughly from III to I during the pulsation cycle (Turner 2012). A typical light curve of a Cepheid is skewed and periodic, ranging from 1 to 50 days.

We find seven Cepheid variables (Table 4 at CDS) of which five were previously known. V1319 Cyg has been previously classified as an SRa type, probably due to its longer period. On the other hand, the folded light curve shows a classical skewed Cepheid shape and the spectral classification of K0I, determined from our observations at Tartu Observatory, is in accordance with a Cepheid rather than SR type of star. Of the two previously unknown Cepheid candidates, NGC 6913-36 exhibits classical Cepheid phase curve shape and has a spectral class estimation of "f" (photometrically determined F type) based on Vilnius photometric system (Milašius

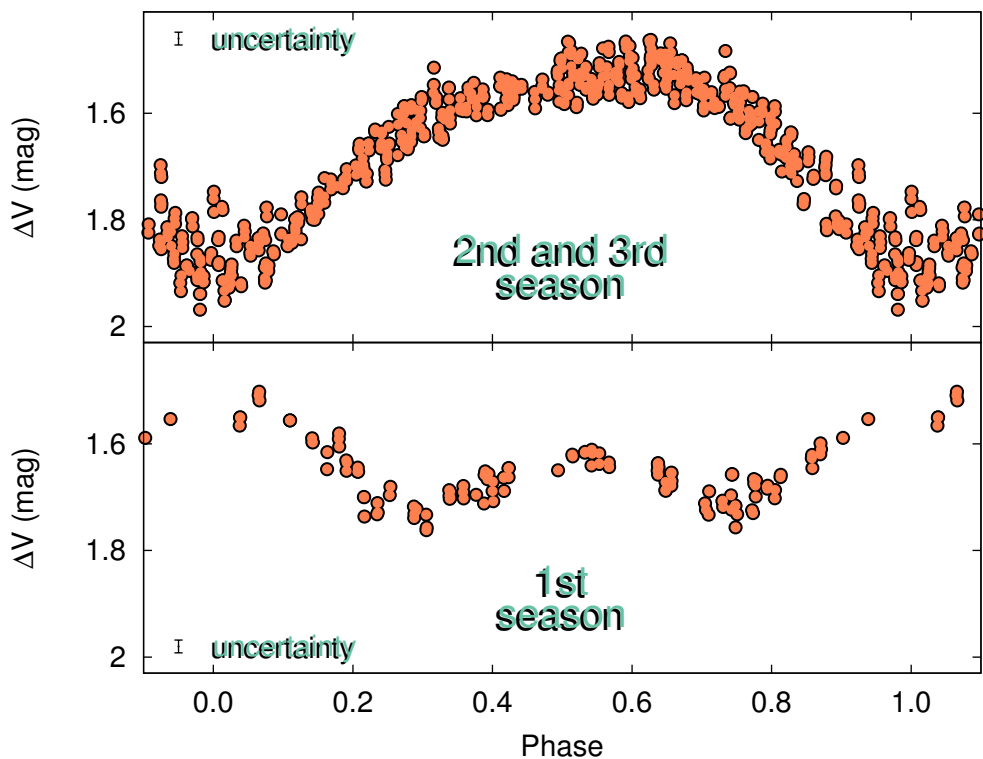


Figure 3.6: Folded light curve of a Cepheid NSVS 5731720. The data in the lower panel are from the first season and in the upper panel from second and third season. Both of them have been folded with the same period of 3.20612. The first season shows binary-like shape and a phase shift of around 0.6.

et al. 2013). The second candidate, 2MASS J20173903+3804143, is added as a candidate because of its brightness, period length and phase curve shape, although the photometric scatter is too high to distinguish between a noisy sinusoidal shape and a classical Cepheid shape.

We note that for the Cepheid NSVS 5731720, only the last two seasons can be used to fold the light curve nicely with the period (Fig. 3.6). The first season has approximately half the amplitude of the latter two, and when folded with the same period of 3.20612 days, the V passband light curve exhibits a binary-like shape with two unequal maxima. There is also a phase shift of 0.6 between the first two seasons. We are unable to explain this behaviour with systematic effects.

3.3.9 Other variables

There is one previously known γ Doradus star V1132 Cas (Table 5 at CDS) for which we confirm the period of 0.626 days (Wyrzykowski et al. 2002). As γ Dor stars have masses of $1.5 - 1.8M_{\odot}$ and are of luminosity type IV–V (Aerts et al. 2010), the apparent magnitude of 8.16 mag for V1132 Cas suggests that it is a nearby field star.

There are an additional 80 variable stars that we could not classify due to the lack of spectral or pulsational information (Table 10 at CDS). We find periods for 13 of these unclassified objects (Table 10 at CDS), ranging from 0.5 to 102 days. V1156 Cas and TYC 3695-992-1 have previously determined periods but as the stars are too faint in our data we were unable to confirm them. This applies to many of the other unclassified objects as they are usually fainter. A number of these unclassified stars have also previously been poorly studied.

3.3.10 Further discussion

We present some light curve examples in Fig. 3.4. These phase curves show the difference in scatter for one bright and one faint star for which we managed to find a period. V359 Per is a SPB star with V magnitude of 9.06 and shows a scatter of around 0.02 mag. 2MASS J23163318+6031477 is a fainter β Cep star with V magnitude of 15.188 and shows a scatter of around 0.15 mag. While it is below our limiting magnitude for the NGC 7510 field, the high amplitude of 0.489 mag is enough to detect the period. We did not find any previous variability information on this star from any database, probably due to its low brightness

Fig. 3.5 is an example of irregular or semi-regular behaviour. V504 Per in the upper panel is a Be star with one of the most numerous outburst counts, showing five major outbursts during the observing campaign. OQ Cep in the lower panel is an M7 type star exhibiting SR variation of over four magnitudes during the second observing season, the highest amplitude variation across all our data. We also find a semi-regular period of 385 days, based on the first two seasons, which is comparable to the previous period determination of 370 days (Alfonso-Garzón et al. 2012).

Despite finding variability in previously known objects, our photometric depth does not always allow us to find periodicities to compare with already published values. Saesen et al. (2013) monitored NGC 884 over three observing seasons and found periods for 131 stars in their field. Eight of them match our listed variables and of these, we determined a period for only one object due to our limiting magnitude in the NGC 869/884 field.

We present the amplitude distribution of variable stars in Fig. 3.7. The effective temperatures corresponding to specific spectral types found in the literature are acquired from Tables 7–9 in Currie et al. (2010). In case there was no luminosity class

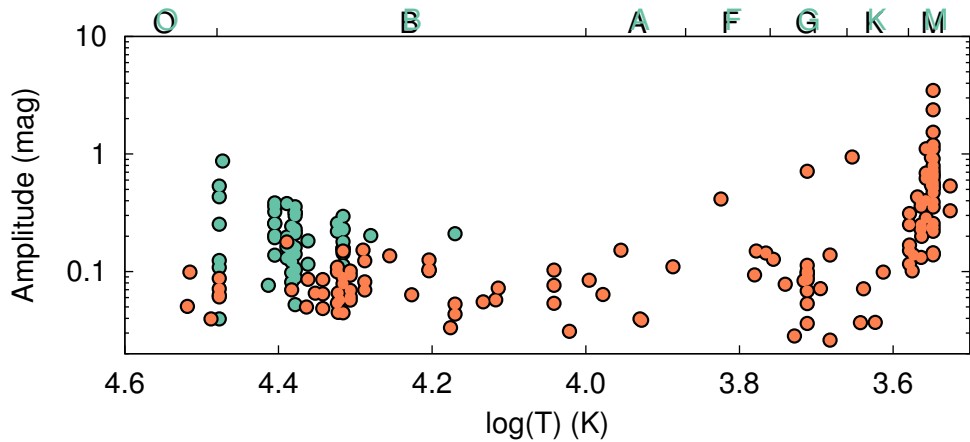


Figure 3.7: Light curve amplitude as a function of effective temperature for all variables except eclipsing binaries. Be stars are marked with green circles and others with orange circles.

determined, their temperature is given as their spectral subgroup mean temperature. The figure shows that the late-type stars have a larger variability amplitude compared to the rest of the selection. Be stars skew the amplitude of hotter stars towards higher values due to their outbursts but as their variability is caused by the circumstellar disk instead of their intrinsic pulsations, they are marked separately with green circles.

To test the suitability of the matches to eclipsing binary and pulsating variable categories, we use the FATS skewness and kurtosis statistics. Eclipses in eclipsing binaries cause the magnitude distribution to have a tail towards the fainter magnitudes and therefore positive skewness values, whereas pulsating stars have a close to zero or negative skewness values due to a more even magnitude distribution. This separates the two groups, eclipsing binaries and pulsating stars, on the skewness-kurtosis plane.

Fig. 3.8 shows the skewness-kurtosis plane for all the eclipsing binaries and pulsating stars we detected in our fields. The pulsating stars clump up on the left side of the diagram and the eclipsing binaries are in a long tail in the right-upper part of the diagram with the two types having a separation around a skewness value of 0.5 as indicated by Graczyk & Eyer (2010). The collection of binary stars up to a skewness value of 1 consists of ellipsoidal variables that show sinusoidal light curves similar to other pulsating stars but are a little more skewed due to irregularities in the uneven maxima of two consecutive periods. The open circles represent our binary candidates (where no orbital periods were found) and they follow the skewness-kurtosis trend of the other binaries.

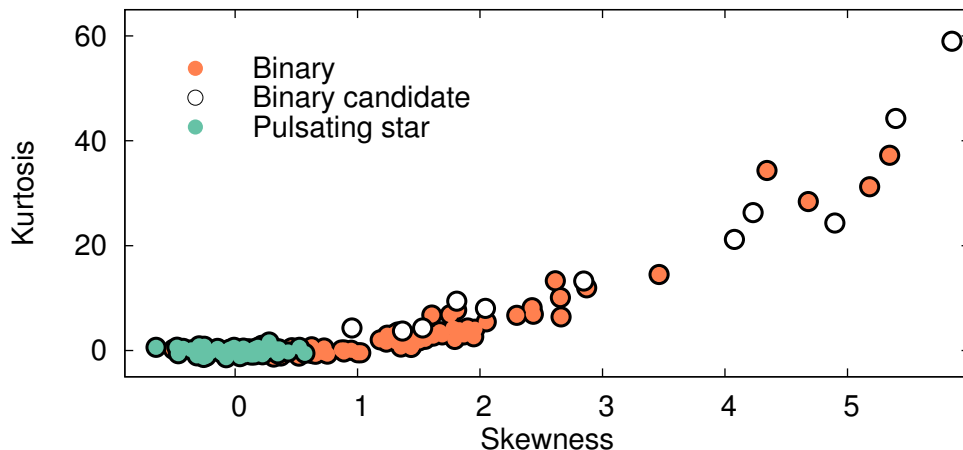


Figure 3.8: Skewness-Kurtosis diagram for the eclipsing binaries (orange points) and pulsating variables (green points). Binary candidates are open circles, following the skewness-kurtosis trend of other binaries.

Although the initial aim was to study the relation between the variability of massive stars and their age, the low amount of the variable stars having a cluster membership probability over 50% makes it statistically infeasible as the ages of most stars could not be determined. In order to look for any correlations, we separated the stars into groups based on their variability type and spectral classifications. But from the remaining 53 cluster members in 8 different classes, we did not find any correlation between the age of the star and any light curve feature from FATS. Fortunately, following Wright et al. (2015), stellar ages for most stars could be calculated with enough precision when combined with the upcoming Gaia distance measurements. We will revisit the problem when stellar ages for massive stars are more readily available.

3.4 Cluster membership analysis

We determined cluster memberships from the cluster membership probabilities of individual objects in Milky Way Star Clusters Catalogue (MWSC) (Kharchenko et al. 2013). Omitting eclipsing binaries, 35 out of the 275 intrinsically variable stars were found to be probable cluster members. This makes the total cluster membership fraction for variable stars less than 13% (membership fractions for individual types are given in Table 3.3). This cluster membership fraction amongst our mostly massive variable stars seems a little low when considering that the spatial concentration of

massive stars should be highest in young open clusters and OB associations. Therefore, we decided to study this in more detail.

Using a limiting magnitude of 14 mag that is close to the limiting magnitude of our observations, we find a total of 21 792 stars around our observed clusters in the MWSC database. Applying the same membership criteria as we did with our variable stars (kinematic probability ($P_{\text{kin}} > 50\%$) and photometric probabilities ($P_{\text{JKs+PJH}} > 100\%$), we find that 11% of all those stars are cluster members. Thus the cluster membership fraction among variable stars is comparable to all of the stars around clusters according to the MWSC.

One of our goals in monitoring stellar clusters of different ages was to study massive stars in various evolutionary phases. To find independent stellar ages, we need accurate membership information for these stars. To this end, we compared MWSC catalogue to other works to test the reliability of their cluster membership estimations. Wright et al. (2015) studied 167 probable cluster members in the Cygnus OB2 association. Matching their 167 cluster members with MWSC database, we find that out of 155 matched stars, only 51 are probable cluster members according to MWSC.

The DAML02 database (Dias et al. 2002) also includes membership probabilities for stars around clusters although their sample size is much smaller than in MWSC. For example, in Berkeley 87 open cluster DAML02 has 157 nearby stars whereas MWSC has 23 567. Matching the two data sets, we find 141 common stars. For this sample, DAML02 gives a membership fraction of 72% (membership probability over 50%) whereas MWSC gives a fraction of 29%. This shows that MWSC underestimates the cluster membership fraction compared to other works. But as it is the only database that covers most of our observed stars, we were obliged to use it for its completeness.

In order to find an upper limit to the cluster membership fraction, we studied the spatial distribution of variable stars in the plane of the sky and measured how variable stars are positioned around stellar clusters. For each star, we calculated the relative distance to the centre of its closest cluster $d' = d/r_C$, where d is the angular distance and r_C is the angular cluster radius from MWSC. This cluster radius is defined as the distance from the cluster centre to where the surface density of stars becomes equal to the average density of the surrounding field. Based on these distances, we calculated the probability densities of finding a star at a certain relative distance from the centre of any cluster. We used the bootstrapping technique to get the probability density of all stars with 99.7% (3σ) confidence limits.

The resulting probability density functions (PDF) can be seen in Fig. 3.9. Panel (a) represents the combined distribution of α Cyg, β Cep, Be, SPB, Cepheid, γ Doradus, Wolf-Rayet and late-type variables. This distribution shows that there are rela-

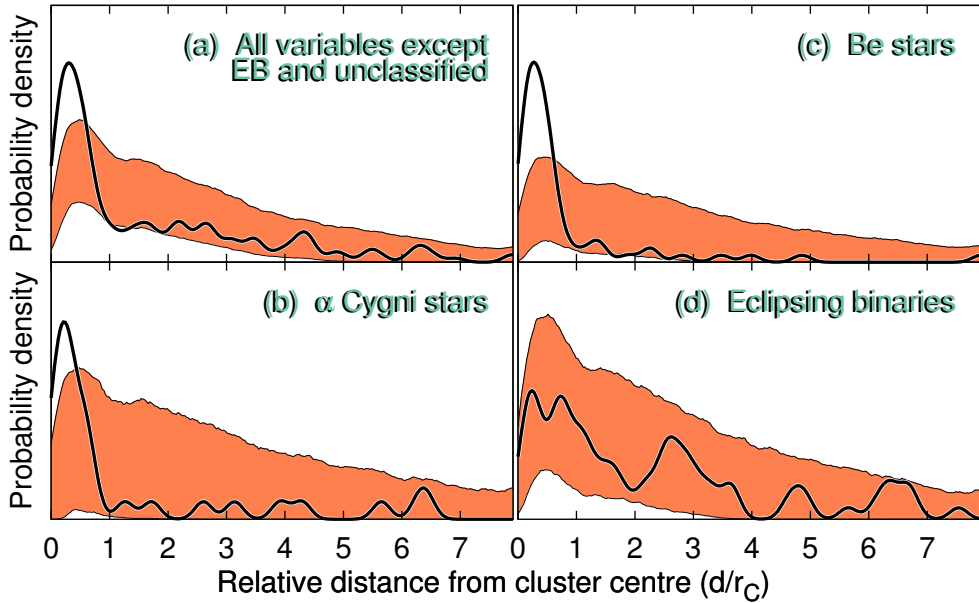


Figure 3.9: Probability density of variable stars at relative distance from the cluster centre. The coloured area represents the 99.7% confidence limits calculated from all stars in our fields. The solid line is the probability density calculated only from the labelled types of variables.

tively more variable stars inside one unit of cluster radius than there are non-variable stars (represented by the coloured area). Panels (b) and (c) show the PDF for α Cygni and Be type stars, respectively. They both display the same signal as the combined distribution, albeit the 3σ confidence area is larger due to smaller sample size. The PDF on panel (d), on the other hand, consists of eclipsing binaries and shows no deviation from the 3σ level. This means that eclipsing binaries have no positional preferences in relation to the clusters. As the variability of binaries is not intrinsic, we omitted them together with unclassified variables from panel (a).

The distribution of all stars shows a maximum at around $0.5 r_C$ with the width of the excess around $1 r_C$ which is to be expected from the definition of the cluster radius. The maximum of our observed variable stars in the plane of the sky is at around $0.3 r_C$, meaning that the stars in the core of the clusters are more likely variable than the stars at the edges of the clusters.

Integrating the PDF of variable stars to one cluster radius, we find that 35% of variable stars are located inside the clusters. As we studied the spatial distribution in the plane of the sky, this can only be the upper limit of the cluster membership

fraction due to fore- and background object contamination.

These examples indicate that the cluster membership probabilities in MWSC might be too strict and thus the membership fraction of 13% amongst our variable stars is underestimated and can go as high as 35%. We did not use DAML02 database for cluster memberships, as their sample size is much smaller and did not include many of our variable stars. But luckily, the reliability of membership probabilities will improve with the arrival of Gaia's more accurate distance, proper motion and radial velocity data as it measures even the brightest of sources in our fields (Gaia Collaboration et al. 2016).

CHAPTER 4

PERIOD CHANGE OF SELECTED MASSIVE BINARIES

The previous chapter described our obtained catalogue and gave a general overview of the type of variable stars we found. But one of the reasons to obtain the full light curve database was to analyse specific objects in more detail. For this, we chose to study the period change of eclipsing binary systems in Cygnus OB2 region.

As mentioned in chapter 1.1, up to 90% of massive stars can reside in multiple star systems. Massive binary systems and their binarity fractions have been studied in various environments for many decades (eg. Garmany et al. 1980; Abt et al. 1990; Duchêne et al. 2001). As stellar multiplicity is caused by the star formation process, determining the frequency and characteristics of multiple star systems can serve as a posteriori tests for star formation theories (Duchêne & Kraus 2013). Binary systems can also give us more insight in the mass loss of massive stars and their evolution in relation to that.

Mass loss in binary systems mostly comes from the mass transfer via Roche-lobe overflow (RLOF) when the primary star's photosphere crosses the inner Lagrange point and starts to exchange mass with its companion (Smith 2014). Mass loss via RLOF exceeds the mass loss via stellar winds and rotation. Mass transfer rates from RLOF depend inversely proportionally on the mass ratio $q = M_2/M_1$, ($q \leq 1$), on the initial orbital separation and it is much more rapid when the donor is a post-main-sequence star compared to it being a main-sequence star (Lauterborn (1970)). While RLOF is happening during a main-sequence phase, mass-transfer rates lessen as the orbit widens until q approaches unity. While the mass is transferred, the mass centre of the interacting binary system shifts towards the mass-receiving star. As a result of the conservation of angular momentum, this mass transfer causes a change in the system's orbital period: the period increases while the mass is transferred to the more massive star, and vice versa. The period also increases when mass is lost from the system through stellar winds.

Thus, mass loss in a binary system can be evaluated from the change in their orbital period. It is possible to measure mass-loss rates from stellar winds and from mass transfer between the binary components (Singh & Chaubey 1986).

Period change (\dot{P}) in binary systems has been commonly evaluated by measuring the times of minimum of the primary eclipses and then comparing these times to the calculated ephemerides for the eclipses. The period change value is then acquired by fitting a polynomial model through the observed minus calculated ($O - C$) data points (Lohr et al. 2012). There are automated codes to extract $O - C$ diagrams from high cadence data (eg. Liakos 2015; Tezcan et al. 2015) but they do not work well with

archival data where measurements have a much lower cadence.

Instead of using the $O - C$ diagrams, there is an alternative method to estimate period change values – by fitting the data to parametrised phenomenological model curves (Mikulášek 2015). This method requires empirical or calculated model phase curves with free parameters for period and period change values. These parameter values can then be found by minimising the difference between the data and the model curves. One upside to this method is that, instead of only the times of eclipse minimum, all of the available data can be used to constrain the parameters.

To study the period change in our observed massive binaries, we developed our own Bayesian parameter estimation method based on model curve fitting. The idea was to analyse available radial-velocity and photometric data of selected binaries by fitting a set of parameters to all of the data simultaneously. As our campaign was only three years long, we had to incorporate literature data to increase the time base and thus improve the accuracy of parameter estimation.

The time base is important in period change studies because a constant change in period introduces a gradual shift in eclipse timings for each consecutive orbit. This causes a measurable cumulative phase shift over many orbital periods. The longer the time base, the more apparent the shift becomes. So having data sets that have been measured widely apart in time, increases the accuracy of the period change assessments.

Figure 4.1 illustrates the cumulative effect of the period change for Schulte 5 with two different data sets that were observed 45 years apart. These phase curves were generated using a constant period of 6.59799 days and a common epoch of periastron. Both of the datasets have been vertically shifted to mean zero magnitude. The visible phase shift is due to the period change during the 2490 orbits that have occurred in between the data sets.

We concentrated our work on eclipsing binaries from the Cygnus OB2 region. The stellar association Cygnus OB2 is one of the most massive and richest associations known in our Galaxy, containing at least 60 O-type stars (Negueruela et al. 2008). Determined from the stellar evolution models, the age of the cluster is found to be 1–7 Myr (Wright et al. 2015). It is a dynamically young sub-structured and unbound association that is located in the molecular cloud complex Cygnus X, and its total estimated mass is $(1.6 \pm 0.3) \times 10^4 M_{\odot}$ (Wright et al. 2014). We chose Cygnus OB2 because of the amount of previously published data for massive binaries in that region. As we wanted to incorporate radial-velocity data with photometric data, we based our target selection on the Cygnus OB2 Radial Velocity Survey (RVS) (Kiminki et al. 2007, 2008, 2009, 2012; Kobulnicky et al. 2014).

In total, there were six suitable eclipsing binaries: A36, MT059, MT696, MT720, Schulte 3, and Schulte 5 that were present in both RVS and our data. We also chose

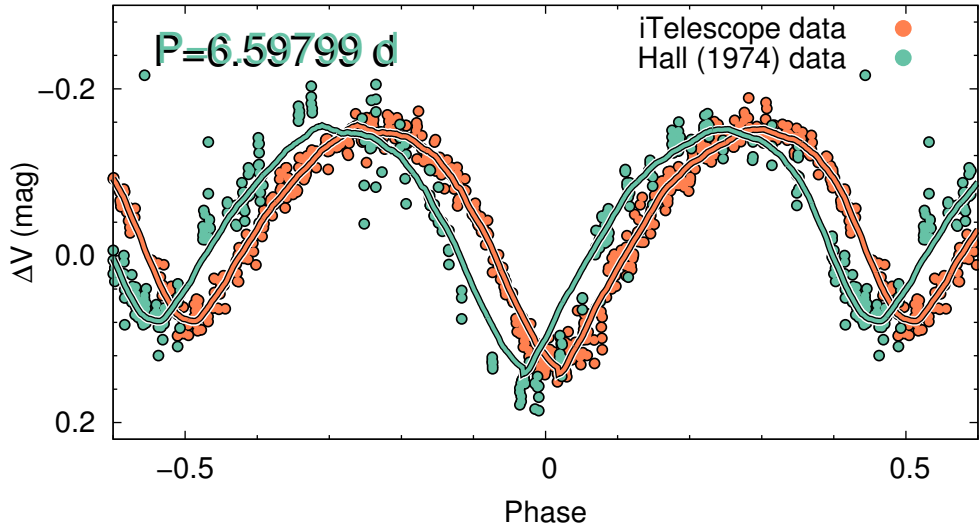


Figure 4.1: V -filter phase diagram of Schulte 5, folded with a constant period. The iTelescope data (orange points) and Hall (1974) data (green points) have been obtained 45 years apart. Solid lines are smoothed empirical light curves. The visible phase shift is due to the cumulative effect of period change (\dot{P}).

an additional massive binary, B17, to complete the set. We used the same naming conventions as in the Cygnus OB2 RVS papers: the MT names from Massey & Thompson (1991), Schulte from Schulte (1958), and A36 and B17 from Comerón et al. (2002). Therefore, some of the names used in this chapter differ from the ones published at CDS because of the different naming scheme. For comparison, we give the same internal ID-s for the Cygnus OB2 field in Table 4.1 and in Table 1 at CDS.

4.1 Compiled data

As mentioned above, we combined new photometric observations with photometry and radial-velocity data from the literature. This work contained two original sets of observational data. The descriptions of the observations and data reduction is described in Chapter 2.

The first photometric data set was the main iTelescope T4 observations in 2011–2013. The analysis was done using aperture photometry measurements, except for MT720, which required PSF photometry due to a neighbouring star contaminating the aperture. To minimise observational errors, we used the nightly mean instrumental differential photometry values instead of single data points. To minimise the

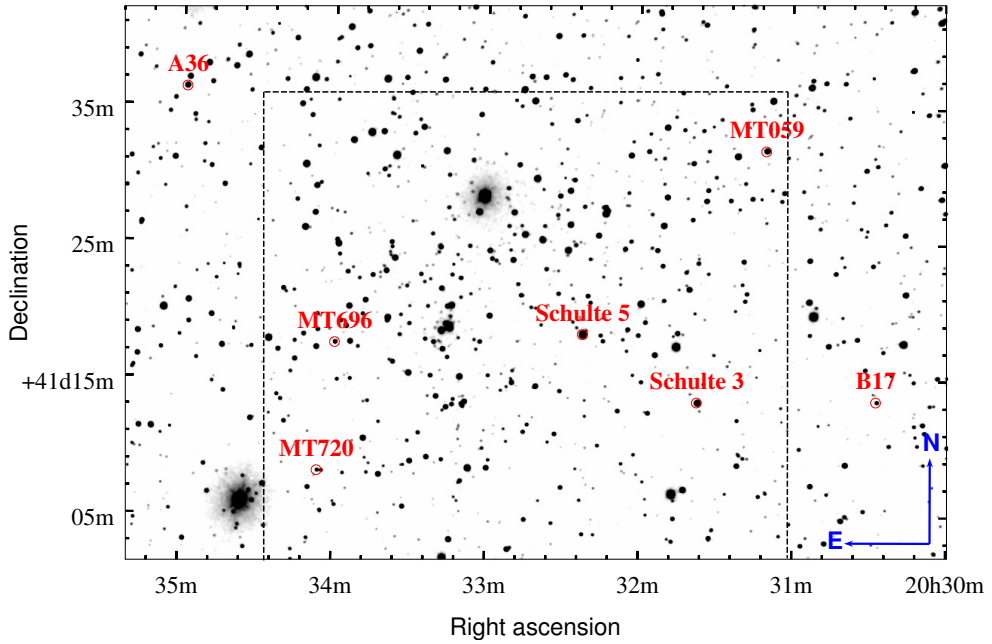


Figure 4.2: Full frame of the Cygnus OB2 region from our first data set (T4) with the selected binaries shown in red. The dashed line indicates the FOV of our second data set (RAITS).

aforementioned scattered light problem, we carefully chose the comparison stars for MT696 and MT720 to be in close proximity on the frame.

The second photometric data set was obtained in 2013–2014 with the RAITS telescope, located in Tõravere, Estonia. Five consecutive exposures were taken with each of the *BVRI* filter during an observation. The CCD frames were reduced and magnitudes were extracted by aperture photometry and PSF photometry using the same method as with the T4 data.

Figure 4.2 shows the FOV of the two telescopes we used to obtain the original data. The FOV of RAITS has about a quarter less total area than the FOV from T4 telescope. Thus, two of the seven programme stars, A36 and B17, fell outside of the RAITS FOV.

In addition to the RAITS and T4 photometric data, we also combined all of the available photometry and RV data from the literature. References to the data that we used for each star are given in Table 4.1. Below, we give a brief overview of these data.

Table 4.1: References to the data used in the period change analysis.

Star	ID	RA Hour	DEC Deg	References
A36	48	20:34:58.8	+41:36:17	1,2,3
B17	158	20:30:27.3	+41:13:25	1,2
MT059	42	20:31:10.5	+41:31:54	1,2,4,5
MT696	117	20:33:59.5	+41:17:35	1,4,6,7
MT720	224	20:34:06.0	+41:08:09	1,4,5
Schulte 3	18	20:31:37.5	+41:13:21	1,2,4,5,8
Schulte 5	5	20:32:22.4	+41:18:19	1,2,4,8,9,10, 11,12,13,14,15,16

References. (1) iTelescope (our data set 1); (2) NSVS^a; (3) Kiminki et al. (2009); (4) RAITS (our data set 2); (5) Kiminki et al. (2008); (6) Souza et al. (2014); (7) Kiminki et al. (2012); (8) IOMC^b; (9) Sazonov (1961); (10) Hall (1974); (11) HIPPARCOS^c; (12) Linder et al. (2008); (13) Miczaika (1953); (14) Bohannan & Conti (1976); (15) Rauw et al. (1999); (16) Wilson & Abt (1951).

^a<http://skydot.lanl.gov/nsvs/nsvs.php>

^b<https://sdc.cab.inta-csic.es/omc/index.jsp>

^c<http://www.rssd.esa.int/SA/HIPPARCOS/apps/PlotCurve.html>

The previously mentioned Cygnus OB2 RVS is a spectroscopic survey of unbiasedly chosen 128 stars of which 83 are B-type and 45 are O-type stars. They have used Keck+HIRES spectrograph (1999–2001), the Lick+Hamilton echelle spectrograph (1999–2000), the WIYN+Hydra spectrograph (2001–2008), and a longslit optical spectrograph with a 2.3 m telescope at the Wyoming Infrared Observatory (2011–2013, 2014 May). The Cygnus OB2 RVS data that we used were attained between 1999 and 2009. The longest data set of 43 measurements (1999–2007) is that for MT059. Schulte 3 and A36 have the fewest observations (~15) and a time base of one year, while MT720 has 32 observations in two years and MT696 has 31 measurements with the time base of 30 days. Unfortunately they did not have any RV data for B17. The only published RV data for B17 that we found (Stroud et al. 2010) is not publicly available and only shown on a figure as a phase curve.

The Northern Sky Variability Survey (NSVS) covers the entire northern sky in an unfiltered optical region, ranging from 8 to 15.5 magnitudes from the Robotic Optical Transient Search Experiment (ROTSE-I) (Woźniak et al. 2004). Except for MT696, 170 data points were obtained within one year (April – December, 1999) for all of our selected stars. The data set for MT720 was available, but due to large photometric errors, the signal of its eclipses was unattainable, and we had to exclude it from our

analysis. The errors for NSVS data sets are typically larger than our own data sets because their data quality is limited by a severe blending that is due to the 14 arcsec pixel size.

The Hipparcos catalogue data (van Leeuwen 2007) are available only for the brightest star in our selection, Schulte 5, because of the limiting magnitude of Hipparcos observations. The available data span over three years, from the end of 1989 to the beginning of 1993, with one hundred broad-band measurements.

The Optical Monitoring Camera (OMC) on board the ESA International Gamma-Ray Astrophysics Laboratory (INTEGRAL) mission consists of $5^\circ \times 5^\circ$ FOV photometric camera observing in the Johnson *V* band (Mas-Hesse et al. 2003). From its launch in 2002, it has observed thousands of variable stars preselected from existing variable star catalogues. The only stars in our selection that have been observed by IOMC are Schulte 3 and Schulte 5. There have been more than 5000 observations made between 2002 and 2009 (which is our longest time series from a single source), and their optical accuracy is roughly on the same level with NSVS photometry.

Souza et al. (2014) have been monitoring MT696 since 2010 in two 5 nm wide filters centred on the continuum and $H\alpha$ (645 and 656 nm, respectively). Their photometric data span over three years from 2010 to the end of 2013 and consist of 105 observations. These data and the RV data of Kiminki et al. (2012) were the only published time series of MT696 at the time of writing Paper II.

For Schulte 5 we have the longest time base, with measurements from 12 different sources. The first published measurements for Schulte 5 are the times of minimum from 1898, although the accuracy of those measurements was doubtful for the authors themselves (Sazonov 1961). During a five-month period in 1952, Miczaika (1953) obtained 36 measurements with a photoelectric equipment on the 32 cm refractor at the Heidelberg Observatory. Hall (1974) observed Schulte 5 photoelectrically for 142 times with a 60 cm Seyfert reflector during the period from 1967 to 1970 using a set of closely matching *UBV* passband filters. Linder et al. (2009) acquired over 300 exposures during a campaign of 14 nights in 1998 with five filters, three of which were centred on different emission-line wavelengths found in various subsets of Wolf-Rayet objects. The other two were centred on line-free areas (around 5057 and 6051 Å). For our period change analysis we chose only the measurements taken with the continuum narrow-band filters because the emission line data also indicate variability that is not directly related to the eclipses of the binary.

RV data for Schulte 5 are available from three sources (Wilson & Abt 1951; Bohannon & Conti 1976; Rauw et al. 1999). All the observations span three years (1946–1949, 1971–1974, and 1994–1997) and consist of 42, 7, and 25 measurements, respectively. Schulte 5 has the longest time base for RV data because it is the only binary in our selection on which more than one RV observation campaign has been

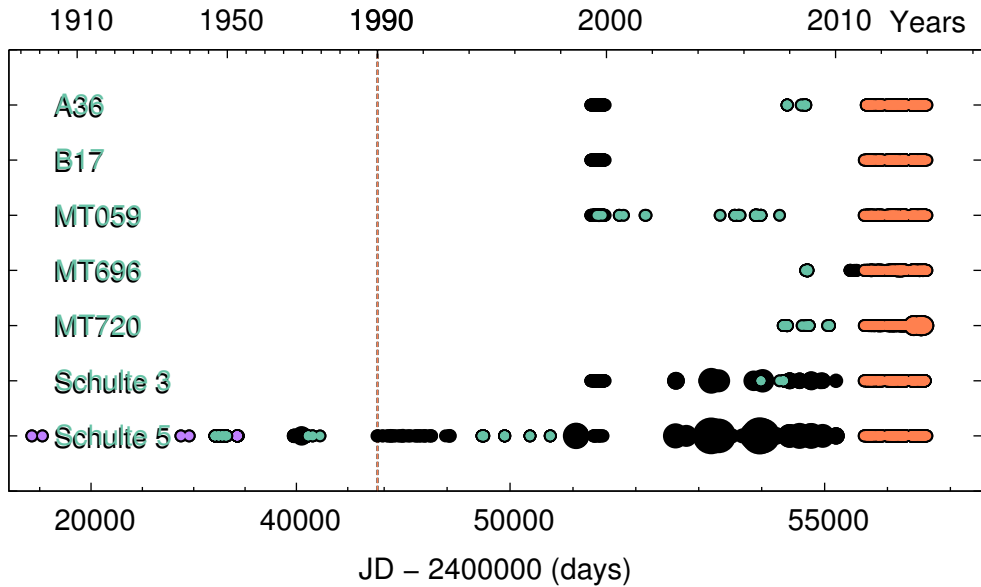


Figure 4.3: Available data shown in time domain with reduced Julian dates at the bottom and calendar years at the top. Point sizes are indicating the number of measurements in a one-day bin. We have changed the scale of the plot in the middle (dashed line) to better show the data available from 1990 onwards. Orange points indicate our photometric data sets, green points are the available RV data, purple points show the times of minimum from Sazonov (1961), and black points are all other available photometric data listed in Table 4.1.

carried out.

All the available data points are shown in Fig. 4.3 to illustrate the time base for each star. It can be seen from the figure that Schulte 5 is by far the most frequently observed star in our selection, while the other massive binaries have scarcely been studied. Our analysis mostly depends on three sources: our own two data sets from 2011 to 2014, NSVS, and Cygnus OB2 RVS. While Schulte 5 has a time base of 116 years, all the other binaries have a time base shorter than 15 years. The long time base for Schulte 5 is an excellent testbed to validate our algorithm for the upcoming 100-year window in time-domain astronomy (Grindlay et al. 2012) that will be available with the digitization of various photographic plate archives.

4.2 Bayesian approach for parameter estimation

The usual method of measuring the period change values is to determine the ephemeris of the eclipses and then fit a polynomial to the observed minus calculated ($O - C$) data points. We used an alternative Bayesian approach of simultaneously fitting all available observational data, light curves, times of minimum, and RV data to the model curves. Instead of only relying on the precise measurements of the times of minimum of the eclipses, we can improve our statistical uncertainties by incorporating additional measurements.

Our method consists of two distinctive steps: acquiring the model curves and then assessing the period (P) and period change (\dot{P}) values that simultaneously fit the data to these curves. We assumed that the shape of the model curves remains constant throughout the whole data series.

For the initial assessment of P , we used our results from the PDM method. This initial period was necessary to fold the photometric and RV data for input to the modelling software. For the modelling we used PHysics Of Eclipsing BinariEs (PHOEBE¹, legacy version 0.31a), a binary modelling software based on the Wilson-Devinney code (Wilson & Devinney 1971). The modelling was carried out using RV data from Kiminki et al. (2008, 2009, 2012); Bohannan & Conti (1976); Rauw et al. (1999) and photometric data from our 2011–2013 data set. The spectral classes for the objects were taken from Kobulnicky et al. (2014), and they were used as an input for the initial temperature (Gray 2001) and mass values (Martins et al. 2005) for the models. The resulting model parameters for masses (M_1, M_2), mass ratio (q), radii (R_1, R_2), temperatures (T_1, T_2), and orbital parameters are presented in Table 4.2.

The phased curves from PHOEBE software were then used as input to the Bayesian inference tool called MultiNest (Feroz & Hobson 2008; Feroz et al. 2009, 2013). The Bayesian parameter estimation method is a Monte Carlo algorithm that calculates the ephemerides of the star as

$$\text{HJD} = \text{HJD}_0 + PE + \frac{1}{2}\dot{P}PE^2, \quad (4.1)$$

where E is the cycle number.

Using a random walk approach, we assessed the values of P and \dot{P} that best fit the data to the model curve. By comparing folded light curves and folded RV curves to the model curves, we obtained the likelihoods of the parameter fits. The less the model and data differ from each other, the higher is the likelihood value. The global maximum of the likelihood posterior is the best fit of the parameters in conjunction with the model curves. We assumed the posterior to be Gaussian, and

¹<http://phoebe-project.org/>

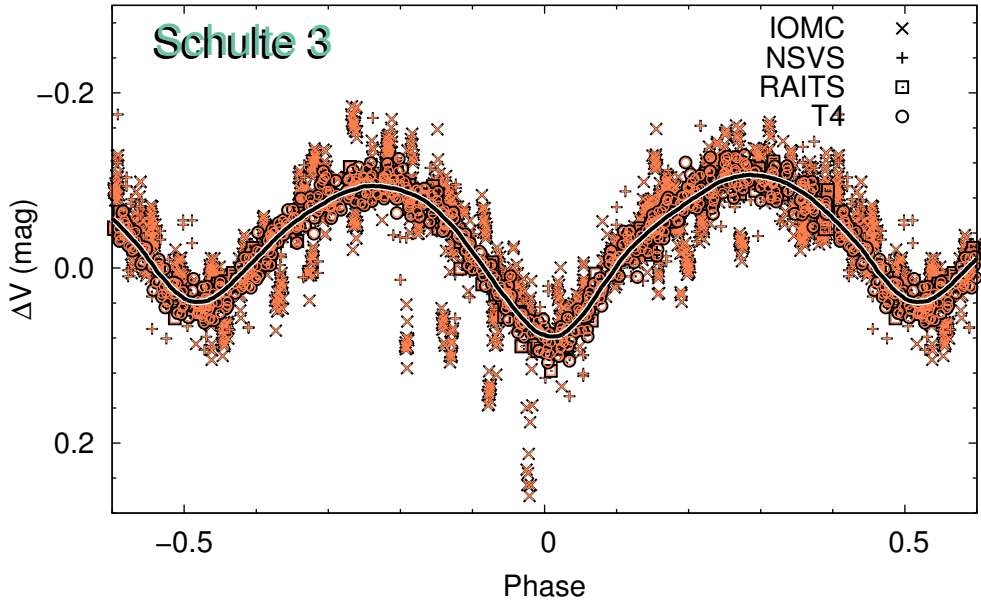


Figure 4.4: Empirical model curve for Schulte 3. The data sets are combined from four different sources. The model is constructed by iteratively sigma clipping the data from a kernel smoothed curve.

thus the parameter fit errors are given as a standard deviation. To minimise the errors, we fixed the value of HJD_0 for every star to the observation time of the faintest data point in the T4 data set.

For the period change analysis, we used one model light curve for all the photometric filters because the fitting of the ephemerides mainly depends on the time domain as opposed to the small differences in eclipse depths from different filters. This was mainly done to minimise the binary modelling required.

To test whether the PHOEBE model phased light curve causes any systematic errors in the period change determination, we constructed empirical model light curves for our selected stars. All the results for P and \dot{P} were obtained using both the PHOEBE model and the empirical model. As there were not enough RV data distributed over the full orbital phase, no accurate empirical RV model curve could be derived.

An empirical model phased curve used for Schulte 3 is given in Figure 4.4. The data consist 2931 photometric measurements from four sources with the largest contribution from IOMC. Measurements have been shifted to a zero mean and a first estimation of the period change has been accounted for using the PHOEBE model.

The empirical model curve was smoothed with a second order polynomial fit in a 0.07 wide kernel. The data were then iteratively sigma clipped with a two sigma cut-off and a new model was made after every iteration.

The errors for each photometric data set were obtained separately as the standard deviation of the difference between the data points and the empirical light curve. The errors for RV data were taken from the respective papers, and the errors for the times of minimum in Sazonov (1961) were given as the timing error of the observations. These errors determined the weight of each data set in the final period change analysis.

Conventionally, $O - C$ diagrams are constructed using only precisely measured photometric times of the eclipses where the times are obtained by continuous monitoring of the selected star during an eclipse. Any RV data are usually completely ignored or only the times of conjunctions are used in the $O - C$ analysis. In our case, however, RV data can be fitted together with any photometric data. This method is especially useful for sparsely covered time series of the eclipses and only approximate times of the minima. This can either be due to observational difficulties or when working with older data that have not been optimised in time domain for this type of studies.

In general, our method can be used for any data coming from all-sky-covering campaigns. They usually provide unevenly spaced observation epochs that make it harder to detect the times of minimum but on the other hand have a long time-series for many objects. Our simultaneous fitting of data with the appropriate weights provides a solution that is not dependent on the measurement errors of any single minimum and also improves the statistical significance of the period assessment because more data points are used. Previous works for finding period change using all of the available data have been carried out for RR_d type stars (Paparo et al. 1998) and for selected eclipsing binaries (Wilson & Van Hamme 2014).

The downside of our method is that one needs the exact model phased light curve and RV curve of the binary to compare the data to. These can be difficult to obtain as every binary has somewhat different phased curves that can only be acquired by binary modelling. But modelling requires both RV and photometric data that is not always readily available. Empirical curves are easier to obtain but they are biased by the uncertainties of the data.

4.3 Parameters for selected massive binaries

We present the binary parameters in Table 4.2 and estimated orbital ephemerides in Table 4.3. We give one-sigma likelihood-estimation uncertainties for P and \dot{P} , formal

Table 4.2: Binary parameters from the PHOEBE modelling software.

Parameter	A36	B17	MT059	MT696
$M_1 (M_\odot)$	22.41 ± 2.96	–	21.23 ± 6.24	14.00 ± 0.81
$M_2 (M_\odot)$	15.32 ± 2.02	–	6.22 ± 1.83	12.67 ± 0.73
q	0.68 ± 0.04	–	0.29 ± 0.01	0.91 ± 0.03
$R_1 (R_\odot)$	16.08 ± 0.27	–	12.51 ± 0.10	5.92 ± 0.09
$R_2 (R_\odot)$	13.48 ± 0.30	–	5.89 ± 0.21	5.63 ± 0.09
T_1 (K) (fixed)	27000	–	38000	32000
T_2 (K)	22924 ± 38	–	18966 ± 98	31070 ± 25
i ($^\circ$)	71.76 ± 0.11	–	68.18 ± 0.13	81.87 ± 0.06
$a (R_\odot)$	39.43 ± 1.45	–	36.34 ± 3.46	16.23 ± 0.24
e	0.01 ± 0.001	–	0.14 ± 0.002	0 (fixed)
ω ($^\circ$)	350	–	189	0 (fixed)
Spectral class	B0Ib+B0III	O7:+O9:	O8V+B	O9.5V+B0V
Parameter	MT720	Schulte 3	Schulte 5	
$M_1 (M_\odot)$	18.52 ± 1.51	32.73 ± 7.04	38.18 ± 5.21	
$M_2 (M_\odot)$	13.19 ± 1.07	17.21 ± 3.70	10.24 ± 1.40	
q	0.71 ± 0.03	0.53 ± 0.05	0.27 ± 0.03	
$R_1 (R_\odot)$	9.93 ± 0.59	18.40 ± 0.41	27.16 ± 0.34	
$R_2 (R_\odot)$	8.47 ± 0.38	13.50 ± 0.34	15.15 ± 0.20	
T_1 (K) (fixed)	29800	41200	36100	
T_2 (K)	19202 ± 80	29702 ± 37	23681 ± 112	
i ($^\circ$)	71.09 ± 0.28	57.47 ± 0.09	64.65 ± 0.05	
$a (R_\odot)$	35.52 ± 0.78	43.72 ± 2.63	53.90 ± 2.08	
e	0.34 ± 0.005	0.015 ± 0.001	0 (fixed)	
ω ($^\circ$)	298	0	0 (fixed)	
Spectral class	B0-B1V+B1-B2V	O6IV:+O9III	O7Ianf+Ofpe/WN9	

Notes. Parameters in this table are the primary and the secondary component masses (M_1 , M_2), the mass ratio M_1/M_2 (q), the primary and the secondary component radii (R_1 , R_2), the primary and the secondary component temperatures (T_1 , T_2), the inclination angle (i), the semi-major axis (a), the eccentricity of the system (e), the argument of periastron (ω), and the binary spectral classes that are taken from Kobulnicky et al. (2014). The temperature for the primary component was fixed according to the spectral class (Gray 2001).

Table 4.3: Orbital ephemerides from the Bayesian parameter estimation algorithm.

Parameter	A36	B17	MT059	MT696
HJD ₀	56282.520	56383.961	56535.672	56181.719
P_{emp} (d)	4.676040(21)	4.021767(38)	4.852281(39)	1.46918869(22)
\dot{P}_{emp} ($\times 10^{-8}$)	3.8 ± 1.3	1.1 ± 1.6	-4.7 ± 1.7	-0.37 ± 0.08
P_{model} (d)	4.676040(19)	4.021719(39)	4.852265(26)	1.46918857(24)
\dot{P}_{model} ($\times 10^{-8}$)	3.9 ± 1.3	-0.8 ± 1.7	-3.6 ± 1.2	-0.46 ± 0.08
	MT720	Schulte 3	Schulte 5	
HJD ₀	56585.602	56264.633	56182.906	
P_{emp} (d)	4.3619709(98)	4.745964(15)	6.597989(24)	
\dot{P}_{emp} ($\times 10^{-8}$)	8.1 ± 2.1	-1.5 ± 1.0	1.16 ± 0.03	
P_{model} (d)	4.3617773(96)	4.745998(29)	6.5980120(30)	
\dot{P}_{model} ($\times 10^{-8}$)	-11.7 ± 3.2	0.0 ± 0.9	1.30 ± 0.03	

Notes. We list the epoch of periastron (HJD₀), period (P), and the rate of period change (\dot{P}). The parameters P and \dot{P} are calculated using empirical (emp) and PHOEBE (model) phased light curves. HJD₀ is fixed in both cases.

errors from PHOEBE for T_2 , i , e and calculated formal errors² for M_1 , M_2 , R_1 , R_2 and a .

The binary parameters (Table 4.2) were obtained with the PHOEBE software where RV data were fitted alongside photometric data. The binary parameter values were not fine-tuned for each individual star as they are a by-product of acquiring model phase curves. The parameter modelling is degenerate between many of the parameters, which means that adding high-resolution spectra for precise temperature and spectral-type measurements would constrain the models further.

There are no parameters for B17 because the only available RV data from Comerón et al. (2002) are published as a phased graph with no available ephemerides. Without RV data, no orbital parameters or masses can be modelled accurately. In addition, the RV data for MT059 are only available for the primary component, and thus the model binary parameters are only one of the possible parameter fits because of the degeneracy of the mass ratio. All the fits of our data to the acquired binary models are presented in Figs. 4.6 – 4.11.

Table 4.3 lists the parameter estimations for orbital ephemerides. The period values were calculated using both empirical (emp) and PHOEBE (model) phased light curves. The epoch of periastron (HJD₀) was fixed to the observation time of the faintest data point in the T4 data set. The given period (P) is calculated as the length of a period that follows right after the HJD₀ date. Finally, the rate of period

²http://phoebe-project.org/1.0/docs/phoebe_manual.pdf

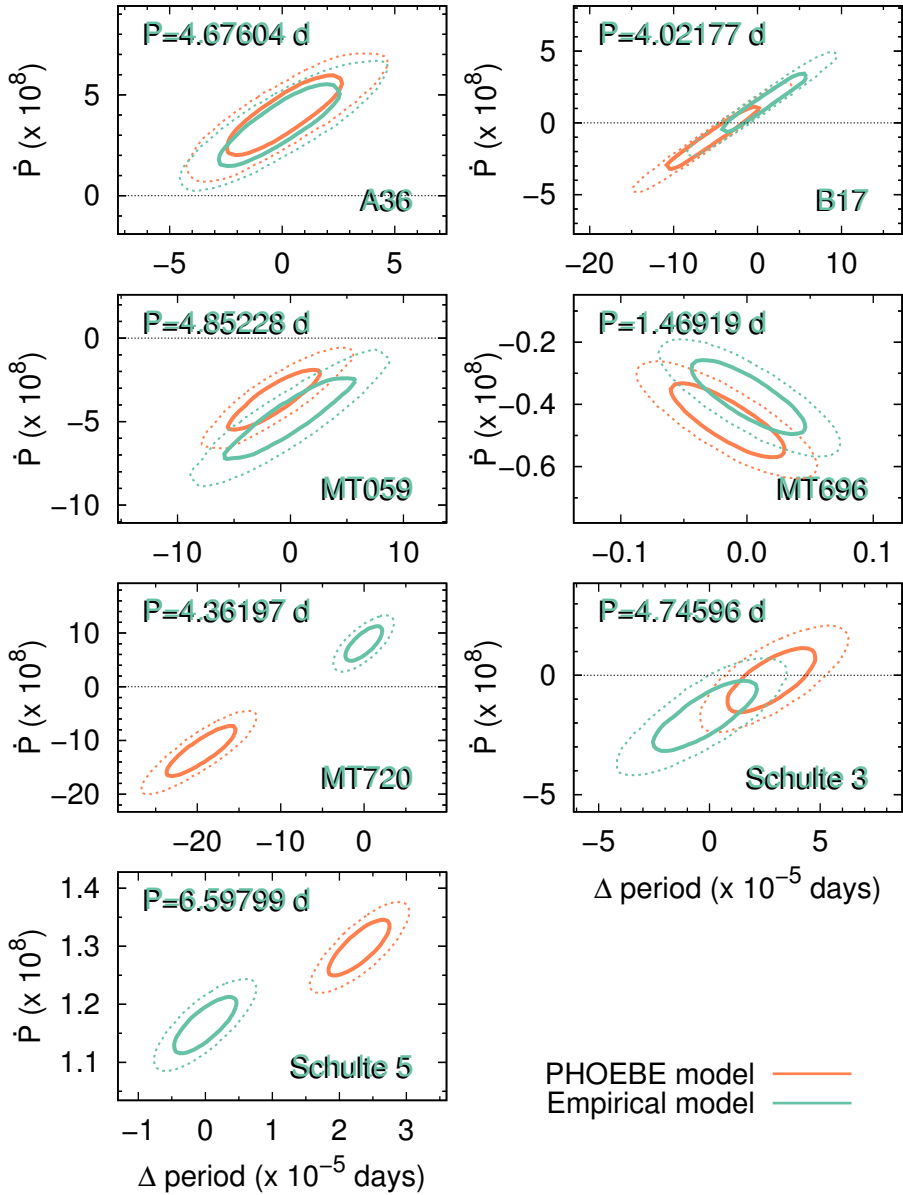


Figure 4.5: Parameter estimates for period and period change. Periods are given as a difference from the P_{emp} value (see Table 4.3). The green line represents the results for an empirical phase model, and the orange line represents the results for the calculated PHOEBE phase model. The inner contour is the 68% and outer dashed contour is the 95% confidence level.

change (\dot{P}) shows how much the period value changes with every consecutive cycle. A negative value means that the system is speeding up (the period is shortening) while a positive value means that the opposite is true.

Figure 4.5 shows the parameter P and \dot{P} estimates for both the empirical and the PHOEBE model folded light curves. The shape of the resulting parameter estimation likelihood cloud shows the amount of degeneracy of the two parameters as well as the uncertainties in the parameter estimations. As a result of the degeneracy of P and \dot{P} , the given uncertainties for these parameters are determined by marginalised distributions. If we had also fitted the HJD_0 value, the results would have been degenerated between all three of those parameters. Therefore, the value of HJD_0 was fixed to reduce the systematic errors of the two fitted parameters. The distance between the locations of the parameter estimation likelihood clouds shows the systematic errors that arise from different model curve shapes, and the sizes of those clouds show the statistical errors. One has to pay extra attention to the modelling of the folded light curves because they can introduce some systematic errors compared to the true light curve.

Appendix A in paper II describes the model fits for each of the dataset separately. The visual comparison between the data and the models can be used to assess the applicability of the final resulting parameters.

The results between empirical and PHOEBE folded light curve models in Fig. 4.5 look consistent for most cases. The posteriors for Schulte 5 seem to disagree with each other, but because the uncertainties in the parameter estimation are so small, they actually agree quite well. The resulting uncertainties for Schulte 5 are very small because its time base is the longest of our selected objects. The results for MT720 show a very large systematic error between the two models. This is due to the relatively short time base as well as the difference between the shape of these two model folded light curves.

For four stars, we detect a non-zero period change values. The strongest evidence for period change is found for Schulte 5, while MT696 also shows period change at three-sigma confidence level and A36 and MT059 at two-sigma confidence level. MT059 and MT696 exhibit a negative period change, while A36 and Schulte 5 have a positive period change. Our calculations for B17, MT720, and Schulte 3 do not indicate any change in their periods.

The approach in this work does not take into account any cyclic patterns of period changes that may come from the light travel time effect through the presence of a third body in the system or from stellar magnetic activity cycles (Liao & Qian 2010). The data for most of our selected stars have a relatively short time base compared to the typical periods of the third orbiting body or magnetic cycles, therefore we have opted to exclude a cyclic pattern as a free parameter because this would artificially

introduce a new degeneracy to the fit. Any cyclic patterns in the period change are sources of possible errors in our results. Neither did we take into account the apsidal motion (Sterne 1939) in binaries with eccentric orbits (MT720 and MT059). The apsidal motion would visibly alter the shape of light and RV curves, but we did not see this in our data sets (see Appendix A in paper II).

We then used our estimated period change values to derive mass-loss rates for two distinctive cases. For an assumed conservative mass exchange between the two components with constant system orbital angular momentum and system mass, the mass transfer rate can be calculated as case I in Singh & Chaubey (1986):

$$\dot{M}_1 = \frac{1}{3} \frac{M_1 M_2}{M_1 - M_2} \frac{\dot{P}}{P}. \quad (4.2)$$

We can also assume that the mass is lost solely through stellar wind (case IV in Singh & Chaubey 1986):

$$\dot{M}_1 = -\frac{1}{2}(M_1 + M_2) \frac{\dot{P}}{P}. \quad (4.3)$$

These equations measure the amount of mass arriving (mass-gain rate) or leaving (mass-loss rate) the primary component. The mass transfer Eq. (4.2) shows that a negative period change value, quickening of the period, indicates that the mass is being transferred from the primary to the secondary component and a positive value indicates the opposite. Equation (4.3) shows the amount of mass being lost from the primary component due to stellar wind. This is only written for the primary component as a more massive star is usually more evolved and exhibits stronger stellar wind.

Table 4.4 summarises the primary component mass-loss rates calculated for both conservative mass exchange as well as mass loss through stellar wind using the two acquired period change values of \dot{P}_{emp} and \dot{P}_{model} . Equations (4.2) and (4.3) are for the idealised occurrences where no other effect interferes with the period-change value. The primary component mass-loss values in Table 4.4 represent isolated cases through either conservative mass exchange or stellar wind. They do not indicate the real values of the mass loss as in reality the mass loss is a combination of different factors. To constrain the mass-loss values further, some additional method to find the strength of stellar wind (radio observations or analysis of the stellar-wind-induced spectral line profiles) has to be included.

In the next sections we compare our results to the previous findings and present some of the problems that we came across.

Table 4.4: Mass transfer and mass loss through stellar wind rates for our selected stars. No mass loss through stellar wind is given for the negative \dot{P} value as this would indicate a positive mass loss from the primary. The errors are calculated using the P , \dot{P} , M_1 , and M_2 uncertainties. The errors for MT696 are large as a result of the similar companion masses.

Star	used \dot{P} value	\dot{M}_1 mass transfer ($10^{-6} M_{\odot}\text{yr}^{-1}$)	\dot{M}_1 stellar wind ($10^{-6} M_{\odot}\text{yr}^{-1}$)
A36	\dot{P}_{emp}	48 ± 19	-56 ± 19
	\dot{P}_{model}	50 ± 21	-58 ± 19
B17		no mass estimates	no mass estimates
MT059	\dot{P}_{emp}	-10.5 ± 4	–
	\dot{P}_{model}	-8.0 ± 3	–
MT696	\dot{P}_{emp}	-41 ± 160	–
	\dot{P}_{model}	-50 ± 254	–
MT720	\dot{P}_{emp}	104 ± 30	-10.7 ± 4.2
	\dot{P}_{model}	-149 ± 45	–
Schulte 3	\dot{P}_{emp}	-13.9 ± 10.2	–
	\dot{P}_{model}	0.001 ± 8.8	–
Schulte 5	\dot{P}_{emp}	3.0 ± 0.2	-15.6 ± 0.7
	\dot{P}_{model}	3.4 ± 0.2	-17.4 ± 0.8

Notes. The two period change values (\dot{P}_{emp} and \dot{P}_{model}) for each star are given in Table 4.3. B17 has no calculated mass-loss rates as there are no mass estimates.

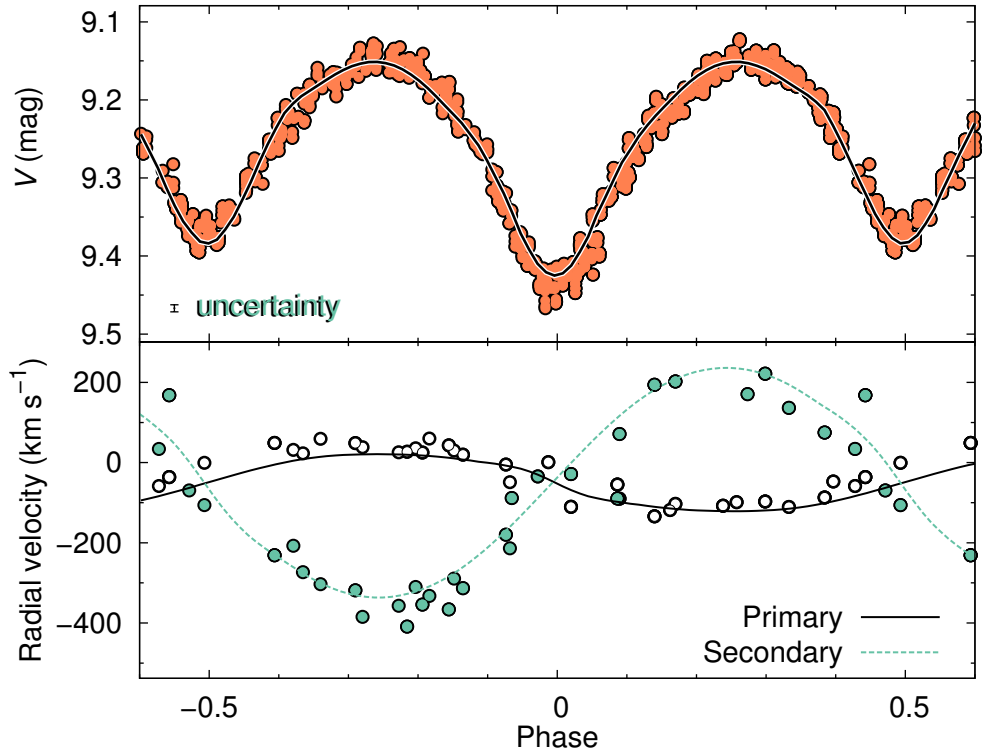


Figure 4.6: Binary modelling for Schulte 5 with the PHOEBE software. The upper panel shows our photometric iTelescope data (data set 1) with the model curve (solid line), and the lower panel shows combined radial-velocity data from Bohannan & Conti (1976) and Rauw et al. (1999) with the model curves for both primary and secondary components.

4.3.1 Schulte 5

Schulte 5 (V729 Cyg, BD +40° 4220) is an eclipsing binary of two O-type supergiants (Kobulnicky et al. 2014). There is also evidence for a third non-thermal radio source around the binary with a period of 6.7 years (Kennedy et al. 2010; Cazorla et al. 2014).

Linder et al. (2009) assumed the orbital solution from Rauw et al. (1999) to derive the absolute masses of the components ($M_1 = 31.9 \pm 3.2 M_\odot$ and $M_2 = 9.6 \pm 1.1 M_\odot$). Our modelling reveals similar masses for the components, $38.2 \pm 5.2 M_\odot$ and $10.2 \pm 1.4 M_\odot$, respectively.

Martins et al. (2005) have calculated a grid of models for O type stars using CMFGEN (Hillier & Miller 1998) atmosphere code, and they include theoretical spectroscopic masses for them. For the primary component of spectral type O7I, the spectroscopic mass would be $M_{\text{spec}} = 40.91 M_{\odot}$. The authors note that one should take care in dealing with their spectroscopic modelled masses as the uncertainty may be as high as 35 to 50%. Nevertheless, our resulting mass for the primary is closer to the theoretical value than to the result from Linder et al. (2009).

We chose Schulte 5 (Fig. 4.6) as a testbed for our period change study because the eclipse-timing method for period change as well as the mass-loss rates have been studied on multiple occasions. Previous assessments for the mass-loss rates from stellar wind were derived by Persi et al. (1990) from infrared observations $\dot{M} = 2.5 \times 10^{-5} M_{\odot}\text{yr}^{-1}$, by Conti & Howarth (1999) combined with multi-frequency radio observations $\dot{M} = (3.7 \pm 1.3) \times 10^{-5} M_{\odot}\text{yr}^{-1}$, and by Linder et al. (2009) using the period change rate of observed times of minimum $\dot{M} = (2.1 \pm 0.6) \times 10^{-5} M_{\odot}\text{yr}^{-1}$.

Following the calculation from Eq. (4.2), Linder et al. (2009) found a mass-transfer rate $\dot{M}_1 = (4.7 \pm 1.5) \times 10^{-6} M_{\odot}\text{yr}^{-1}$, which they argued against because this value was lower than expected from the previous assessments derived from the infrared and radio data. Using the masses obtained from our PHOEBE model and the P and \dot{P} from our Bayesian parameter estimation method, we also obtain similar mass-loss rates of $\dot{M}_1 = (3.0 \pm 0.2) \times 10^{-6} M_{\odot}\text{yr}^{-1}$ and $\dot{M}_1 = (3.4 \pm 0.2) \times 10^{-6} M_{\odot}\text{yr}^{-1}$ depending on the applied period change value. This difference between the Linder et al. (2009) \dot{M}_1 value and our values is mostly due to the difference in the period change values. The value from Linder et al. (2009), $\dot{P} = (1.9 \pm 0.5) \times 10^{-8}$, is higher than our obtained value of $\dot{P}_{\text{emp}} = (1.16 \pm 0.03) \times 10^{-8}$ and thus their mass-loss rate is also slightly higher. Our period change value is probably more accurate because we have a time base that is longer by over 40 years.

Yaşarsoy & Yakut (2014) found a period change of $P/\dot{P} \sim 9.4 \times 10^5$ from eclipse timings by acquiring new observations on 65 observing nights from 2010 to 2011 in Bessel *UBVRI* bands. With their given period of $P = 6.597981$ d, we can calculate $\dot{P} = 7.01913 \times 10^{-6}$, which is much higher than the value of $\dot{P} = (1.16 \pm 0.03) \times 10^{-8}$ that we obtained. It may be possible that their given P/\dot{P} value is in the units of years instead of days as one might assume from their period value. In this case, the value $\dot{P} = 1.92305 \times 10^{-8}$ agrees with the value of \dot{P} from Linder et al. (2009). They also modelled the masses of the primary ($31.6 \pm 2.9 M_{\odot}$) and secondary ($8.8 \pm 0.3 M_{\odot}$) component. If we use their data for calculating mass loss through mass transfer, we obtain $\dot{M}_1 = 4.325 \times 10^{-6} M_{\odot}\text{yr}^{-1}$, which is very similar to the mass-loss rate that Linder et al. (2009) obtained, but differs from ours due to the value of period change and obtained component masses.

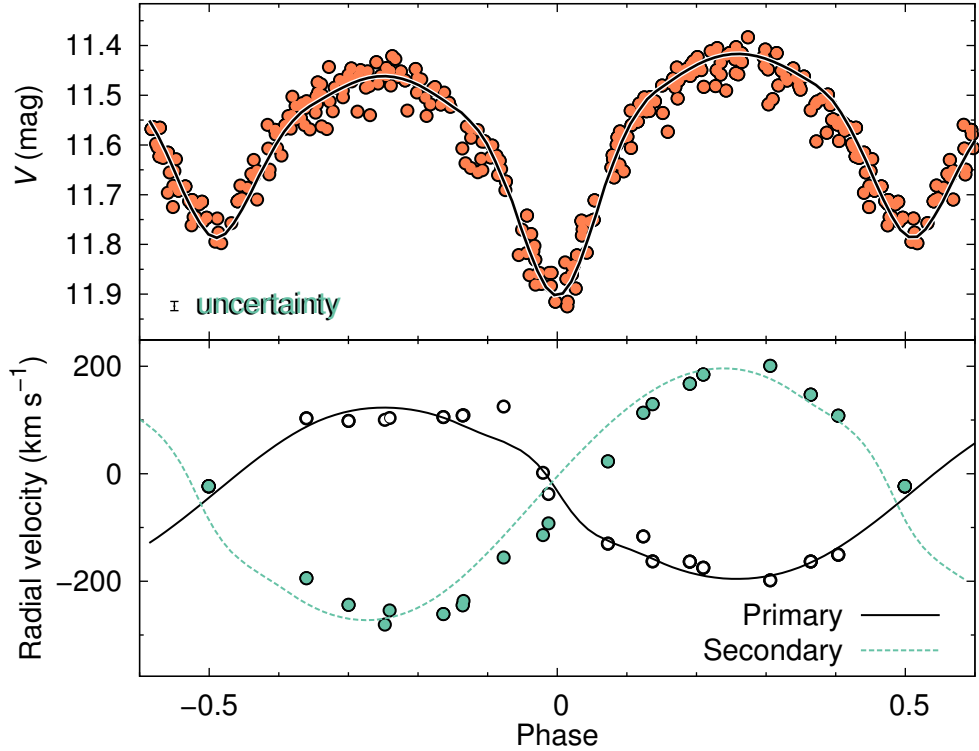


Figure 4.7: Binary modelling for A36 with the PHOEBE software. Designations of lines, labels, and photometric data set are the same as in Fig. 4.6. Radial-velocity data are taken from Kiminki et al. (2009).

We find that the mass-loss rate through stellar wind (Eq. (4.3)) for Schulte 5 is $\dot{M}_1 = (-1.56 \pm 0.07) \times 10^{-5} M_{\odot}\text{yr}^{-1}$ or $\dot{M}_1 = (-1.74 \pm 0.08) \times 10^{-5} M_{\odot}\text{yr}^{-1}$ depending on the \dot{P} value, which are comparable to the result of Linder et al. (2009) ($\dot{M}_1 = (-2.1 \pm 0.6) \times 10^{-5} M_{\odot}\text{yr}^{-1}$). The previous mass-loss rate assessments of the stellar wind from radio and infrared observations have confirmed the value to be close to our finding. This indicates that the period change of the system is caused by the mass loss from stellar wind of the primary component instead of the mass transfer from the secondary component.

4.3.2 A36

A36 (Fig. 4.7) was first named in a paper by Comerón et al. (2002), who listed it as a possible binary. The eclipsing nature of A36 was found from NSVS data (Otero

2008; Hoffman et al. 2009) and it is classified as an Algol/ β Lyrae candidate. Kiminki et al. (2009) determined the spectral type as a B0Ib+B0III system on the basis that the light curve and spectra show similar component temperatures and luminosities with differences in specific lines.

Our calculated mass ratio for the binary system is 0.66 and is within error limits of the Kiminki et al. (2009) estimation of 0.70 ± 0.06 . They give a period of $P = 4.6752 \pm 0.0007$ d that is slightly different from our result of $P = 4.67604 \pm 0.00002$ d. This is mainly due to A36 having fewer observations in the Radial Velocity Survey to precisely determine the period. We find the period change from the combination of two models to be $\dot{P} = (3.85 \pm 1.3) \times 10^{-8}$, thus the mass loss by direct mass transfer would be $\dot{M}_1 = (4.9 \pm 2.0) \times 10^{-5} M_{\odot}\text{yr}^{-1}$ and by stellar wind $\dot{M}_1 = (-5.7 \pm 1.9) \times 10^{-5} M_{\odot}\text{yr}^{-1}$.

The value of \dot{M}_1 by stellar wind is too high for a B0Ib star because the maximum empirical estimates for mass-loss rates are typically lower than $10^{-5} M_{\odot}\text{yr}^{-1}$ (Vink et al. 2000; Puls et al. 2006). Therefore, the change in period must be caused by the mass transfer from the secondary to the primary. This also indicates that A36 is experiencing the Algol paradox (Pustyl'nik 1998) where the secondary, less massive, component is more evolved (filling its Roche lobe).

This paradox seems to contradict the stellar evolution theory which states that the evolutionary time-scales are proportionally shorter, the more massive the star is. Especially, as binary stars are thought to have formed at the same time and, thus, are the same age. The paradox can be resolved by the mass transfer between the components. When the originally more massive star has filled its Roche lobe, it will start losing its mass to the less massive companion. Eventually, the two components will switch places and the less evolved star will be more massive and vice versa.

The spectral classification by Kiminki et al. (2009) seems to contradict our conclusion because the less evolved secondary (B0III) could not be a donor star as it could not fill its Roche lobe before the more evolved primary (B0Ib). But this conclusion is still viable if the luminosity class of the primary component could be lowered. Our PHOEBE modelling results for the stellar radii and masses also support the argument that the primary component is closer to the luminosity class III.

4.3.3 B17

B17 was first discussed by Comerón et al. (2002), who discovered that it displays emission in the Brackett γ line (the B notation in front of the star number), which is an indicator of high mass-loss rate typical of the evolved stellar stages. It is a massive evolved binary system with a spectral classification estimation of O7Ia+O9I supergiants. Hoffman et al. (2009) classified it as an Algol/ β Lyrae type using NSVS data.

For B17 we could not use any spectroscopic data. Stroud et al. (2010) have done an extensive photometric and spectroscopic campaign on B17, but their data are unfortunately not publicly available and they are only presented in a phased form on a graph. Their determined period of 4.02174 ± 0.00003 d coincides with ours, and because the time base between the NSVS photometry data and their observed spectra was only four years, they did not discuss any possibility of a period change. We did not find any indication of a period change within the binary system with values of $\dot{P}_{\text{emp}} = (1.1 \pm 1.6) \times 10^{-8}$ and $\dot{P}_{\text{model}} = (-0.8 \pm 1.7) \times 10^{-8}$, and therefore we find no mass loss in the system. No stellar parameters were modelled either because there were no available RV data.

4.3.4 MT059

MT059 (Schulte 1) is an O8V type star with a B, possibly later than B1V, type companion. Kiminki et al. (2008) have only measured radial velocities for the primary component and did not detect any spectral features of the companion, which indicates that the luminosity ratio has to be lower than $L_2/L_1 \lesssim 0.2$. For their primary component mass assessment, they used the theoretical mass for a spectral type O8V from Martins et al. (2005) with a value of $M_{\text{spec}} = 21.95 M_{\odot}$. They concluded that due to the absence of spectral signatures of the secondary component, the interpolation from its spectral type yields the mass of the secondary companion to be $5.1 M_{\odot} \lesssim M_2 \lesssim 13.8 M_{\odot}$ and the mass ratio $0.24 \pm 0.02 \lesssim q \lesssim 0.64 \pm 0.03$.

Our resulting mass ratio falls on the lower side of their prediction with a value of 0.29, and the masses we obtained agree with the previously mentioned predictions with values of $M_1 = 21.23 \pm 6.24 M_{\odot}$ and $M_2 = 6.22 \pm 1.83 M_{\odot}$. There are no RV data for the secondary companion, therefore we cannot independently assess the mass ratio, and thus the mass ratio is degenerate with the other stellar parameters. The semi-major axis of the system also yields large formal errors, which lead to large errors in the mass assessments. The modelled light curve (upper panel in Fig. 4.8) indicates the presence of a reflection effect (phase ~ 0.2) that is only loosely supported by the data. A reflection effect is the heating of a star by its companion that results in an increased radiative brightness on the side facing that companion as the temperature increases (Kallrath & Milone 2009). A more thorough investigation is needed to determine whether this effect is from the observational uncertainties or from the underlying physics of the system.

MT059 is indicated by Kiminki et al. (2008) as a SB1-type binary without mentioning its eclipsing nature. Our observations and NSVS photometric data show clear eclipses from the photometric folded light curve. The binary has an eccentricity of 0.14, which is also notable from the uneven timings in phase space between the primary and secondary eclipse.

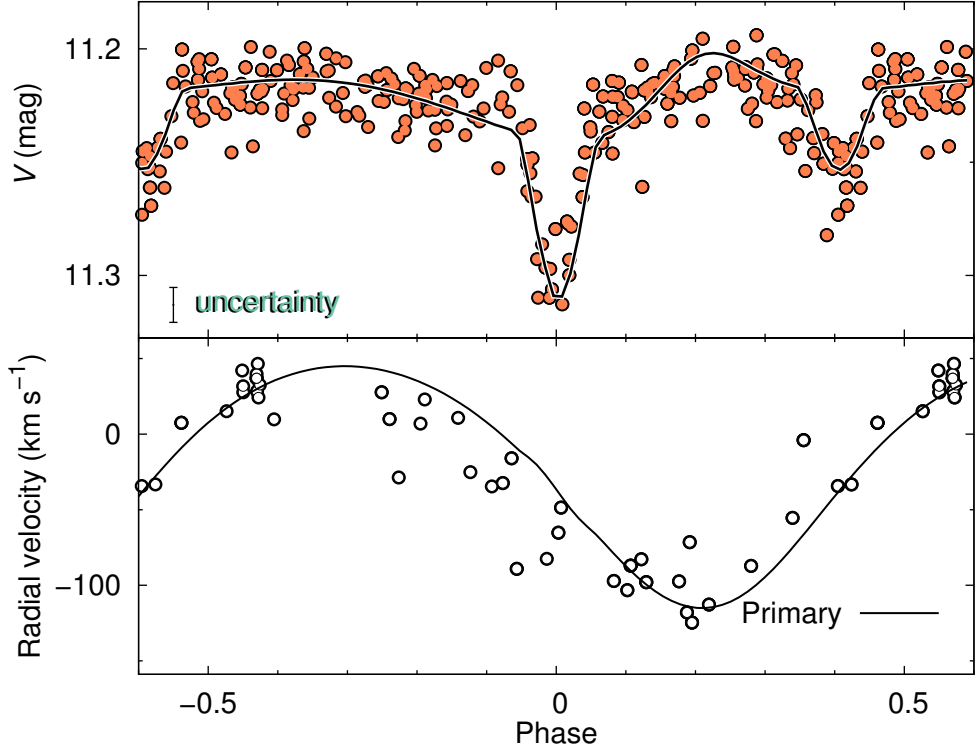


Figure 4.8: Binary modelling for MT059 with the PHOEBE software. Designations of lines, labels, and photometric data set are the same as in Fig. 4.6. Radial-velocity data are taken from Kiminki et al. (2008).

We find that MT059 has the highest period change value out of all of our selected binary systems ($\dot{P}_{\text{emp}} = (-4.7 \pm 1.7) \times 10^{-8}$ or $\dot{P}_{\text{model}} = (-3.6 \pm 1.7) \times 10^{-8}$). This is due to the RV observations, which are also visibly shifted in our PHOEBE modelling (Fig. 4.8). The mass loss through conservative mass exchange with the results from our empirical model is $\dot{M}_1 = (-10.5 \pm 4) \times 10^{-6} M_{\odot} \text{yr}^{-1}$. As the period change is negative, the mass loss from stellar wind cannot be calculated using Eq. (4.3) because it would result in a positive \dot{M}_1 value, and therefore the period change must be from mass transfer from the primary to the secondary component.

4.3.5 MT696

MT696 (Fig. 4.9) is a binary system of an O9.5V spectral type primary and an early-B type companion. Rios & DeGioia-Eastwood (2004) were the first to report the

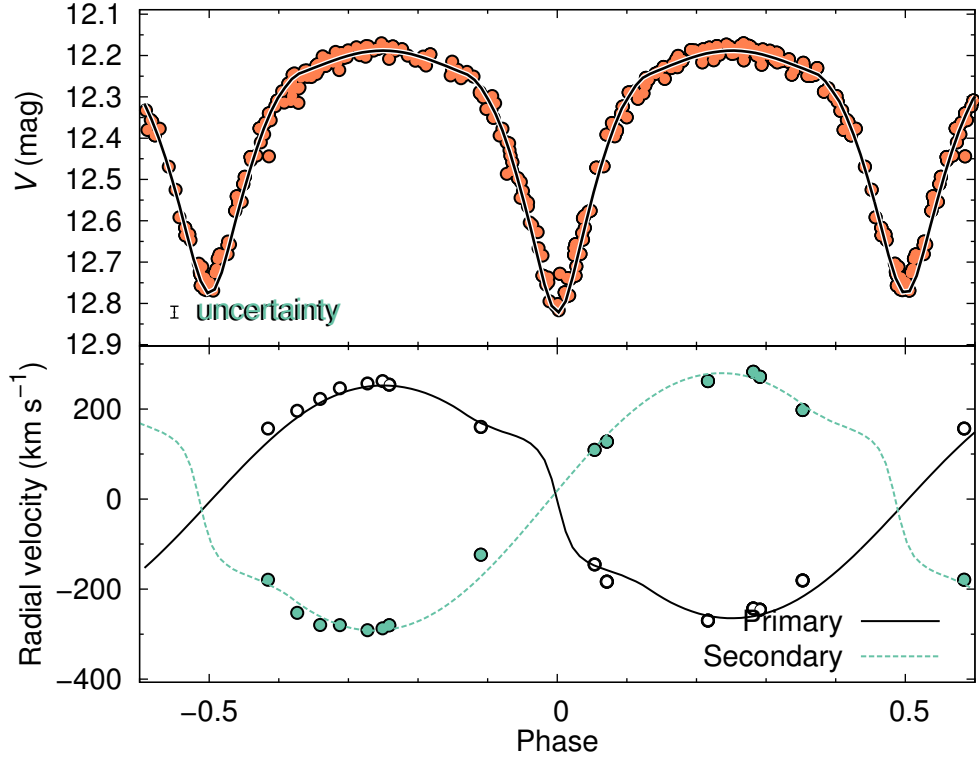


Figure 4.9: Binary modelling for MT696 with the PHOEBE software. Designations of lines, labels, and photometric data set are the same as in Fig. 4.6. Radial-velocity data are taken from Kiminki et al. (2012).

eclipsing binary status of MT696, indicating that it might be a W UMa type binary with a 1.46-day period. Kiminki et al. (2008) argued that the early spectral types of the components, the absence of emission features, and a period longer than one day suggest MT696 to be β Lyr type instead. They also improved the period estimate to 1.4692 ± 0.0005 days and estimated the inclination to be near 80° and the mass ratio q to be 0.85 ± 0.03 , which are close to our estimates. Their minimum mass estimates are $15.1 \pm 0.7 M_\odot$ for the primary and $12.8 \pm 0.5 M_\odot$ for the secondary component, while our modelling gives full component masses with values of $14.00 \pm 0.81 M_\odot$ and $12.67 \pm 0.73 M_\odot$, respectively. According to Martins et al. (2005), the mass for spectral type O9.5V is $M_{\text{spec}} = 16.46 M_\odot$. Our mass estimates are within errors of the minimum masses from Kiminki et al. (2008), but lower than the theoretical primary mass, which means that our resulting masses might be underestimated. Another pos-

sibility is that the spectral types and thus the masses of the binary components might not be accurately determined by Kobulnicky et al. (2014).

Souza et al. (2014) found the period to be 1.46919 ± 0.00006 d, and they did not find any period change in their two-year-long data set. We, on the other hand, found the period change at three-sigma confidence level with the value of $\dot{P}_{\text{emp}} = (-0.37 \pm 0.08) \times 10^{-8}$ and $\dot{P}_{\text{model}} = (-0.46 \pm 0.08) \times 10^{-8}$. This is the lowest value of a period change amongst our studied binaries. As a result of the low value for the period change and the similar masses for the binary components, the errors for conservative mass-loss rates are very high because the total error depends both on the period change uncertainty as well as the difference between the companion masses. The acquired mass-loss rate for direct mass transfer is then $\dot{M}_1 = (-0.4 \pm 1.6) \times 10^{-4} M_{\odot}\text{yr}^{-1}$, and it is dominated by the measurement errors of the stellar masses.

4.3.6 MT720

Kiminki et al. (2012) have observed MT720 (Fig. 4.10) and measured its radial velocities on 32 occasions, noting that no known photometric variability has been studied before. They indicated the period of the system to be 4.3622 ± 0.0003 days (compared to our $P_{\text{emp}} = 4.36197 \pm 0.00001$ and $P_{\text{model}} = 4.36177 \pm 0.00001$ days) and an eccentricity of 0.35 ± 0.02 , which is evident from the RV curve. They also found minimum masses from the RV curve and suggested the spectral type of the binary system to be B0–B1V + B1–B2V. Their calculated minimum masses of $M_1 \geq 15.5 M_{\odot}$ and $M_2 \geq 11.1 M_{\odot}$ are in accordance with our modelling results for the component total masses of $M_1 = 18.52 \pm 1.51 M_{\odot}$ and $M_2 = 13.19 \pm 1.07 M_{\odot}$. Two years later Salas et al. (2014) conducted a 1.5-year-long photometric survey in Cygnus OB2 and included MT720 as a confirmed eclipsing binary with a period of 4.3619 ± 0.0001 days. Our photometric data also show clear evidence of eclipsing nature of the binary.

At first we noticed that in phase space the primary eclipse coincided with the RV curve when the more massive star was eclipsing the secondary component, indicating that it must be less luminous. After modelling the light curve, it turns out that because of the high eccentricity of the system, the primary eclipse depth lessened into what we see as a secondary eclipse. This effect is due to the combination of the high eccentricity and a low inclination angle, resulting in a partial eclipsing of the primary component by the secondary star. The model in Fig. 4.10 is acquired by introducing a phase shift of 0.45 so the secondary eclipse would coincide with a phase zero point.

Modelled stellar parameters for MT720 are more prone to errors because of the poor fit between the data and the model. As can be seen in Fig. 4.10, the secondary eclipse in the observations is narrower than the model curve. Our period change

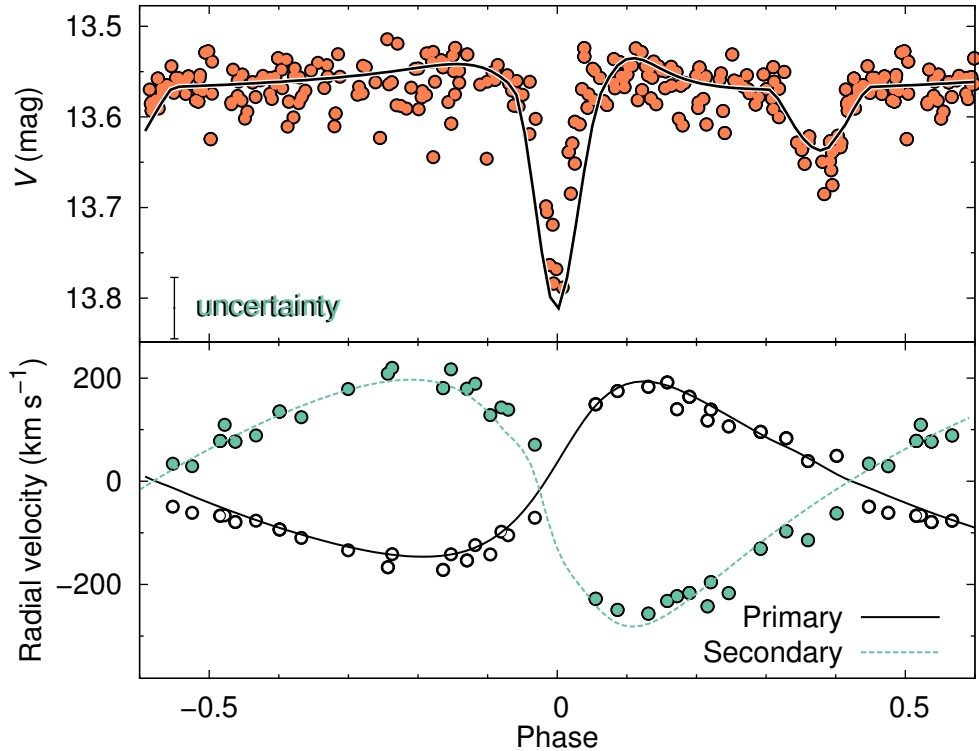


Figure 4.10: Binary modelling for MT720 with the PHOEBE software. Designations of lines, labels, and photometric data set are the same as in Fig. 4.6. Radial-velocity data are taken from Kiminki et al. (2008).

modelling for this system has a strong systematic effect that is due to the differences between the two phased light curve models. The above-mentioned modelling discord arises because MT720 has the largest photometric uncertainties as it is the faintest object in our selection. The systematic errors between the models prevent us from finding any reliable evidence for the period change in MT720.

4.3.7 Schulte 3

Schulte 3 (Fig. 4.11) is a massive binary system consisting of O6IV: and O9III stellar type components. Kiminki et al. (2008) found a mass ratio of $q = 0.44 \pm 0.08$, which agrees within errors with our result of 0.53 ± 0.05 , but differs from the theoretical mass ratio of $q = 0.64$ for O6IV: + O9III binary system (Martins et al. 2005). Our modelled masses ($M_1 = 32.73 \pm 7.04 M_\odot$ and $M_2 = 17.21 \pm 3.70 M_\odot$) agree with

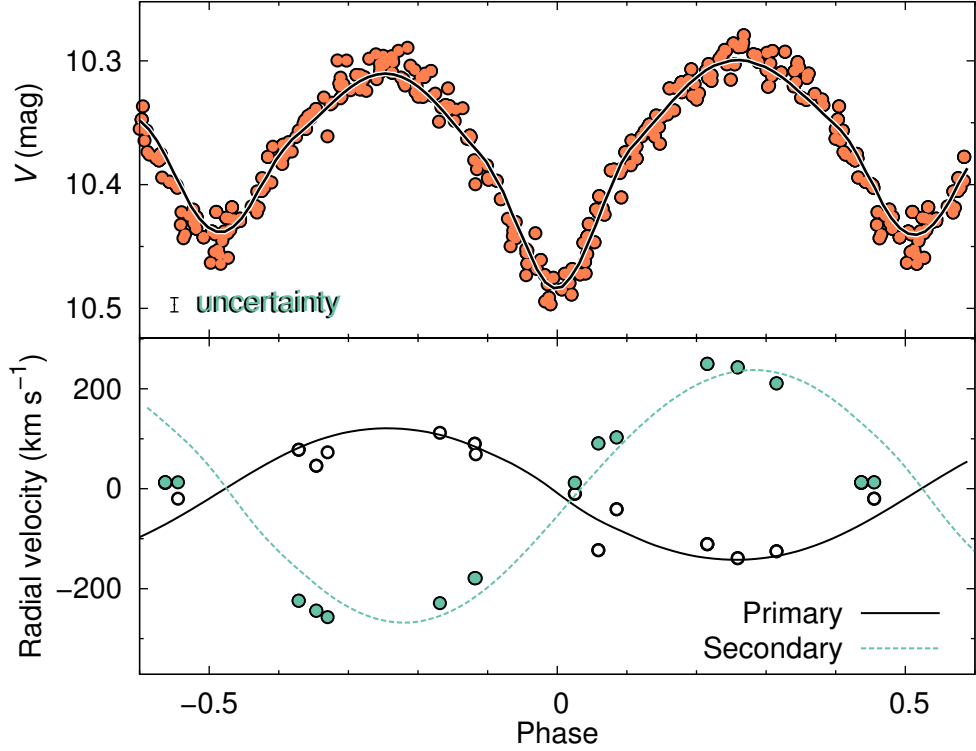


Figure 4.11: Binary modelling for Schulte 3 with the PHOEBE software. Designations of lines, labels, and photometric data set are the same as in Fig. 4.6. Radial-velocity data are taken from Kiminki et al. (2008).

their minimum mass predictions of $M_1 \geq 17.2 M_\odot$ and $M_2 \geq 7.6 M_\odot$. Our acquired primary component mass is also close to the theoretical spectroscopic mass of O6V ($M_{\text{spec}} = 31.73 M_\odot$), but the theoretical mass value for the secondary component ($M_{\text{spec}} = 23.07 M_\odot$) is higher than our result.

Kiminki et al. (2008) argued that the difference between the mass ratios is due to the mass transfer between the components. The period we find coincides with their result ($P = 4.7459 \pm 0.0003$ days) within the errors, but we did not detect any notable period change in the system. Our period change value for empirical model is $\dot{P}_{\text{emp}} = (-1.5 \pm 1.0) \times 10^{-8}$, which does not imply a non-zero value at two-sigma confidence level, and for PHOEBE model the value is $\dot{P}_{\text{model}} = (0.0 \pm 0.9) \times 10^{-8}$. These values show clear evidence for no period change within the system and indicate no mass transfer between the components.

CHAPTER 5

SUMMARY

The formation and evolution of massive stars is still an open question as physical phenomena like core convective overshooting, internal stellar rotation and angular momentum distribution inside massive stars are poorly understood. The field of asteroseismology helps us explore these stellar interiors by observing the surface oscillations of stars. Although, space missions (CoRoT, MOST, Kepler) have made asteroseismic observations of hundreds of solar-like stars during the last decade, our knowledge of massive stars is relatively poor due to the small number of them observed from space. Ground-based observations can not achieve the precision for proper asteroseismic analysis but, for massive stars with suitably large brightness amplitudes, they can be used to expand on the known asteroseismic constraints. Furthermore, automated small ground telescopes have been used in many variable-star all-sky surveys and their availability makes them especially useful for studying bright (massive) stars with good temporal coverage.

In order to study massive stars in different evolutionary phases, we monitored 22 northern open clusters and associations in 2011–2013 across 15 fields in four constellations. Using a small-aperture automated telescopes, we optimised our observations for the brightest stars in each field and obtained light curves for over 25 000 stars. The fields were monitored using a 0.25-m telescope in New Mexico, as well as a 0.31-m and 1.5-m telescopes in Tõravere.

Based on the variability index method we found 354 variable stars in the fields. We used a discrete Fourier transform code called SigSpec to obtain periods for pulsating stars and phase dispersion minimum algorithm to fine-tune the periods for eclipsing binaries. In addition to the pulsational information, we used a pulsation HR diagram to classify our variable stars. We classified 80 eclipsing binaries, 31 α Cyg, 13 β Cep, 62 Be, 16 SPB, 7 Cepheid, 1 γ Doradus, 3 WR and 63 late-type stars. We compared our results with the Variable Star Index (VSX) to identify possible first discoveries of variability amongst the detected variable stars. We found 47 eclipsing binaries, 10 α Cyg, 11 β Cep, 29 Be, 15 SPB, 2 Cepheid, 1 WR and 33 late-type stars that are absent in the VSX database. An additional 70 variable stars could not be classified due to the lack of spectral or pulsational information.

We found that 13% of the variable stars are cluster members based on the membership information in the Milky Way Star Clusters Catalogue (MWSC). We also found that MWSC membership estimations are lower compared to other membership estimations. Analysing the probability density function of variable stars, we found the upper limit of membership fraction to be 35%.

Mass loss in massive stars determines the evolution of their temperature, luminosity and even the type of supernova explosion in their final evolutionary phases. Mass-loss rates in binary stellar systems can be measured from the change in their eclipse timings, indicating either a spin-up or slow-down of the system and thus a change in their periods. To study mass-loss rates in eclipsing massive binaries, we used a Bayesian approach to determine the period change of seven massive binaries in the Cygnus OB2 association.

For this, we used archival photometry and RV data together with our own photometric observations. Our observations were essential in the period-change analysis for A36, B17, MT696, and MT720 because they increased the time base up to 13 years. We noted for the first time the eclipsing nature of MT059.

We showed that by applying the Bayesian parameter estimation method the period change can be calculated using all the available data simultaneously for any binary star. Using all data points in contrast to using only the times of minimum, improves the statistical significance of the calculations and opens up new data sets that can be included in the analysis. This is especially important with the trend to digitise archives of photographic plates because it adds new historical observations that were not optimised for the eclipses of binaries, which means that the times of minimum may be difficult to obtain.

Out of the selected seven binaries, four of them showed evidence of a non-zero period change at two-sigma confidence level. For three stars we reported the period change for the first time. Our calculations confirmed the previous assessments for \dot{P} of a star Schulte 5. We also showed that the change in period in Schulte 5 originates from the stellar wind from the primary component. Two of the systems, B17 and Schulte 3, showed period change values close to zero, indicating that there is no mass transfer between the binary components or that the period change values are too low for us to estimate them reliably with the available data. Our method had systematic errors in fitting the period and period change parameters for MT720, and thus we did not derive any reliable values for that system. Two of the systems, MT059 and MT696, had negative \dot{P} values that showed mass transfer from the primary to the secondary component. We argued that the change in period for A36 might stem from mass transfer from the secondary component to the primary, indicating a more evolved secondary stellar component.

In the end, we carried out a three-year observational campaign with the goal to observe and study the most luminous variable stars in selected fields. The resulting database is listed in The Strasbourg astronomical Data Center (CDS¹), divided into different variability types. Alongside the database, the light curve data for all of the variable stars were also made available to be used by the community in future studies.

¹<http://cdsarc.u-strasbg.fr/viz-bin/qcat?J/A+A/598/A108>

CHAPTER 6

KOKKUVÕTE (SUMMARY IN ESTONIAN)

Massiivsete tähtede muutlikkuse uuring Linnutee täheparvedes

Käesoleva töö eesmärk oli uurida massiivsete tähtede heleduse muutlikkust erineva vanusega Linnutee täheparvedes. Massiivsed tähed arenevad päikesesarnastest tähtedest märgatavalt kiiremini ning lõpetavad oma elu supernoovadena. Oma elu jooksul läbivad nad mitmeid etappe, mille jooksul erinevad füüsilised protsessid põhjustavad nende heleduse muutlikkust. Uurides massiivseid tähti erinevate vanustega täheparvedes (tähtede vanus on sarnane täheparve vanusega), on võimalik vaadeldud tähtede muutlikkuse kaudu hinnata neis toimuvaid protsesse.

Selleks viisime 2011 suvest kuni 2013 talveni läbi vaatluskampania 22 põhjataeva hajusparves ja OB-assotsiatsioonis. Vaatlesime kolme erineva teleskoobiga: 0.25-m robotteleskoobiga New Mexicos, USA-s ning 0.31-m ja 1.5-m teleskoopidega Tõraveres, Eestis. Kokku jälgisime kampania käigus 15 erinevat vaatlusalala ja mõõtsime üle 25 000 tähe heleduskõvera.

Meie poolt määratud muutlikkuse indeksi alusel leidsime oma vaatlusandmetest 354 muutlikku tähte. Muutlikkuse indeks on määratud kui ööde jooksul mõõdetud heleduste keskmise hajuvuse osakaal kogu heleduskõvera hajuvusest. Konstantsete tähtede jaoks ei muutu tähe heledused erinevate ööde vahel, samas kui muutlikel tähtedel on järjestikustel öödel vägagi erinevad heledused. Selles töös on muutlikeks tähtedeks loetud kõik tähed, mille muutlikkuse indeks ületab väärtust 1.5, ning konstantseteks tähtedeks kõik tähed, mille väärtus jääb 1 lähedale.

Järgnevalt analüüsisime me muutlike tähtede perioodilisust ning klassifitseerisime neid muutlikkuse rühmadesse. Me kasutasime SigSpeci nimelist sagedusanalüüsi programmi, et määrata muutlike tähtede pulseerimisperioodid. Kaksik-tähtede perioodide täpsemaks määramiseks kasutasime lisaks faasi minimeerimise meetodit, kuna see töötab paremini ebakorrapäraste heleduskõverate korral. Kasutades leitud pulseerimisperioode ning muutlikkuse diagramme, klassifitseerisime me vastleitud tähed nende heleduse käitumise järgi muutlikkuse rühmadesse. Need rühmad on määratud tähes toimuvate füüsiliste protsesside järgi ning meie poolt avastatud tähed kuuluvad neist üheksasse rühma, millest pea kõik asuvad HR diagrammi ülemises osas (piirkonnas, mida mööda kulgeb massiivsete tähtede elutee).

Me võrdlesime oma muutlike tähtede nimekirja tuntud muutlike tähtede andmebaasiga VSX, et teha kindlaks potentsiaalsed esmaavastused. VSX-i andmebaasis on üle 400 000 muutliku tähe, mis pärinevad nii arvukatest ületaeava muutlikkuse uuringutest kui ka üksikkasutajate panustest. 62%-le meie poolt leitud muutlikele tähtedele ei leidunud VSX andmebaasist vastet. See tähendab, et suure tõenäosusega

oleme me esimesed, kes mõõtsid nende tähtede heleduse pikemaajalist muutlikkust.

Me määrasime muutlike tähtede täheparvedesse kuuluvust *Milky Way Star Cluster Catalogue* (MWSC, Linnutee täheparvede kataloog) põhjal ning avastasime, et täheparvedesse kuuluvate liikmete osakaal oli ainult 13%. Võrreldes teiste andmebaasidega, oli MWSC liikmemäär protsent tunduvalt madalam. Kahjuks aga oli MWSC ainus andmebaas, kus kõik meie vaadeldud tähed esindatud olid. Uurides muutlike tähtede põhjal tehtud parve kuuluvuse tõenäosustihedust, leidsime me liikmemäär osakaalu ülempiiriks kuni 35%, mis on märgatavalt suurem kui MWSC põhjal leitu.

Edasi uurisime üksikasjalikumalt varjutusmuutlike kaksiktähtede (kaks tähte, mis tiirlevad ümber ühise massikeskme) perioodimuutust. Kaksiktähe tiirlemisperiood muutub, kui kaksiktähe komponentide kaugus massikeskme ümber ei ole fikseeritud. Kaugus massikeskmest on määratud tähtede massisuhtega, mis muutub, kui ühelt tähelt kandub aine üle teisele tähele või tähetuulte tõttu kandub aine süsteemist välja. Kui tähed triivivad massikeskmele lähemale, siis nende tiirlemisperiood lüheneb (negatiivne perioodimuutus) ja kui eemale, siis periood pikeneb (positiivne perioodimuutus). Teades perioodimuutuse väärtust, on võimalik arvutada tähe massikadu, millest omakorda sõltub kõikide massiivsete tähtede arengukäik.

Perioodimuutuste uurimisteks valisime seitse massiivset kaksiktähte Luige tähtkujust. Lisaks omaenda vaatlustele kasutasime ka kõiki avalikult kättesaadavaid fotomeetriliste ja spektroskoopiliste vaatluste tulemusi. Meie vaatlused olid määravaks nelja kaksiktähe (A36, B17, MT696 ja MT720) perioodimuutuse uurimisel, kuna pikendasid ajalist baasi kuni 13 aasta võrra. Meie olime ka esimesed, kes mõõtsid varjutusi tähes MT059. Lisaks perioodimuutusele modelleerisime me ka kõigi uuritavate tähtede orbitaal- ja stellaarparameetrid, mis annab parema ülevaate tähtede masside, temperatuuride, kauguste ja suuruste kohta süsteemis.

Perioodimuutuse arvutamiseks kasutasime me uudset meetodit, milles analüüsiiti samaaegselt ühe tähe kõiki mõõdetud heledusi ja radiaalkiirusi. Monte Carlo algoritmiga otsisime kogu andmestikust kõige paremini sobivat perioodi ja perioodimuutuse väärtust, sobitades andmeid eelnevalt arvatud tähemudelitega. Tavaliselt uuritakse perioodimuutust varjutuse miinimumide ajalise nihke meetodil, milles kasutatakse ainult fotomeetriliste varjutuste keskpunkte ja ülejäänud andmestik jäetakse kõrvale. Meie meetodiga saab aga analüüsida kõiki fotomeetrilisi vaatlusi koos radiaalkiirustega ning sedasi tunduvalt vähendada statistilist müra. See muutub eriti oluliseks, kui lõppeb ülemaailmne vanade fotoplaatide digitaliseerimise buum. Siis avaldub sajakonna aasta jagu ajaloolisi andmeid, mis aga tavaliselt ei ole optimeeritud kaksiktähtede varjutuste keskpunktide mõõtmiseks. Meie meetodiga on võimalik neid vanu andmeid kasutada hoolimata sellest, kuidas vaatlused on läbi viidud.

Seitsmest uuritud kasiktähest neljal leidsime nullist erineva perioodimuutuse ning neist kolmel ei olnud varem perioodimuutust üldse uuritud. Meie arvutused kinnitasid varem leitud perioodimuutuse tähe Schulte 5 jaoks ning me näitasime, et leitud perioodimuutus on tingitud peakomponendi tähetuulest. Kahe tähe, B17 ja Schulte 3, jaoks näitasid meie arvutused, et perioodimuutust ei ole toimunud. Sellest võib eeldada, et nendes süsteemides ei kandu ainet ühelt komponendilt teisele. Kahjuks ilmnisid tähe MT720 parameetrite arvutamisel süstemaatilised vead ning me ei jõudnud kindla tulemuseni. Me leidsime, et süsteemides MT059 ja MT696 on periood lühenenud täheaine ülekandumisel peakomponendilt sekundaarile. Viimase tähe, A36, perioodimuutus oli positiivne, mis viitab, et aine kandub sekundaarkomponendilt peakomponendile. See aga tähendab, et väiksema massiga sekundaarkomponent peab olema kiiremini evolutsioneerunud ja A36 näol on tegemist nn. Algoli paradoksi süsteemiga.

Meie töö põhitulemuseks oli kolmeaastane vaatluskampaania, mille käigus uurisime Linnutee hajusparvede heledaimaid tähti. See tulemus on avaldatud andmebaasina Starsbourg'i astronoomilises andmekeskuses (CDS¹) grupeerituna erinevatesse muutlikkuse rühmadesse. Lisaks andmebaasile on seal avaldatud ka kõikide muutlike tähtede heleduskõverad, mida on kõigil võimalik avalikult kasutada tulevastes tähemuutlikkuse uurimistöodes.

¹<http://cdsarc.u-strasbg.fr/viz-bin/qcat?J/A+A/598/A108>

BIBLIOGRAPHY

- Abt, H. A., Gomez, A. E., & Levy, S. G. 1990, *The frequency and formation mechanism of B2-B5 main-sequence binaries*, ApJS, 74, 551
- Aerts, C. 2015, *Massive Star Asteroseismology in Action*, in IAU Symposium, Vol. 307, *New Windows on Massive Stars*, ed. G. Meynet, C. Georgy, J. Groh, & P. Stee, 154
- Aerts, C., Christensen-Dalsgaard, J., & Kurtz, D. W. 2010, *Asteroseismology*
- Aerts, C., Zwitter, K., Marcos-Arenal, P., et al. 2013, *Ensemble Asteroseismology of the Young Open Cluster NGC 2244*, ArXiv e-prints
- Alfonso-Garzón, J., Domingo, A., Mas-Hesse, J. M., & Giménez, A. 2012, *The first INTEGRAL-OMC catalogue of optically variable sources*, A&A, 548, A79
- Baker, N. & Kippenhahn, R. 1962, *The Pulsations of Models of δ Cephei Stars. With 17 Figures in the Text*, ZAp, 54, 114
- Balona, L. A. 1995, *Tests of the Pulsation and Starspot Models for the Periodic Be-Stars*, MNRAS, 277, 1547
- Barbon, R. & Hassan, S. M. 1996, *A new study of the young open cluster NGC 7510.*, A&AS, 115, 325
- Baume, G., Vázquez, R. A., & Carraro, G. 2004, *The young open cluster Markarian 50*, MNRAS, 355, 475
- Becker, S. A. 1998, *The Variable Star Menagerie*, in *Astronomical Society of the Pacific Conference Series*, Vol. 135, *A Half Century of Stellar Pulsation Interpretation*, ed. P. A. Bradley & J. A. Guzik, 12
- Bedding, T. R. 2014, *Solar-like oscillations: An observational perspective*, ed. P. L. Pallé & C. Esteban, 60
- Bertin, E. 2011, *Automated Morphometry with SExtractor and PSFEx*, in *Astronomical Society of the Pacific Conference Series*, Vol. 442, *Astronomical Data Analysis Software and Systems XX*, ed. I. N. Evans, A. Accomazzi, D. J. Mink, & A. H. Rots, 435
- Bertin, E. & Arnouts, S. 1996, *SExtractor: Software for source extraction.*, A&AS, 117, 393
- Bohannon, B. & Conti, P. S. 1976, *Spectroscopic studies of O-type binaries. I. BD +40 4220: an enigma ripe for resolution.*, ApJ, 204, 797
- Bohlin, R. C. 2014, *Hubble Space Telescope CALSPEC Flux Standards: Sirius (and Vega)*, AJ, 147, 127
- Breger, M., Stich, J., Garrido, R., et al. 1993, *Nonradial Pulsation of the Delta-Scuti Star Bu-Cancri in the Praesepe Cluster*, A&A, 271, 482

- Brickhill, A. J. 1991, *The pulsations of ZZ Ceti stars. III - The driving mechanism*, MNRAS, 251, 673
- Cazorla, C., Nazé, Y., & Rauw, G. 2014, *Wind collisions in three massive stars of Cygnus OB2*, A&A, 561, A92
- Chapellier, E., Rodríguez, E., Auvergne, M., et al. 2011, *The γ Doradus CoRoT target HD 49434. II. Frequency analysis of the CoRoT data*, A&A, 525, A23
- Chaplin, W. J. & Miglio, A. 2013, *Asteroseismology of Solar-Type and Red-Giant Stars*, ARA&A, 51, 353
- Cherepashchuk, A. M. & Khaliullin, K. F. 1973, *Narrow-band photoelectric photometry of the Wolf-Rayet eclipsing binary V444 Cygni in the continuum ($\lambda\lambda$ 4244-7512 Å)*, AZh, 50, 516
- Choi, H. S., Kim, S.-L., Kang, Y. H., & Park, B.-G. 1999, *Search for variable stars in the open cluster NGC 7654*, A&A, 348, 789
- Clementini, G., Ripepi, V., Leccia, S., et al. 2016, *Gaia Data Release 1. The Cepheid and RR Lyrae star pipeline and its application to the south ecliptic pole region*, A&A, 595, A133
- Comerón, F., Pasquali, A., Rodighiero, G., et al. 2002, *On the massive star contents of Cygnus OB2*, A&A, 389, 874
- Conti, P. S. & Howarth, I. D. 1999, *1-m spectroscopy of normal OB stars*, MNRAS, 302, 145
- Currie, T., Hernandez, J., Irwin, J., et al. 2010, *The Stellar Population of h and χ Persei: Cluster Properties, Membership, and the Intrinsic Colors and Temperatures of Stars*, ApJS, 186, 191
- Dambis, A. K., Glushkova, E. V., Berdnikov, L. N., Joshi, Y. C., & Pandey, A. K. 2017, *Investigation of open clusters based on IPHAS and APASS survey data*, MNRAS, 465, 1505
- De Cat, P., Briquet, M., Aerts, C., et al. 2007, *Long term photometric monitoring with the Mercator telescope. Frequencies and mode identification of variable O-B stars*, A&A, 463, 243
- Deeming, T. J. 1975, *Fourier Analysis with Unequally-Spaced Data*, Ap&SS, 36, 137
- Dias, W. S., Alessi, B. S., Moitinho, A., & Lépine, J. R. D. 2002, *New catalogue of optically visible open clusters and candidates*, A&A, 389, 871
- Duchêne, G. & Kraus, A. 2013, *Stellar Multiplicity*, ARA&A, 51, 269
- Duchêne, G., Simon, T., Eislöffel, J., & Bouvier, J. 2001, *Visual binaries among high-mass stars. An adaptive optics survey of OB stars in the NGC 6611 cluster*, A&A, 379, 147
- Eyer, L. & Mowlavi, N. 2008, *Variable stars across the observational HR diagram*, Journal of Physics Conference Series, 118, 012010
- Eyer, L., Palaversa, L., Mowlavi, N., et al. 2012, *Standard candles from the Gaia*

- perspective*, Ap&SS, 341, 207
- Fabricius, C., Makarov, V. V., Knude, J., & Wycoff, G. L. 2002, *Henry Draper catalogue identifications for Tycho-2 stars*, A&A, 386, 709
- Feroz, F. & Hobson, M. P. 2008, *Multimodal nested sampling: an efficient and robust alternative to Markov Chain Monte Carlo methods for astronomical data analyses*, MNRAS, 384, 449
- Feroz, F., Hobson, M. P., & Bridges, M. 2009, *MULTINEST: an efficient and robust Bayesian inference tool for cosmology and particle physics*, MNRAS, 398, 1601
- Feroz, F., Hobson, M. P., Cameron, E., & Pettitt, A. N. 2013, *Importance Nested Sampling and the MultiNest Algorithm*, ArXiv e-prints
- Gaia Collaboration, Brown, A. G. A., Vallenari, A., et al. 2016, *Gaia Data Release 1. Summary of the astrometric, photometric, and survey properties*, ArXiv e-prints
- Garmany, C. D., Conti, P. S., & Massey, P. 1980, *Spectroscopic studies of O type stars. IX - Binary frequency*, ApJ, 242, 1063
- Georgy, C., Granada, A., Ekström, S., et al. 2014, *Populations of rotating stars. III. SYCLIST, the new Geneva population synthesis code*, A&A, 566, A21
- Glebbeek, E., Gaburov, E., Portegies Zwart, S., & Pols, O. R. 2013, *Structure and evolution of high-mass stellar mergers*, MNRAS, 434, 3497
- Gomez-Forellad, J. M. 2000, *SAO 23170, a New Beta Cep in the Stellar Cluster H VI 33*, Information Bulletin on Variable Stars, 4924
- Gough, D. 2003, *On the Principal Asteroseismic Diagnostic Signatures*, Ap&SS, 284, 165
- Gough, D. O. 2002, *On the Hydrodynamics of Stellar Pulsation and Stability (invited review)*, in *Astronomical Society of the Pacific Conference Series*, Vol. 259, IAU Colloq. 185: Radial and Nonradial Pulsations as Probes of Stellar Physics, ed. C. Aerts, T. R. Bedding, & J. Christensen-Dalsgaard, 37
- Goupil, M. J., Samadi, R., Lochard, J., Dziembowski, W. A., & Pamyatnykh, A. 2004, *Inferring information about rotation from stellar oscillations*, in *ESA Special Publication*, Vol. 538, *Stellar Structure and Habitable Planet Finding*, ed. F. Favata, S. Aigrain, & A. Wilson, 133
- Graczyk, D. & Eyser, L. 2010, *The Light Curve Statistical Moments Analysis: The Identification of Eclipsing Binaries*, Acta Astron., 60, 109
- Gray, R. 2001, in 2, Vol. 2, *Encyclopedia of Astronomy and Astrophysics*, 1st edn., ed. P. Murdin (Institute of Physics), 717
- Greisen, E. W. & Calabretta, M. R. 2002, *Representations of world coordinates in FITS*, A&A, 395, 1061
- Grindlay, J., Tang, S., Los, E., & Servillat, M. 2012, *Opening the 100-Year Window for Time-Domain Astronomy*, in *IAU Symposium*, Vol. 285, *New Horizons in Time Domain Astronomy*, ed. E. Griffin, R. Hanisch, & R. Seaman, 29

- Grunhut, J. H., Wade, G. A., & MiMeS Collaboration. 2012, *The Incidence of Magnetic Fields in Massive Stars: An Overview of the MiMeS Survey Component*, in *Astronomical Society of the Pacific Conference Series*, Vol. 465, *Proceedings of a Scientific Meeting in Honor of Anthony F. J. Moffat*, ed. L. Drissen, C. Robert, N. St-Louis, & A. F. J. Moffat, 42
- Gummersbach, C. A. & Kaufer, A. 1996, *The Hot Star Newsletter*, 22, 16
- Guzik, J. A. 2011, *Recent advances in modeling stellar interiors*, *Ap&SS*, 336, 95
- Hall, D. S. 1974, *The O9+Of eclipsing binary V729 Cygni in Cygnus OB2*, *Acta Astron.*, 24, 69
- Handler, G. 2013, *Asteroseismology*, ed. T. D. Oswalt & M. A. Barstow, 207
- Hardorp, J., Rohlf, K., Slettebak, A., & Stock, J. 1959, *Luminous stars in the Northern Milky Way. Part I*, *Hamburger Sternw. Warner & Swasey Obs.*
- Hillier, D. J. & Miller, D. L. 1998, *The Treatment of Non-LTE Line Blanketing in Spherically Expanding Outflows*, *ApJ*, 496, 407
- Hirschi, R. & et al. 2006, *Stellar evolution of massive stars at very low metallicities (With 10 Figures)*, in *Reviews in Modern Astronomy*, Vol. 19, *Reviews in Modern Astronomy*, ed. S. Roeser, 101
- Hoffman, D. I., Harrison, T. E., Coughlin, J. L., et al. 2008, *New β Lyrae and Algol Candidates from the Northern Sky Variability Survey*, *AJ*, 136, 1067
- Hoffman, D. I., Harrison, T. E., & McNamara, B. J. 2009, *Automated Variable Star Classification Using the Northern Sky Variability Survey*, *AJ*, 138, 466
- Huber, D., Ireland, M. J., Bedding, T. R., et al. 2012, *Fundamental Properties of Stars Using Asteroseismology from Kepler and CoRoT and Interferometry from the CHARA Array*, *ApJ*, 760, 32
- Humphreys, R. M. 1978, *Studies of luminous stars in nearby galaxies. I. Supergiants and O stars in the Milky Way.*, *ApJS*, 38, 309
- Joshi, U. C., Sanwal, B. B., & Sagar, R. 1983, *Photometry of the open cluster NGC 6913*, *PASJ*, 35, 405
- Kallrath, J. & Milone, E. F. 2009, *Eclipsing Binary Stars: Modeling and Analysis*
- Kennedy, M., Dougherty, S. M., Fink, A., & Williams, P. M. 2010, *Modeling the Radio Emission from Cyg OB2 No. 5: A Quadruple System?*, *ApJ*, 709, 632
- Kennicutt, R. C. & Evans, N. J. 2012, *Star Formation in the Milky Way and Nearby Galaxies*, *ARA&A*, 50, 531
- Khalack, V. 1996, *Fast narrow-band photometry of the WR141 (WN6)*, in *Liege International Astrophysical Colloquia*, Vol. 33, *Liege International Astrophysical Colloquia*, ed. J. M. Vreux, A. Detal, D. Fraipont-Caro, E. Gosset, & G. Rauw, 239
- Kharchenko, N. V., Piskunov, A. E., Röser, S., Schilbach, E., & Scholz, R.-D. 2005, *Astrophysical parameters of Galactic open clusters*, *A&A*, 438, 1163
- Kharchenko, N. V., Piskunov, A. E., Schilbach, E., Röser, S., & Scholz, R.-D. 2013,

- Global survey of star clusters in the Milky Way. II. The catalogue of basic parameters*, A&A, 558, A53
- Kim, D.-W., Protopapas, P., Bailer-Jones, C. A. L., et al. 2014, *The EPOCH Project. I. Periodic variable stars in the EROS-2 LMC database*, A&A, 566, A43
- Kiminki, D. C. & Kobulnicky, H. A. 2012, *An Updated Look at Binary Characteristics of Massive Stars in the Cygnus OB2 Association*, ApJ, 751, 4
- Kiminki, D. C., Kobulnicky, H. A., Ewing, I., et al. 2012, *Additional Massive Binaries in the Cygnus OB2 Association*, ApJ, 747, 41
- Kiminki, D. C., Kobulnicky, H. A., Gilbert, I., Bird, S., & Chunev, G. 2009, *Five More Massive Binaries in the Cygnus OB2 Association*, AJ, 137, 4608
- Kiminki, D. C., Kobulnicky, H. A., Kinemuchi, K., et al. 2007, *A Radial Velocity Survey of the Cyg OB2 Association*, ApJ, 664, 1102
- Kiminki, D. C., McSwain, M. V., & Kobulnicky, H. A. 2008, *New Massive Binaries in the Cygnus OB2 Association*, ApJ, 679, 1478
- Kjeldsen, H. & Frandsen, S. 1992, *High-precision time-resolved CCD photometry*, PASP, 104, 413
- Kobulnicky, H. A. & Fryer, C. L. 2007, *A New Look at the Binary Characteristics of Massive Stars*, ApJ, 670, 747
- Kobulnicky, H. A., Kiminki, D. C., Lundquist, M. J., et al. 2014, *Toward Complete Statistics of Massive Binary Stars: Penultimate Results from the Cygnus OB2 Radial Velocity Survey*, ApJS, 213, 34
- Koen, C. & Eyer, L. 2002, *New periodic variables from the Hipparcos epoch photometry*, MNRAS, 331, 45
- Kosovichev, A. G. 2011, *Advances in Global and Local Helioseismology: An Introductory Review*, in Lecture Notes in Physics, Berlin Springer Verlag, Vol. 832, Lecture Notes in Physics, Berlin Springer Verlag, ed. J.-P. Rozelot & C. Neiner, 3
- Kourniotis, M., Bonanos, A. Z., Soszyński, I., et al. 2014, *Variability of massive stars with known spectral types in the Small Magellanic Cloud using 8 years of OGLE-III data*, A&A, 562, A125
- Krumholz, M. R., Matzner, C. D., & McKee, C. F. 2006, *The Global Evolution of Giant Molecular Clouds. I. Model Formulation and Quasi-Equilibrium Behavior*, ApJ, 653, 361
- Langer, N. 2012, *Presupernova Evolution of Massive Single and Binary Stars*, ARA&A, 50, 107
- Larson, R. B. & Starrfield, S. 1971, *On the formation of massive stars and the upper limit of stellar masses.*, A&A, 13, 190
- Lauterborn, D. 1970, *Evolution with mass exchange of case C for a binary system of total mass $7 M_{\text{sun}}$.*, A&A, 7, 150
- Lee, O. J., Baldwin, R. J., Hamlin, D. W., et al. 1943, *Dearborn catalog of faint red*

- stars : titanium oxide stars in zones -4.5[degrees] to +13.5[degrees]*, *Annals of the Dearborn Observatory*, 5
- Leighton, R. B., Noyes, R. W., & Simon, G. W. 1962, *Velocity Fields in the Solar Atmosphere. I. Preliminary Report.*, *ApJ*, 135, 474
- Liakos, A. 2015, *AbsParEB and InPeVEB: Software for the Calculation of Absolute and Orbital Period Changes Parameters of Eclipsing Binaries*, in *Astronomical Society of the Pacific Conference Series*, Vol. 496, *Living Together: Planets, Host Stars and Binaries*, ed. S. M. Rucinski, G. Torres, & M. Zejda, 286
- Liao, W.-P. & Qian, S.-B. 2010, *The most plausible explanation of the cyclic period changes in close binaries: the case of the RS CVn-type binary WW Dra*, *MNRAS*, 405, 1930
- Linder, N., Rauw, G., Manfroid, J., et al. 2008, *VizieR Online Data Catalog: Multiwavelength study of Cyg OB2 5 (Linder+, 2009)*, *VizieR Online Data Catalog*, 349, 50231
- Linder, N., Rauw, G., Manfroid, J., et al. 2009, *A multiwavelength investigation of the massive eclipsing binary Cygnus OB2 #5*, *A&A*, 495, 231
- Lohr, M. E., Norton, A. J., Kolb, U. C., et al. 2012, *Period decrease in three Super-WASP eclipsing binary candidates near the short-period limit*, *A&A*, 542, A124
- Maciejewski, G. & Niedzielski, A. 2007, *CCD BV survey of 42 open clusters*, *A&A*, 467, 1065
- Mackenzie, C., Pichara, K., & Protopapas, P. 2016, *Clustering-based Feature Learning on Variable Stars*, *ApJ*, 820, 138
- Maeder, A. 2009, *Physics, Formation and Evolution of Rotating Stars*
- Manfroid, J. 1995, *Stellar calibration of CCD flat fielding.*, *A&AS*, 113, 587
- Marchenko, S. V., Moffat, A. F. J., & Eenens, P. R. J. 1998, *The Wolf-Rayet Binary WR 141 (WN5O + O5 V-III) Revisited*, *PASP*, 110, 1416
- Martins, F., Schaerer, D., & Hillier, D. J. 2005, *A new calibration of stellar parameters of Galactic O stars*, *A&A*, 436, 1049
- Mas-Hesse, J. M., Giménez, A., Culhane, J. L., et al. 2003, *OMC: An Optical Monitoring Camera for INTEGRAL. Instrument description and performance*, *A&A*, 411, L261
- Mason, B. D., Hartkopf, W. I., Gies, D. R., Henry, T. J., & Helsel, J. W. 2009, *The High Angular Resolution Multiplicity of Massive Stars*, *AJ*, 137, 3358
- Massey, P., DeGioia-Eastwood, K., & Waterhouse, E. 2001, *The Progenitor Masses of Wolf-Rayet Stars and Luminous Blue Variables Determined from Cluster Turnoffs. II. Results from 12 Galactic Clusters and OB Associations*, *AJ*, 121, 1050
- Massey, P., Johnson, K. E., & DeGioia-Eastwood, K. 1995, *The Initial Mass Function and Massive Star Evolution in the OB Associations of the Northern Milky Way*, *ApJ*, 454, 151

- Massey, P. & Thompson, A. B. 1991, *Massive stars in CYG OB2*, AJ, 101, 1408
- Mennickent, R. E., Pietrzyński, G., Gieren, W., & Szewczyk, O. 2002, *On Be star candidates and possible blue pre-main sequence objects in the Small Magellanic Cloud*, A&A, 393, 887
- Miczaika, G. R. 1953, *Light-Variability of the Of-Type Spectroscopic Binary BD+40 4220*, PASP, 65, 141
- Mikulášek, Z. 2015, *Phenomenological modelling of eclipsing system light curves*, A&A, 584, A8
- Milašius, K., Boyle, R. P., Vrba, F. J., et al. 2013, *Seven-color Photometry and Classification of Stars in the Direction of Open Cluster M 29 (NGC 6913) in Cygnus*, Baltic Astronomy, 22, 181
- Monteiro, H., Dias, W. S., & Caetano, T. C. 2010, *Fitting isochrones to open cluster photometric data. A new global optimization tool*, A&A, 516, A2
- Moravveji, E., Guinan, E. F., Shultz, M., Williamson, M. H., & Moya, A. 2012, *Asteroseismology of the nearby SN-II Progenitor: Rigel. I. The MOST High-precision Photometry and Radial Velocity Monitoring*, ApJ, 747, 108
- Morris, S. L. 1985, *The ellipsoidal variable stars*, ApJ, 295, 143
- Nedoroščík, J., Vaňko, M., & Pribulla, T. 2015, *Eclipsing binaries in ASAS and NSVS databases: Fourier analysis*, Contributions of the Astronomical Observatory Skalnaté Pleso, 45, 17
- Negueruela, I., Marco, A., Herrero, A., & Clark, J. S. 2008, *New very massive stars in Cygnus OB2*, A&A, 487, 575
- Neilson, H. R. & Ignace, R. 2015, *Period change and stellar evolution of β Cephei stars*, A&A, 584, A58
- Nicholson, M. & Scottish, C. 2006, *Three New Variable Stars in Cygnus*, Open European Journal on Variable Stars, 30, 1
- Norton, A. J., Wheatley, P. J., West, R. G., et al. 2007, *New periodic variable stars coincident with ROSAT sources discovered using SuperWASP*, A&A, 467, 785
- Nun, I., Protopapas, P., Sim, B., et al. 2015, *FATS: Feature Analysis for Time Series*, ArXiv e-prints
- Oliveira, A. F., Monteiro, H., Dias, W. S., & Caetano, T. C. 2013, *Fitting isochrones to open cluster photometric data. III. Estimating metallicities from UBV photometry*, A&A, 557, A14
- Otero, S. A. 2008, *New eclipsing binaries found in the NSVS database II*, Open European Journal on Variable Stars, 83, 1
- Paczyński, B. 2000, *Monitoring All Sky for Variability*, PASP, 112, 1281
- Paczyński, B., Szczygieł, D. M., Pilecki, B., & Pojmański, G. 2006a, *Eclipsing binaries in the All Sky Automated Survey catalogue*, MNRAS, 368, 1311
- Paczyński, B., Szczygieł, D. M., Pilecki, B., & Pojmański, G. 2006b, *Eclipsing bina-*

- ries in the All Sky Automated Survey catalogue*, MNRAS, 368, 1311
- Pandey, A. K. 1986, *Photometry of open cluster STOCK 17*, Bulletin of the Astronomical Society of India, 14, 20
- Pandey, A. K., Nilakshi, Ogura, K., Sagar, R., & Tarusawa, K. 2001, *NGC 7654: An interesting cluster to study star formation history*, A&A, 374, 504
- Pandey, A. K., Upadhyay, K., Ogura, K., et al. 2005, *Stellar contents of two young open clusters: NGC 663 and 654*, MNRAS, 358, 1290
- Paparo, M., Saad, S. M., Szeidl, B., et al. 1998, *Period changes in both modes of RR_d stars in M15*, A&A, 332, 102
- Park, W., Pak, S., Shim, H., et al. 2016, *Photometric transformation from RGB Bayer filter system to Johnson-Cousins BVR filter system*, Advances in Space Research, 57, 509
- Persi, P., Tapia, M., Rodriguez, L. F., Ferrari-Toniolo, M., & Roth, M. 1990, *Thermal and non-thermal radio emission from Cygnus OB2 No. 5*, A&A, 240, 93
- Pichara, K., Protopapas, P., & León, D. 2016, *Meta-classification for Variable Stars*, ApJ, 819, 18
- Pigulski, A., Kopacki, G., & Kołaczkowski, Z. 2001, *The young open cluster NGC 663 and its Be stars*, A&A, 376, 144
- Pigulski, A. & Pojmański, G. 2008, *β Cephei stars in the ASAS-3 data. II. 103 new β Cephei stars and a discussion of low-frequency modes*, A&A, 477, 917
- Pigulski, A., Pojmański, G., Pilecki, B., & Szczygiel, D. M. 2009, *The All Sky Automated Survey. The Catalog of Variable Stars in the Kepler Field of View*, Acta Astron., 59, 33
- Piskunov, A. E., Belikov, A. N., Kharchenko, N. V., Sagar, R., & Subramaniam, A. 2004, *On the determination of age and mass functions of stars in young open star clusters from the analysis of their luminosity functions*, MNRAS, 349, 1449
- Pojmanski, G. 1997, *The All Sky Automated Survey*, Acta Astron., 47, 467
- Pojmanski, G., Pilecki, B., & Szczygiel, D. 2005, *The All Sky Automated Survey. Catalog of Variable Stars. V. Declinations 0 arcd - +28 arcd of the Northern Hemisphere*, Acta Astron., 55, 275
- Portegies Zwart, S. F., McMillan, S. L. W., & Gieles, M. 2010, *Young Massive Star Clusters*, ARA&A, 48, 431
- Puls, J., Markova, N., Scuderi, S., et al. 2006, *Bright OB stars in the Galaxy. III. Constraints on the radial stratification of the clumping factor in hot star winds from a combined H_{α} , IR and radio analysis*, A&A, 454, 625
- Pustyl'nik, I. 1998, *The Early History of Resolving the Algol Paradox*, Astronomical and Astrophysical Transactions, 15, 357
- Rauer, H., Catala, C., Aerts, C., et al. 2014, *The PLATO 2.0 mission*, Experimental Astronomy, 38, 249

- Rauw, G., Vreux, J.-M., & Bohannon, B. 1999, *The Interacting Early-Type Binary BD +40 4220 (V729 Cyg): Modeling the Colliding Winds Region*, ApJ, 517, 416
- Reegen, P. 2007, *SigSpec. I. Frequency- and phase-resolved significance in Fourier space*, A&A, 467, 1353
- Rios, L. Y. & DeGioia-Eastwood, K. 2004, *A New Very Early Contact Binary in Cyg OB2*, in Bulletin of the American Astronomical Society, Vol. 205, American Astronomical Society Meeting Abstracts, 905
- Rivinius, T., Carciofi, A. C., & Martayan, C. 2013, *Classical Be stars. Rapidly rotating B stars with viscous Keplerian decretion disks*, A&A Rev., 21, 69
- Rosseland, S. & Randers, G. 1938, *On the Stability of Pulsating Stars*, Astrophysica Norvegica, 3, 71
- Rucinski, S. M. 2007, *The short-period end of the contact binary period distribution based on the All-Sky Automated Survey*, MNRAS, 382, 393
- Saesen, S., Briquet, M., Aerts, C., Miglio, A., & Carrier, F. 2013, *Pulsating B-type Stars in the Open Cluster NGC 884: Frequencies, Mode Identification, and Asteroseismology*, AJ, 146, 102
- Saio, H., Georgy, C., & Meynet, G. 2013, *Evolution of blue supergiants and α Cygni variables: puzzling CNO surface abundances*, MNRAS, 433, 1246
- Salas, J., Maíz Apellániz, J., & Barbá, R. H. 2014, *A photometric variability study of massive stars in Cygnus OB2*, ArXiv e-prints
- Sana, H., de Mink, S. E., de Koter, A., et al. 2012, *Binary Interaction Dominates the Evolution of Massive Stars*, Science, 337, 444
- Sanner, J., Geffert, M., Brunzendorf, J., & Schmoll, J. 1999, *Photometric and kinematic studies of open star clusters. I. NGC 581 (M 103)*, A&A, 349, 448
- Sazonov, V. 1961, *V 729 Cygni*, Peremennye Zvezdy, 13, 445
- Schmidt, E. G. 2013, *Type II Cepheid Candidates. IV. Objects from the Northern Sky Variability Survey*, AJ, 146, 61
- Schulte, D. H. 1958, *New Members of the Association VI Cygni. II.*, ApJ, 128, 41
- Shin, M.-S., Yi, H., Kim, D.-W., Chang, S.-W., & Byun, Y.-I. 2012, *Detecting Variability in Massive Astronomical Time-series Data. II. Variable Candidates in the Northern Sky Variability Survey*, AJ, 143, 65
- Singh, M. & Chaubey, U. S. 1986, *Mass loss from Wolf-Rayet stars*, Ap&SS, 124, 389
- Skiff, B. A. 2014, *VizieR Online Data Catalog: Catalogue of Stellar Spectral Classifications (Skiff, 2009-2016)*, VizieR Online Data Catalog, 1
- Smith, N. 2014, *Mass Loss: Its Effect on the Evolution and Fate of High-Mass Stars*, ARA&A, 52, 487
- Souza, S. P., Beltz-Mohrmann, G., & Sami, M. 2014, *The Light Curve and Period of MT696*, Journal of the American Association of Variable Star Observers

- (JAAVSO), 42, 154
- St-Louis, N., Chené, A.-N., Schnurr, O., & Nicol, M.-H. 2009, *A Systematic Search for Corotating Interaction Regions in Apparently Single Galactic Wolf-Rayet Stars. I. Characterizing the Variability*, ApJ, 698, 1951
- Stankov, A. & Handler, G. 2005, *Catalog of Galactic β Cephei Stars*, ApJS, 158, 193
- Stein, R. F. & Nordlund, A. 1989, *Topology of convection beneath the solar surface*, ApJ, 342, L95
- Stellingwerf, R. F. 1978, *Period determination using phase dispersion minimization*, ApJ, 224, 953
- Sterken, C. & Manfroid, J., eds. 1992, *Astrophysics and Space Science Library*, Vol. 175, *Astronomical Photometry, A Guide*, 288
- Sterne, T. E. 1939, *Apsidal motion in binary stars*, MNRAS, 99, 451
- Straižys, V., Milašius, K., Boyle, R. P., et al. 2014, *The Enigma of the Open Cluster M29 (NGC 6913) Solved*, AJ, 148, 89
- Stroud, V. E., Clark, J. S., Negueruela, I., et al. 2010, *The eclipsing, double-lined, Of supergiant binary Cygnus OB2-B17*, A&A, 511, A84
- Suzuki, T. K., Nakasato, N., Baumgardt, H., et al. 2007, *Evolution of Collisionally Merged Massive Stars*, ApJ, 668, 435
- Tassoul, M. 1980, *Asymptotic approximations for stellar nonradial pulsations*, ApJS, 43, 469
- Tetzlaff, N., Neuhäuser, R., Hohle, M. M., & Maciejewski, G. 2010, *Identifying birth places of young isolated neutron stars*, MNRAS, 402, 2369
- Tezcan, C. T., Šenavci, H. V., & Yorukoglu, O. 2015, *A GUI for Analyzing the Period Changes of Eclipsing Binary Stars: ANGORA*, in *Astronomical Society of the Pacific Conference Series*, Vol. 496, *Living Together: Planets, Host Stars and Binaries*, ed. S. M. Rucinski, G. Torres, & M. Zejda, 290
- Turner, D. G. 2012, *Classical Cepheids After 228 Years of Study*, *Journal of the American Association of Variable Star Observers (JAAVSO)*, 40, 502
- Tuvikene, T. 2012, *CCD photometry of variable stellar sources*, PhD thesis, Vrije Universiteit Brussel
- van Leeuwen, F. 2007, *Validation of the new Hipparcos reduction*, A&A, 474, 653
- Vanbeveren, D., De Loore, C., & Van Rensbergen, W. 1998, *Massive stars*, A&A Rev., 9, 63
- Verner, G. A., Elsworth, Y., Chaplin, W. J., et al. 2011, *Global asteroseismic properties of solar-like oscillations observed by Kepler: a comparison of complementary analysis methods*, MNRAS, 415, 3539
- Vink, J. S., ed. 2015, *Astrophysics and Space Science Library*, Vol. 412, *Very Massive Stars in the Local Universe*
- Vink, J. S., de Koter, A., & Lamers, H. J. G. L. M. 2000, *New theoretical mass-loss*

- rates of O and B stars*, A&A, 362, 295
- Vink, J. S., de Koter, A., & Lamers, H. J. G. L. M. 2001, *Mass-loss predictions for O and B stars as a function of metallicity*, A&A, 369, 574
- Walker, G. A. H., Kuschnig, R., Matthews, J. M., et al. 2005, *MOST Detects g-Modes in the Be Star HD 163868*, ApJ, 635, L77
- White, T. R., Bedding, T. R., Stello, D., et al. 2011, *Asteroseismic Diagrams from a Survey of Solar-like Oscillations with Kepler*, ApJ, 742, L3
- Wiedemair, C., Sterken, C., Eenmäe, T., et al. 2016, *CCD photometry of CY Aquarii IV. The 2012-2015 seasons*, Journal of Astronomical Data, 22, 1
- Willette, G. T. 1994, *Stochastic excitation of the solar oscillations by turbulent convection*, PhD thesis, California Institute of Technology
- Wilson, O. C. & Abt, A. 1951, *The Of-Type Spectroscopic Binary BD+40 4220.*, ApJ, 114, 477
- Wilson, R. E. & Devinney, E. J. 1971, *Realization of Accurate Close-Binary Light Curves: Application to MR Cygni*, ApJ, 166, 605
- Wilson, R. E. & Van Hamme, W. 2014, *Unification of Binary Star Ephemeris Solutions*, ApJ, 780, 151
- Wolff, S. C., Strom, S. E., & Rebull, L. M. 2011, *The Evolution of Circumstellar Disks Surrounding Intermediate-mass Stars: IC 1805*, ApJ, 726, 19
- Woźniak, P. R., Vestrand, W. T., Akerlof, C. W., et al. 2004, *Northern Sky Variability Survey: Public Data Release*, AJ, 127, 2436
- Wright, C. O., Egan, M. P., Kraemer, K. E., & Price, S. D. 2003, *The Tycho-2 Spectral Type Catalog*, AJ, 125, 359
- Wright, N. J., Drew, J. E., & Mohr-Smith, M. 2015, *The massive star population of Cygnus OB2*, MNRAS, 449, 741
- Wright, N. J., Parker, R. J., Goodwin, S. P., & Drake, J. J. 2014, *Constraints on massive star formation: Cygnus OB2 was always an association*, MNRAS, 438, 639
- Wyrzykowski, L., Pietrzynski, G., & Szewczyk, O. 2002, *Variable Stars in the Field of Young Open Cluster NGC 581*, Acta Astron., 52, 105
- Yaşarsoy, B. & Yakut, K. 2014, *An interacting O + O supergiant close binary system: Cygnus OB2-5 (V729 Cyg)*, New A, 31, 32
- Yadav, R. K. S., Kumar, B., Subramaniam, A., Sagar, R., & Mathew, B. 2008, *Optical and near-infrared photometric study of the open cluster NGC 637 and 957*, MNRAS, 390, 985

ACKNOWLEDGEMENTS

I would like to thank my supervisors for helping me carry out this full-time project - ranging from the observations to the resulting databases. Their help was very appreciated, guiding me through my studies and helping me find the right tools for data handling, analysis and interpretation. I am grateful to Tõnis Eenmäe for teaching me the ins and outs of observational astronomy and how to squeeze out better quality from my raw data. Special thanks goes to Taavi Tuvikene for improving my critical thinking of written English and manuscript preparation. His help was also crucial in the setting up of my reduction and calibration pipelines.

This work was supported by institutional research funding of the Estonian Ministry of Education and Research (IUT26-2, IUT40-1, IUT40-2), by the Estonian Research Council grants 8906 and PUTJD5, and by the European Regional Development Fund (TK133).

APPENDIX

Table 1: Observed eclipsing binaries.

Field	ID	Designation	RA J2000	DEC J2000	Cluster membership	Spectral type	V (mag)	Amp. (mag)	Period (days)	VSX info	VSX period (days)
Berkeley 86	3	V444 Cyg	20:19:32.4	+38:43:54	-	WN5+O6II-V	7.973	0.336	4.2130	EA/WR	4.2124
Berkeley 86	22	HD 228989	20:20:21.4	+38:42:00	-	O8.5V:+O9.7V:	9.686	0.091	1.7734	-	-
Berkeley 86	52	LS II +38 43	20:19:36.8	+38:35:21	Berkeley 86	B1V	10.676	0.148	1.9102	-	-
Berkeley 86	289	V435 Cyg	20:16:27.0	+38:45:41	-	B3V(e)	12.749	0.659	6.7758	EA/SD	6.7719
Berkeley 86	381	2MASS J20190590+3853009	20:19:05.9	+38:53:01	-	-	12.808	0.569	4.3262	-	-
Berkeley 87	18	BD+36 4063	20:25:40.6	+37:22:27	-	ON9.7Ib	9.656	0.187	4.8121	E/GS	4.8126
Berkeley 87	50	TYC 2697-130-1	20:25:30.6	+37:25:48	-	F5V*	10.736	0.169	0.7726	EA	0.7726
Berkeley 87	87	V2538 Cyg	20:23:33.5	+37:25:45	-	BIII-V*	12.003	0.496	3.1620	EB	3.1616
Berkeley 87	131	TYC 2697-883-1	20:25:38.3	+37:03:11	-	-	12.188	0.183	1.8632	-	-
Berkeley 87	203	2MASS J20222399+3658020	20:22:24.0	+36:58:02	Berkeley 87	-	12.940	0.198	20.3009	-	-
Berkeley 87	251	2MASS J20215480+3654426	20:21:54.8	+36:54:43	-	-	13.324	0.376	6.4827	-	-
Berkeley 87	288	NSV 5733998	20:25:15.8	+37:33:18	-	-	13.139	0.635	1.6691	E	0.8340
Berkeley 87	414	2MASS J20241336+3704436	20:24:13.4	+37:04:44	-	-	13.830	0.668	0.2540	VAR	0.2540
Cygnus OB2	5	BD+40 4220	20:32:22.4	+41:18:19	Cygnus OB2	O7I+O6I+O9V	9.185	0.292	6.5980	EB/D/GS	6.5978
Cygnus OB2	18	BD+40 4212	20:31:37.5	+41:13:21	Cygnus OB2	O6IV+O9III	10.214	0.190	4.7460	EA	4.7463
Cygnus OB2	42	Schulte 1	20:31:10.5	+41:31:54	Cygnus OB2	O8V	11.072	0.089	4.8523	-	-
Cygnus OB2	48	V2550 Cyg	20:34:58.8	+41:36:17	FSR 0236	B0Ib+B0III	11.418	0.447	4.6760	EA	4.6760
Cygnus OB2	117	Schulte 27	20:33:59.5	+41:17:35	Cygnus OB2	O9.5V+B0V	12.203	0.612	1.4692	EW/KE	1.4600
Cygnus OB2	158	V1827 Cyg	20:30:27.3	+41:13:25	FSR 0236	O7I+O9I	13.053	0.509	4.0218	EB	4.0217
Cygnus OB2	187	V2186 Cyg	20:33:10.5	+41:22:22	Cygnus OB2	B0V+B3V	12.958	0.161	2.9787	EA	2.9788
Cygnus OB2	224	[MT91] 720	20:34:06.0	+41:08:09	-	B0.5V+B1.5V	13.415	0.241	4.3620	-	-
Cygnus OB2	362	[MT91] 36	20:30:56.1	+41:28:54	-	-	13.691	0.592	0.6856	EA	0.6858
Cygnus OB2	597	[MT91] 372	20:32:58.9	+41:04:30	-	B0V+B2V	14.958	0.530	2.2279	EA	2.2280
Cygnus OB2	1498	2MASS J20304696+4106392	20:30:47.0	+41:06:39	-	-	13.781	0.379	8.6462	-	-
EO Per	94	2MASS J02511159+5725096	02:51:11.6	+57:25:10	-	-	12.559	0.080	0.7672	EA:	-
EO Per	140	UCAC4 738-028961	02:53:00.5	+57:32:34	-	-	13.025	0.275	2.2368	-	-
IC 1805	41	LS I +61 297	02:34:15.0	+61:24:40	-	B1V	10.937	0.244	3.3674	-	-

Table 1: continued.

Field	ID	Designation	RA J2000	DEC J2000	Cluster membership	Spectral type	V (mag)	Amp. (mag)	Period (days)	VSX info	VSX period (days)
IC 1805	69	V1166 Cas	02:32:09.6	+61:38:24	IC 1805	B1V	11.445	0.637	1.3211	EA	1.3210
IC 1805	160	IC 1805 39	02:30:07.2	+61:31:08	—	A3V	12.864	0.438	1.7626	—	—
NGC 581	20	HD 236763	01:31:31.8	+60:33:36	NGC 581	B5	9.507	0.116	4.1740	—	—
NGC 581	69	V11123 Cas	01:33:16.3	+60:38:01	NGC 581	B2:V	11.200	0.175	4.5022	EA	4.5020
NGC 581	142	V1141 Cas	01:38:18.0	+61:08:35	—	B1:	11.929	0.516	6.9092	EA	6.9092
NGC 663	67	TYC 4032-2795-1	01:46:03.0	+61:26:31	—	—	11.170	0.298	6.1610	EB	6.1610
NGC 663	91	TYC 4032-2513-1	01:47:38.9	+61:01:04	—	B3	11.481	0.203	1.4957	—	—
NGC 663	200	2MASS J01441735+6116503	01:44:17.4	+61:16:50	—	F0III	12.541	0.295	1.5974	—	—
NGC 6913	3	V2031 Cyg	20:23:51.0	+38:29:34	—	F0III	8.645	0.104	2.7046	EA	2.7047
NGC 6913	167	TYC 3152-944-1	20:22:57.2	+38:18:25	—	b3	12.554	0.137	9.7214	—	—
NGC 6913	384	2MASS J20244750+3810584	20:24:47.5	+38:10:58	—	b5V	13.826	0.434	1.9103	—	—
NGC 6913	396	2MASS J20255147+3802425	20:25:51.5	+38:02:43	—	—	13.775	0.481	1.8187	—	—
NGC 6913	444	2MASS J20221996+3812386	20:22:20.0	+38:12:39	—	—	13.998	0.265	2.3788	—	—
NGC 7510	26	HD 240218	23:11:22.6	+60:15:10	—	A2	9.850	0.075	3.3628	—	—
NGC 7510	42	LS III +60 42	23:11:02.9	+60:33:33	—	B0.5V	10.808	0.073	8.4064	—	—
NGC 7510	71	V628 Cas	23:17:25.6	+60:50:43	—	em	11.542	0.000	2.8880	INA	—
NGC 7510	392	QV Cep	23:11:47.8	+60:34:14	—	—	13.501	0.666	0.5552	EA	0.5552
NGC 7510	477	2MASS J23152566+6048592	23:15:25.7	+60:48:59	—	—	13.502	0.489	0.5832	—	—
NGC 7510	912	2MASS J23102945+6029168	23:10:29.4	+60:29:17	—	—	14.741	0.479	6.0826	—	—
NGC 7510	1099	2MASS J23144017+6013054	23:14:40.2	+60:13:05	—	—	14.666	0.711	0.5702	—	—
NGC 7654	16	TYC 4279-1821-1	23:22:40.0	+61:13:33	—	G0V	9.817	0.089	30.9760	—	—
NGC 7654	643	V399 Cas	23:22:25.2	+61:07:47	—	—	13.589	0.408	0.6604	EW	0.6604
NGC 7654	1509	2MASS J23282926+6105510	23:28:29.3	+61:05:51	—	—	14.467	0.755	1.1681	—	—
NGC 869/884	37	V622 Per	02:22:17.7	+57:07:25	NGC 869	B2III	9.287	0.108	5.2145	ELL:	—
NGC 869/884	166	NGC 869 1516	02:20:03.0	+57:11:19	—	B1V	11.029	0.279	1.7334	EB	1.7329
NGC 869/884	246	NGC 869 542	02:18:17.4	+56:55:22	—	—	11.585	0.449	0.7393	S	—
NGC 869/884	300	NGC 884 2351	02:22:15.6	+57:13:29	NGC 869	B4V	11.828	0.221	11.6100	EA:	—
NGC 869/884	354	NGC 884 2646	02:23:04.1	+57:10:09	NGC 869	B2V	12.136	0.356	8.2006	—	—
P Cygni	11	V478 Cyg	20:19:38.7	+38:20:09	—	B0.5IV	8.767	0.392	2.8812	EA/DM	2.8809

Table 1: continued.

Field	ID	Designation	RA J2000	DEC J2000	Cluster membership	Spectral type	V (mag)	Amp. (mag)	Period (days)	VSX info	VSX period (days)
P Cygni	32	LS II +38 32	20:18:09.5	+38:18:28	-	OB-	10.313	0.312	1.6619	EA	-
P Cygni	132	2MASS J20195689+3750073	20:19:56.9	+37:50:07	-	-	12.099	0.348	3.1640	-	-
P Cygni	320	2MASS J20170807+3758584	20:17:08.1	+37:58:58	-	-	13.028	0.583	2.7104	-	-
PZ Cas	21	BD+61 2536	23:49:19.0	+61:57:46	-	OB-	9.602	0.091	1.1047	-	-
PZ Cas	30	2MASS J23461792+6201334	23:46:17.9	+62:01:33	Stock 17	-	10.077	0.177	9.0030	-	-
PZ Cas	51	LS I +61 34	23:44:31.2	+61:59:13	-	OB-	10.716	0.068	3.2740	-	-
PZ Cas	97	LS I +61 51	23:46:08.6	+62:03:01	-	OB-	11.433	0.567	3.3005	-	-
PZ Cas	171	2MASS J23443377+6207168	23:44:33.8	+62:07:17	-	-	12.372	0.201	4.4177	-	-
PZ Cas	217	TYC 4281-1348-1	23:43:44.4	+61:36:55	-	-	12.526	0.173	0.4334	-	-
PZ Cas	250	2MASS J23461052+6137333	23:46:10.5	+61:37:33	-	-	12.731	0.226	1.3156	-	-
PZ Cas	516	2MASS J23483201+6216474	23:48:32.0	+62:16:48	-	-	13.536	0.418	5.4486	-	-
PZ Cas	930	2MASS J23465248+6141157	23:46:52.5	+61:41:16	-	-	14.289	0.634	2.1354	-	-
PZ Cas	1161	2MASS J23454071+6215304	23:45:40.7	+62:15:30	Stock 17	-	14.816	0.000	1.2228	EA	1.2220
Cygnus OB2	173	TYC 3157-779-1	20:31:57.0	+41:12:34	-	-	12.529	0.073	-	-	-
EO Per	98	2MASS J02504641+5734517	02:50:46.4	+57:34:52	-	-	12.438	0.115	-	-	-
EO Per	158	2MASS J02522011+5717211	02:52:20.1	+57:17:21	-	-	13.062	0.162	-	-	-
NGC 663	21	BD+60 306	01:41:44.8	+61:15:15	-	G8III	9.873	0.099	-	EA:	-
NGC 663	172	TYC 4032-2601-1	01:47:39.4	+61:18:21	-	B1Ve	12.383	0.168	-	-	-
NGC 663	565	2MASS J01430579+6053307	01:43:05.8	+60:53:31	-	-	13.352	0.310	-	-	-
NGC 869/884	35	HD 14321	02:20:52.9	+56:55:33	NGC 884	B2III	9.287	0.099	-	-	-
NGC 869/884	48	V621 Per	02:22:09.7	+57:07:02	-	B1.5II	9.440	0.084	-	EA	-
NGC 869/884	88	BD+56 489	02:18:15.1	+57:10:16	-	B3e	10.219	0.147	-	-	-
PZ Cas	37	TYC 4281-1792-1	23:44:32.8	+61:45:00	-	-	10.428	0.229	-	-	-
PZ Cas	1287	2MASS J234444605+6144316	23:44:46.1	+61:44:32	-	-	14.062	0.706	-	-	-

Table 2: Observed β Cephei variables.

Field	ID	Designation	RA J2000	DEC J2000	Cluster membership	Spectral type	V (mag)	Amp. (mag)	Period (days)	VSX info	VSX period (days)
Berkeley 86	5	HD 193032	20:16:40.4	+38:53:57	-	B0.2III	8.308	0.071	0.1808	?	-
Berkeley 86	28	LS II +38 39	20:18:59.4	+38:57:14	-	B1III	10.057	0.179	0.2286	-	-
Berkeley 86	323	2MASS J20194609+3851325	20:19:46.1	+38:51:32	-	-	12.855	0.372	0.1381	-	-
Berkeley 87	55	LS II +36 70	20:22:53.3	+37:06:46	-	OB-	11.093	0.063	0.2158	-	-
Berkeley 87	338	UCAC3 255-208501	20:24:26.8	+37:19:33	-	-	13.468	0.333	0.1986	-	-
NGC 6913	17	HD 229171	20:23:02.9	+38:27:21	-	B2IV	9.380	0.057	0.2855	-	-
NGC 7510	40	LS III +60 58	23:16:12.3	+60:27:24	Markarian 50	OB	10.663	0.053	0.2138	-	-
NGC 7510	84	LS III +60 59	23:16:33.1	+60:28:48	-	OB	11.629	0.050	0.1928	-	-
NGC 7510	232	2MASS J23175230+6025022	23:17:52.3	+60:25:02	-	-	12.725	0.111	0.1651	-	-
NGC 7510	1337	2MASS J23163318+6031477	23:16:33.2	+60:31:48	-	-	15.188	0.489	0.1520	-	-
NGC 869/884	42	V665 Per	02:18:48.0	+57:17:08	NGC 869	B2V	9.441	0.089	0.2423	BCEP	0.2423
NGC 869/884	83	BD+56 586	02:22:36.3	+57:04:54	-	B1V	9.986	0.070	0.1621	-	-
NGC 957	38	TYC 3695-212-1	02:30:34.3	+57:36:34	NGC 957	-	10.819	0.072	0.1904	-	-

Table 3: Observed SPB variables.

Field	ID	Designation	RA J2000	DEC J2000	Cluster membership	Spectral type	V (mag)	Amp. (mag)	Period (days)	VSX info	VSX period (days)
Berkeley 87	118	TYC 2684-312-1	20:23:24.7	+37:13:54	-	-	11.973	0.084	0.8602	-	-
Berkeley 87	240	2MASS J20234453+3713410	20:23:44.5	+37:13:41	Berkeley 87	-	13.048	0.146	3.0662	-	-
Cygnus OB2	81	[MT91] 615	20:33:42.1	+41:07:54	-	B2V	11.405	0.079	0.8139	-	-
Cygnus OB2	190	[MT91] 626	20:33:45.0	+41:22:32	-	-	12.541	0.108	1.1100	-	-
Cygnus OB2	229	[MT91] 29	20:30:53.5	+41:27:01	-	-	12.813	0.120	1.3136	-	-
Gemini OB1	44	HD 252944	06:11:27.7	+23:13:53	-	B9	10.869	0.228	0.3852	-	-
NGC 6913	30	HD 229253	20:24:25.2	+38:29:07	-	B5IV	10.155	0.033	1.5719	-	-

Table 3: continued.

Field	ID	Designation	RA J2000	DEC J2000	Cluster membership	Spectral type	V (mag)	Amp. (mag)	Period (days)	VSX info	VSX period (days)
NGC 6913	36	LS II +38 67	20:22:41.8	+38:10:38	NGC 6913	B3III	10.642	0.064	0.7952	—	—
NGC 6913	1148	HD 229271	20:24:45.9	+37:59:34	—	B9	10.623	0.061	1.3757	—	—
NGC 7510	25	BD+59 2692	23:17:27.3	+60:15:00	—	B7II	9.849	0.058	1.3032	—	—
NGC 7510	35	TYC 4279-2213-1	23:17:48.0	+60:26:49	—	—	10.415	0.040	0.8982	—	—
NGC 7510	482	WRAM 37	23:17:00.7	+60:31:03	—	—	13.547	0.171	3.0937	—	—
NGC 7654	14	BD+60 2549	23:28:10.0	+61:09:06	—	B7V	9.433	0.072	1.2710	—	—
NGC 869/884	30	V359 Per	02:20:15.7	+57:05:55	—	B1.5III	9.060	0.086	1.2309	BCEP:	—
NGC 957	13	BD+56 640	02:31:08.4	+57:31:37	NGC 957	B2III:	9.607	0.100	1.7070	—	—
PZ Cas	404	2MASS J23493339+6157236	23:49:33.4	+61:57:24	—	—	13.245	0.194	1.0504	—	—

Table 4: Observed Cepheid variables.

Field	ID	Designation	RA J2000	DEC J2000	Cluster membership	Spectral type	V (mag)	Amp. (mag)	Period (days)	VSX info	VSX period (days)
Berkeley 86	65	V1319 Cyg	20:20:51.1	+39:00:45	—	K0I*	11.240	0.944	41.3353	SRA	41.8700
NGC 663	28	BY Cas	01:47:11.9	+61:25:21	—	F4Ib	10.369	0.414	3.2221	DCEPS	3.2215
NGC 6913	99	NSVS 5731720	20:23:21.7	+38:00:07	—	k3V:	12.009	0.425	3.2061	CEP	3.2046
NGC 6913	309	NGC 6913 36	20:23:41.2	+38:27:00	—	f	14.032	0.535	3.4379	—	—
NGC 7654	234	PW Cas	23:25:58.5	+61:16:01	—	F8/G0	13.061	0.713	3.9999	DCEP	3.9999
P Cygni	18	TYC 3152-1813-1	20:20:47.1	+38:17:07	—	—	9.987	0.141	2.5164	CEP	2.5137
P Cygni	405	2MASS J20173903+3804143	20:17:39.0	+38:04:14	—	—	13.591	0.506	5.0511	—	—

Table 5: Observed γ Doradus variables.

Field	ID	Designation	RA J2000	DEC J2000	Cluster membership	Spectral type	V (mag)	Amp. (mag)	Period (days)	V SX info	V SX period (days)
NGC 581	7	V1132 Cas	01:33:45.5	+60:37:23	-	F1	8.157	0.097	0.6257	GDOR	0.6258

Table 6: Observed WR variables.

Field	ID	Designation	RA J2000	DEC J2000	Cluster membership	Spectral type	V (mag)	Amp. (mag)	Period (days)	V SX info	V SX period (days)
Berkeley 86	3	V444 Cyg	20:19:32.4	+38:43:54	-	WN5+O6II-V	7.973	0.336	4.2130	EA/WR	4.2124
Berkeley 87	21	WR 141	20:21:31.7	+36:55:13	-	WN5-w+O5V-III	9.840	0.108	-	WR	-
PZ Cas	66	WR 158	23:43:30.6	+61:55:48	-	WN7	11.282	0.073	-	-	-

Table 7: Observed α Cyg variables.

Field	ID	Designation	RA J2000	DEC J2000	Cluster membership	Spectral type	V (mag)	Amp. (mag)	Period (days)	V SX info	V SX period (days)
Berkeley 87	7	HD 229059	20:21:15.4	+37:24:31	-	B2Iabe	8.761	0.136	8.1319	BE	-
Cygnus OB2	33	Schulte 12	20:32:41.0	+41:14:29	FSR 0236	B3.5Ia+	11.702	0.126	-	?	-
Cygnus OB2	35	Schulte 19	20:33:39.1	+41:19:26	Cygnus OB2	B0Iab	10.944	0.063	-	IS:	-
Cygnus OB2	43	[CPR2002] A23	20:30:39.7	+41:08:49	-	B0.7Ib	11.296	0.085	-	-	-
Cygnus OB2	1512	Schulte 18	20:33:30.8	+41:15:23	-	B1Ib	10.860	0.093	-	-	-
EO Per	7	BD+56 733	02:52:40.7	+57:27:52	-	BIII-III*	9.711	0.048	-	-	-
Gemini OB1	1	PU Gem	06:09:44.0	+23:06:49	-	B3Ia	5.749	0.102	-	ACYG	6.8066
NGC 663	5	LS I +61 232	01:46:23.8	+61:15:30	NGC 663	B5Ib	8.472	0.055	-	-	-

Table 7: continued.

Field	ID	Designation	RA J2000	DEC J2000	Cluster membership	Spectral type	V (mag)	Amp. (mag)	Period (days)	VSX info	VSX period (days)
NGC 663	13	LSI +60 183	01:45:56.1	+61:14:05	—	B8Iab	8.928	0.054	—	—	—
NGC 6913	2	HD 194153	20:22:35.6	+38:07:46	—	B1Ia	8.542	0.061	—	—	—
NGC 6913	4	HD 229238	20:24:04.7	+38:32:17	NGC 6913	B0.5Ia	8.942	0.050	—	E:	—
NGC 869/884	1	HD 14433	02:21:55.4	+57:14:35	—	A0I	6.870	0.084	—	?	—
NGC 869/884	2	V551 Per	02:16:51.7	+57:03:19	NGC 869	B1Iab	6.526	0.101	—	ACYG	5.6430
NGC 869/884	3	V520 Per	02:19:04.5	+57:08:08	—	B3I	6.670	0.105	—	IA	1.6254
NGC 869/884	4	HD 14143	02:19:13.9	+57:10:09	—	B3I	6.753	0.102	0.5321	VAR	0.0892
NGC 869/884	5	HD 14542	02:23:00.4	+57:23:13	NGC 869	B8I	7.078	0.103	—	?	—
NGC 869/884	7	V553 Per	02:22:53.5	+57:14:43	—	A2I	7.540	0.152	—	ACYG:	—
NGC 869/884	9	HD 13841	02:16:46.4	+57:01:46	—	B1.5Ib	7.435	0.070	—	?	—
NGC 869/884	13	HD 14443	02:22:00.6	+57:08:42	NGC 869	B1.5II	8.109	0.066	—	?	—
NGC 869/884	25	V757 Per	02:18:23.1	+57:00:37	—	B0.7I	8.477	0.065	0.2453	BCEP	0.1643
NGC 869/884	29	V424 Per	02:21:50.8	+57:23:12	—	B1Ie	8.747	0.057	—	GCAS:	—
NGC 869/884	59	BD+56 596	02:23:11.6	+57:10:20	—	B0II-III*	9.553	0.087	—	?	—
NGC 869/884	195	NSV 776	02:18:57.7	+57:08:18	NGC 869	B2.5II	11.020	0.152	—	BCEP:	—
NGC 957	4	V475 Per	02:26:45.7	+57:40:45	—	B1.5Ia	7.253	0.124	—	ACYG	1.3666
NGC 957	6	HD 15620	02:32:52.9	+57:55:46	—	B8Iab	8.395	0.076	—	?	—
NGC 957	7	HD 15571	02:32:24.8	+57:25:44	—	B1II	8.425	0.065	—	—	—
P Cygni	2	HD 193183	20:17:22.8	+38:14:09	—	B1.5Ib	7.021	0.082	—	?	—
PZ Cas	9	BD+61 2529	23:48:30.0	+61:59:20	—	B1.1Ib	8.680	0.069	—	?	—
PZ Cas	14	BD+60 2615	23:44:42.1	+61:40:05	—	B0.2(I)	9.142	0.061	—	—	—
PZ Cas	20	BD+61 2531	23:48:35.9	+62:14:46	—	B1.2(II)	9.421	0.045	—	—	—

Table 8: Observed variable Be stars.

Field	ID	Designation	RA J2000	DEC J2000	Cluster membership	Spectral type	V (mag)	Amp. (mag)	Period (days)	VSX info	VSX period (days)
Berkeley 87	112	VES 203	20:21:24.9	+37:22:48	-	B0/1Ve	12.141	0.194*	-	?	-
Berkeley 87	124	TYC 2684-476-1	20:21:54.5	+37:00:00	-	em	12.226	0.133	-	-	-
Berkeley 87	462	AS 407	20:21:28.4	+37:26:20	-	B2e	14.228	0.356*	-	-	-
Cygnus OB2	109	[MT91] 213	20:32:13.1	+41:27:24	FSR 0236	B0V	11.266	0.534*	-	BE	-
Cygnus OB2	121	Schulte 30	20:34:43.6	+41:29:05	-	B2IIIe	12.240	0.220*	-	-	-
EO Per	35	EO Per	02:50:38.6	+57:20:10	-	B0ea	10.938	0.872*	-	ISA	-
IC 1805	44	KM Cas	02:29:30.5	+61:29:44	-	B0III	11.219	0.253*	-	SDOR:	-
NGC 581	72	NGC 581 2	01:33:24.3	+60:39:45	-	B2Ve	11.270	0.179	-	?	-
NGC 581	2947	V1122 Cas	01:33:15.1	+60:41:00	-	B0/1Ve	9.712	0.357*	-	BE	-
NGC 663	18	BD+60 358	01:49:38.6	+61:03:02	-	B1Ve*	9.231	0.098	-	-	-
NGC 663	26	BD+60 344	01:46:34.0	+61:09:02	-	B2V	10.043	0.226*	-	-	-
NGC 663	27	V972 Cas	01:45:18.0	+61:06:56	-	B1Ve	10.083	0.081	-	BE	-
NGC 663	32	V985 Cas	01:46:35.5	+61:15:48	-	B2Ve	10.286	0.232*	-	BE	-
NGC 663	46	BD+60 307	01:41:46.5	+61:19:30	-	B2Ve	10.657	0.106	-	-	-
NGC 663	50	V983 Cas	01:46:27.7	+61:12:25	-	Be	10.538	0.317*	-	BE	-
NGC 663	56	LSI +61 238	01:48:23.1	+61:15:53	-	B2Ve	10.867	0.158	-	-	-
NGC 663	96	LSI +60 188	01:46:57.6	+61:01:40	-	B(e)	11.525	0.102	-	-	-
NGC 663	104	LSI +61 220	01:43:40.8	+61:19:47	-	OBe:	11.914	0.298*	-	-	-
NGC 663	122	V975 Cas	01:45:46.4	+61:09:21	-	B1Ve	11.937	0.168	-	BE	-
NGC 663	173	TYC 4032-1819-1	01:46:35.6	+61:13:39	-	B1Ve	12.311	0.149	-	-	-
NGC 663	179	V986 Cas	01:47:03.7	+61:17:32	-	B2Ve	12.281	0.154	-	BE	-
NGC 663	193	V973 Cas	01:45:37.8	+61:07:59	-	B2Ve	12.135	0.295*	-	BE	-
NGC 663	196	V974 Cas	01:45:39.6	+61:12:59	-	B2Ve	12.451	0.105	-	BE	-
NGC 663	2279	V831 Cas	01:47:00.2	+61:21:24	-	B1IIIe	11.366	0.130	-	HMXB/XP	-
NGC 663	2285	V976 Cas	01:45:56.1	+61:12:45	-	B2Ve	12.008	0.113	-	BE	-
NGC 663	2286	V980 Cas	01:46:20.2	+61:14:22	-	B2Ve	11.985	0.158*	-	BE	-
NGC 663	2287	V984 Cas	01:46:30.6	+61:14:29	-	B1Ve	12.085	0.243*	-	BE	-

Table 8: continued.

Field	ID	Designation	RA J2000	DEC J2000	Cluster membership	Spectral type	V (mag)	Amp. (mag)	Period (days)	VSX info	VSX period (days)
NGC 663	2291	V981 Cas	01:46:26.8	+61:07:42	-	B0/1Ve	10.665	0.138	-	BE	-
NGC 663	2317	V978 Cas	01:46:06.1	+61:13:39	-	B0/1Ve	11.509	0.258	-	BE	-
NGC 6913	12	V1322 Cyg	20:23:46.0	+38:30:03	-	B0.2IIIe	9.281	0.040	-	GCAS	-
NGC 6913	91	TYC 3152-1008-1	20:22:19.0	+38:01:48	-	em	11.871	0.160*	-	-	-
NGC 7510	16	HD 218941	23:11:14.8	+60:34:22	NGC 7510	OB+e:	9.678	0.052	-	-	-
NGC 7510	85	TYC 4279-2067-1	23:10:47.5	+60:31:53	-	B0Ve	11.766	0.108	0.5820	-	-
NGC 7654	46	LS III +61 27	23:21:11.4	+61:31:33	-	OB:e:	11.419	0.230	-	-	-
NGC 869/884	31	V356 Per	02:16:57.7	+57:07:49	-	B1III/Ve	9.139	0.163	0.3420	BCEP:	-
NGC 869/884	45	V506 Per	02:21:43.4	+57:07:33	-	B0Ve	9.491	0.433*	-	BE	-
NGC 869/884	51	V502 Per	02:17:44.7	+56:54:00	-	B1Ve	9.560	0.149	-	BE	-
NGC 869/884	53	BD+56 582	02:22:22.7	+57:17:05	-	B1III	9.664	0.196*	-	GCAS	-
NGC 869/884	55	BD+56 534	02:19:26.5	+57:04:42	-	B0Ve	9.649	0.124	-	-	-
NGC 869/884	63	BD+56 493	02:18:18.4	+56:51:02	-	B1IV/Ve	9.686	0.145*	-	-	-
NGC 869/884	65	V503 Per	02:20:39.0	+57:18:43	-	B1.5IIIe	9.811	0.182*	-	BE	-
NGC 869/884	66	V504 Per	02:21:18.1	+57:18:22	-	B1IIIe	9.882	0.379*	-	BE	-
NGC 869/884	87	V507 Per	02:21:52.9	+57:09:59	NGC 869	B0/1Ve	9.822	0.256	-	BE	-
NGC 869/884	89	BD+56 529	02:19:13.7	+57:07:44	-	B1Ve	10.202	0.121	-	?	-
NGC 869/884	102	NGC 884 2649	02:23:04.2	+57:07:39	-	B2e	10.428	0.141	-	-	-
NGC 869/884	104	NGC 884 2804	02:23:33.1	+57:04:33	-	OBe	10.435	0.219*	-	-	-
NGC 869/884	106	BD+56 516	02:18:54.3	+57:09:30	-	B2V	10.386	0.143	-	-	-
NGC 869/884	107	MWC 448	02:23:24.9	+57:19:03	-	B2IIIe	10.763	0.257*	78.5370	-	-
NGC 869/884	112	MWC 447	02:22:47.0	+56:58:06	-	B0e	10.593	0.106	-	-	-
NGC 869/884	123	MWC 39	02:22:04.6	+57:10:39	-	B1.5III	10.645	0.115	-	GCAS:	-
NGC 869/884	130	MWC 711	02:22:48.1	+57:12:01	-	B0/1Ve	10.443	0.204	-	-	-
NGC 869/884	149	LS V +57 16	02:21:57.4	+57:20:22	NGC 869	OB-	10.783	0.206	-	GCAS	-
NGC 869/884	203	NGC 869 1438	02:19:47.8	+57:06:40	-	B2e	11.362	0.317*	-	-	-
NGC 869/884	212	NGC 884 2085	02:21:42.9	+57:05:31	-	B3	11.368	0.162	-	-	-
NGC 869/884	285	NGC 869 1278	02:19:28.9	+57:11:24	-	B0/1Ve	11.694	0.384*	-	GCAS	-
NGC 869/884	4167	NGC 884 1772	02:20:52.8	+57:13:28	-	B2e	11.443	0.211	-	-	-

Table 8: continued.

Field	ID	Designation	RA J2000	DEC J2000	Cluster membership	Spectral type	V (mag)	Amp. (mag)	Period (days)	VSX info	VSX period (days)
NGC 957	46	LS V +57 46	02:33:10.6	+57:32:54	-	B0/1Ve	11.218	0.322*	-	-	-
P Cygni	10	HD 193516	20:19:07.5	+37:46:10	-	BN0.7IVp	8.583	0.076	-	?	-
P Cygni	61	LS II +37 47	20:17:30.2	+38:05:56	-	B5III	10.970	0.210*	-	-	-
PZ Cas	3	V818 Cas	23:49:53.1	+62:12:51	-	B2.3(III)ne	7.800	0.203*	-	BE	-
PZ Cas	8	HD 223044	23:46:00.4	+61:59:28	-	em	8.466	0.089*	-	-	-
PZ Cas	190	GSC 04284-00313	23:41:45.7	+62:04:34	-	em	12.549	0.216	-	-	-

Notes. Be stars with photometric outbursts are marked with an asterisk (*) behind their amplitude value.

Table 9: Observed variable late-type stars.

Field	ID	Designation	RA J2000	DEC J2000	Cluster membership	Spectral type	V (mag)	Amp. (mag)	Period (days)	VSX info	VSX period (days)
Berkeley 86	1	HD 193469	20:18:57.5	+39:00:14	-	K4.5Ib	6.408	0.099	-	?	-
Berkeley 86	18	HD 228689	20:16:23.2	+38:48:16	-	M4	9.792	0.142	-	-	-
Berkeley 87	10	BC Cyg	20:21:38.5	+37:31:59	Berkeley 87	M4I	9.799	0.543	-	SRC	700
Berkeley 87	12	BI Cyg	20:21:21.9	+36:55:56	Berkeley 87	M2/4I	9.526	0.401	-	LC	-
Berkeley 87	23	HD 229105	20:21:56.2	+37:21:29	-	K2II	9.955	0.037	-	-	-
EO Per	3	V648 Cas	02:51:03.9	+57:51:20	-	M2I:	9.189	0.393	-	LC	-
EO Per	5	V637 Cas	02:56:53.2	+57:33:25	-	M1Ib:	9.719	0.138	-	LC	-
EO Per	253	IRAS 02475+5704	02:51:13.9	+57:16:49	-	C	14.4490	9.11	-	L	193
EO Per	354	V500 Cas	02:51:33.0	+57:50:34	-	C	13.7961	5.31	268	M	250
Gemini OB1	2	BU Gem	06:12:19.1	+22:54:31	-	M1-M2Ia-Iab	6.413	0.431	513.8820	SRC	325
Gemini OB1	3	WY Gem	06:11:56.3	+23:12:26	-	M2Iapeb	7.388	0.249	-	LC+E:	23550
Gemini OB1	7	HD 253017	06:11:45.5	+23:01:49	-	M0Ib	9.230	0.116	-	-	-
Gemini OB1	10	HD 252505	06:09:54.8	+22:57:37	-	M5III	10.0690	0.329	-	SRB	64
Gemini OB1	12	HD 253178	06:12:28.9	+22:50:53	-	M2III	10.3050	0.199	-	DCEP-FUI/SR	24

Table 9: continued.

Field	ID	Designation	RA J2000	DEC J2000	Cluster membership	Spectral type	V (mag)	Amp. Period (mag) (days)	VSX info	VSX period (days)
Gemini OB1	34	GSC 01877-01435	06:09:02.3+23:15:46		-	M5III	11.6290.535	41.3160	MISC	42
IC 1805	33	IRAS 02254+6112	02:29:14.0+61:25:54		-	M5	11.4280.237	29.8360	-	-
NGC 581	11	BD+59 274	01:33:29.2+60:38:48		-	M0.5Ib-II	8.543 0.101	-	?	-
NGC 581	36	TYC 4031-1368-1	01:33:33.9+60:42:59		-	M4Iab:	10.9050.236	22.5632	-	-
NGC 581	130	V 472 Cas	01:33:31.9+60:32:47		-	M4:*	12.3710.631	70.2096	LB	-
NGC 663	3	BD+60 327	01:45:38.8+61:02:23		-	K0:III:	8.277 0.138	63.3533	-	-
NGC 663	4	BD+60 321	01:44:21.1+61:17:51		-	K0III	8.256 0.026	-	-	-
NGC 663	8	MLR 106	01:43:10.1+60:55:54		-	G2III	8.977 0.078	-	-	-
NGC 663	9	AZ Cas	01:42:16.5+61:25:16		-	M0Ib:ep+B	9.268 0.311	-	EA/GS	3402
NGC 663	10	V 589 Cas	01:46:05.5+60:59:37		-	M3Iab-Ib	8.886 0.286	-	LC	-
NGC 6913	20	HD 229152	20:22:43.0+38:28:17		-	K2III	9.773 0.037	-	-	-
NGC 6913	87	TYC 3152-1467-1	20:24:17.2+38:31:14		-	G5III	11.8590.084	-	VAR:	-
NGC 6913	164	IRAS 20238+3746	20:25:44.0+37:56:50		-	m4III	13.1680.220	-	-	-
NGC 6913	178	IKY Cyg	20:25:58.1+38:21:08		-	M3Ia	11.3081.108	-	LC	-
NGC 7510	5	HD 240254	23:18:19.2+60:16:22		-	M2	9.105 0.139	-	-	-
NGC 7510	8	BD+59 2678	23:14:51.3+60:44:57	FSR 0422	-	M2Iab	9.506 0.132	-	-	-
NGC 7510	11	V 356 Cep	23:13:31.5+60:30:19		-	M2Ib	10.0610.228	497.72	LC	-
NGC 7510	275	V 563 Cas	23:16:55.3+60:26:01		-	M8.5	15.0062.377	-	M	543
NGC 7510	235	70Q Cep	23:12:57.0+60:34:38		-	M7	12.8253.476	384.9370	SRB	370
NGC 7654	6	BD+60 2524	23:21:29.1+61:06:43		-	G8III	8.824 0.072	-	-	-
NGC 7654	17	TYC 4279-1503-1	23:23:46.1+61:05:55		-	M4	10.4610.144	24.0044	-	-
NGC 7654	26	TYC 4280-1353-1	23:27:39.0+61:17:28	Czemik 43	-	M6	10.8280.257	40.4007	-	-
NGC 7654	70	V 433 Cas	23:25:12.0+61:19:29		-	M6	12.1270.389	-	RCB:	-
NGC 869/884	6	AD Per	02:20:29.0+56:59:35	NGC 869	-	M2I	8.102 0.359	-	SRC	362
NGC 869/884	8	FZ Per	02:20:59.6+57:09:30		-	M0I	8.164 0.250	-	SRC	184
NGC 869/884	10	V 439 Per	02:23:11.1+57:11:58		-	M0I	8.281 0.168	-	LC	-
NGC 869/884	12	V 403 Per	02:23:24.1+57:12:43	NGC 869	-	M0I	8.581 0.151	-	LC:	-
NGC 869/884	16	RS Per	02:22:24.0+57:06:33		-	M4I	8.555 0.932	-	-	-
NGC 869/884	18	BU Per	02:18:53.3+57:25:17		-	M3I	9.368 0.690	411.7000	SRC	367

Table 9: continued.

Field	ID	Designation	RA J2000	DEC J2000	Cluster membership	Spectral type	V (mag)	Amp. (mag)	Period (days)	VSX info	VSX period (days)
NGC 869/884	232	2MASS J02163833+570512402	16:38.3+57:05:13		-	M2:*	12.0810.732	0.0	-	-	-
P Cygni	249	SI * 642	20:16:58.1+38:07:26		-	S	13.1830.659	-	-	-	-
PZ Cas	4	PZ Cas	23:44:03.3+61:47:22	Stock 17		M3Ia	8.990 0.620	-	-	SRC	925
Berkeley 87	128	2MASS J20254911+373218220	25:49.1+37:32:18	MWSC 3336		-	12.9120.354	29.5716	-	-	-
Berkeley 87	171	2MASS J20225899+370513120	22:59.0+37:05:13		-	-	13.1560.132	-	-	-	-
Berkeley 87	262	IRAS 20236+3725	20:25:30.9+37:35:35		-	-	14.0110.447	41.6787	-	-	-
Berkeley 87	312	2MASS J20255026+370146520	25:50.3+37:01:46		-	-	14.9840.793	-	-	L:	179
EO Per	428	IRAS 02472+5710	02:50:54.9+57:22:35		-	-	15.1500.815	-	-	L	-
EO Per	432	2MASS J02550398+575042502	55:04.0+57:50:42		-	-	14.7930.554	-	-	-	-
IC 1805	164	2MASS J02334807+614203602	33:48.1+61:42:04		-	-	13.6010.378	74.51	-	-	-
NGC 581	46	TYC 4031-754-1	01:39:19.3+60:39:38		-	-	11.1780.512	122.3	-	-	-
NGC 7510	854	2MASS J23140953+605033523	14:09.5+60:50:34		-	-	15.2330.488	-	-	-	-
NGC 7654	116	IRAS 23260+6106	23:28:20.4+61:23:19		-	-	12.3930.537	253.7790	-	-	-
NGC 7654	136	IRAS 23269+6105	23:29:10.2+61:22:16		-	-	12.6730.305	38.4499	-	-	-
NGC 7654	686	2MASS J23212953+612144123	21:29.5+61:21:44		-	-	14.8541.104	172.8580	-	-	-
NGC 7654	1340	IRAS 23260+6101	23:28:22.0+61:18:03		-	-	15.0121.197	-	-	-	-
NGC 869/884	405	IRAS 02133+5644	02:16:56.4+56:58:18		-	-	13.1290.468	-	-	-	-
P Cygni	170	IRAS 20150+3808	20:16:51.9+38:18:21		-	-	12.8070.511	-	-	-	-
PZ Cas	98	2MASS J23465305+615529023	46:53.1+61:55:29		-	-	12.1890.575	-	-	-	-
PZ Cas	583	2MASS J23485763+620054923	48:57.6+62:00:55		-	-	14.3850.683	-	-	-	-

Table 10: Observed unclassified variable stars.

Field	ID	Designation	RA J2000	DEC J2000	Cluster membership	Spectral type	V (mag)	Amp. (mag)	Period (days)	VSX info	VSX period (days)
Berkeley 86	7	HD 228898	20:19:17.2	+38:25:50	-	K5	9.169	0.085	-	-	-
Berkeley 86	36	HD 228905	20:19:21.3	+38:24:41	Berkeley 86	OB-	10.229	0.125	-	-	-

Table 10: continued.

Field	ID	Designation	RA J2000	DEC J2000	Cluster membership	Spectral type	V (mag)	Amp. (mag)	Period (days)	VSX info	VSX period (days)
Berkeley 87	4	HD 194709	20:25:42.1	+37:08:43	-	K2	8.387	0.036	-	-	-
Berkeley 87	24	BD+37 3927	20:25:06.9	+37:27:56	-	O8.5I	10.177	0.051	-	-	-
Berkeley 87	26	LS II +37 83	20:22:58.3	+37:14:05	-	OB	10.169	0.036	-	-	-
Berkeley 87	35	LS II +36 66	20:21:37.9	+37:08:15	-	OB	10.621	0.042	-	-	-
Berkeley 87	41	TYC 2684-1267-1	20:20:56.3	+37:07:32	-	K5V*	11.189	0.071	-	-	-
Berkeley 87	49	HD 229142	20:22:32.2	+36:55:55	-	A	10.603	0.040	-	-	-
Berkeley 87	71	TYC 2697-169-1	20:25:02.9	+37:26:36	-	OB:	11.526	0.094	3.7068	-	-
Berkeley 87	92	2MASS J20222298+3712557	20:22:23.0	+37:12:56	-	-	11.796	0.077	0.6094	-	-
Cygnus OB2	10	BD+40 4241	20:35:06.9	+41:20:01	-	-	9.718	0.040	-	-	-
Cygnus OB2	14	Schulte 8C	20:33:18.0	+41:18:31	Cygnus OB2	O5III	10.115	0.039	-	-	-
Cygnus OB2	34	TYC 3161-1060-1	20:33:03.5	+41:27:15	-	-	10.761	0.041	34.7074	-	-
Cygnus OB2	94	Schulte 8D	20:33:16.3	+41:19:02	-	O8.5V	11.920	0.099	-	-	-
Cygnus OB2	126	TYC 3161-1170-1	20:30:01.9	+41:28:21	-	-	11.850	0.084	-	-	-
Cygnus OB2	197	[MT91] 152	20:31:51.3	+41:23:23	-	G3V	12.674	0.144	-	-	-
Cygnus OB2	212	[MT91] 115	20:31:37.3	+41:23:36	FSR 0236	G6V	12.951	0.127	-	-	-
EO Per	8	BD+56 739	02:54:50.8	+57:26:36	-	B2III	9.704	0.054	-	-	-
EO Per	17	TYC 3709-420-1	02:53:28.5	+57:48:41	-	A1V*	10.590	0.064	-	-	-
EO Per	62	2MASS J02505003+5752025	02:50:50.0	+57:52:03	-	-	12.676	0.120	-	-	-
EO Per	161	2MASS J02532561+5734465	02:53:25.6	+57:34:46	-	-	13.567	0.167	-	-	-
EO Per	193	2MASS J02505080+5746415	02:50:50.8	+57:46:42	-	-	13.835	0.211	22.7993	-	-
EO Per	201	2MASS J02554267+5721199	02:55:42.7	+57:21:20	-	-	13.571	0.206	51.5116	-	-
NGC 581	2935	BD+59 288	01:37:29.0	+60:34:57	-	F2	10.231	0.101	-	-	-
NGC 663	15	LS I +60 191	01:47:20.2	+61:07:55	NGC 663	B2V	9.068	0.045	-	-	-
NGC 663	41	TYC 4032-2137-1	01:46:07.0	+61:11:51	-	B3	10.471	0.066	-	-	-
NGC 663	86	TYC 4032-3085-1	01:49:43.6	+61:25:40	-	G0	11.468	0.090	-	-	-
NGC 663	90	TYC 4032-1627-1	01:49:07.2	+61:05:21	NGC 663	B3	11.445	0.066	-	-	-
NGC 663	105	TYC 4031-1261-1	01:41:59.4	+61:21:23	-	-	11.732	0.094	-	-	-
NGC 663	184	V1156 Cas	01:46:39.8	+61:09:52	-	-	12.303	0.096	-	BCEP	0.2764
NGC 663	524	2MASS J01471474+6127387	01:47:14.7	+61:27:39	-	-	14.110	0.373	47.7310	-	-

Table 10: continued.

Field	ID	Designation	RA J2000	DEC J2000	Cluster membership	Spectral type	V (mag)	Amp. (mag)	Period (days)	VSX info	VSX period (days)
NGC 6913	6	HD 229153	20:22:45.3	+37:57:41	-	O9.7III	9.132	0.040	-	-	-
NGC 6913	8	HD 194356	20:23:47.1	+37:58:58	-	B9.5V	8.625	0.031	-	-	-
NGC 6913	24	TYC 3152-196-1	20:25:02.9	+38:02:35	-	k0.5III	10.222	0.037	-	-	-
NGC 6913	40	HD 229233	20:23:59.0	+38:33:36	-	A4V	10.590	0.039	-	?	-
NGC 6913	41	LS II +37 93	20:25:58.8	+38:08:46	-	OB-	10.811	0.046	-	-	-
NGC 6913	48	LS II +38 62	20:22:07.6	+38:23:51	-	B5III	10.745	0.053	-	-	-
NGC 6913	76	TYC 3152-1235-1	20:24:55.2	+38:33:27	-	F5	11.352	0.053	-	-	-
NGC 6913	108	2MASS J20223358+3804105	20:22:33.6	+38:04:11	-	f2IV	11.703	0.056	-	-	-
NGC 6913	127	TYC 3152-450-1	20:23:04.7	+38:26:57	-	A5	12.006	0.059	-	VAR:	-
NGC 6913	150	TYC 3152-340-1	20:25:08.7	+38:29:23	-	A6IV	12.149	0.110	0.5274	-	-
NGC 6913	300	2MASS J20242110+3810010	20:24:21.1	+38:10:01	-	g:	13.272	0.145	4.8150	-	-
NGC 7510	7	HD 240221	23:12:12.2	+60:39:59	-	B5III	8.765	0.043	-	-	-
NGC 7510	12	TYC 4279-711-1	23:11:30.2	+60:47:02	-	-	9.720	0.075	-	-	-
NGC 7510	14	TYC 4279-334-1	23:16:00.9	+60:18:41	-	G5IV	9.638	0.028	-	-	-
NGC 7510	22	LS III +60 53	23:13:11.0	+60:42:20	-	B	10.392	0.088	-	-	-
NGC 7510	44	LS III +59 52	23:14:02.9	+60:14:34	-	OB-	10.681	0.031	-	-	-
NGC 7510	45	TYC 4279-2508-1	23:17:52.2	+60:32:19	-	A3III	10.696	0.040	-	-	-
NGC 7510	48	2MASS J23175940+6047486	23:17:59.4	+60:47:49	-	-	11.402	0.108	101.6920	-	-
NGC 7510	57	TYC 4279-2336-1	23:13:49.0	+60:23:59	-	-	11.111	0.043	-	-	-
NGC 7510	75	2MASS J23181916+6019065	23:18:19.2	+60:19:07	-	-	11.859	0.102	-	-	-
NGC 7510	77	TYC 4279-1959-1	23:18:18.0	+60:36:43	-	-	11.326	0.055	-	-	-
NGC 7510	95	GSC 04279-02000	23:10:27.6	+60:31:07	-	K0	12.067	0.068	-	-	-
NGC 7510	116	TYC 4279-877-1	23:16:01.9	+60:11:48	-	-	11.806	0.052	-	-	-
NGC 7510	161	2MASS J23180979+6045083	23:18:09.8	+60:45:08	FSR 0422	-	12.282	0.092	-	-	-
NGC 7510	224	2MASS J23112618+6040222	23:11:26.2	+60:40:22	-	-	12.749	0.196	-	-	-
NGC 7510	375	2MASS J23165008+6018047	23:16:50.1	+60:18:05	-	-	13.273	0.155	0.3798	-	-
NGC 7510	2356	2MASS J23173196+6041026	23:17:32.0	+60:41:03	-	-	13.017	0.131	-	-	-
NGC 7654	5	BD+60 2537	23:25:09.3	+61:22:00	NGC 7654	K2	8.919	0.113	-	-	-
NGC 7654	56	TYC 4279-785-1	23:22:14.6	+61:41:31	-	F2	10.938	0.097	-	-	-

Table 10: continued.

Field	ID	Designation	RA J2000	DEC J2000	Cluster membership	Spectral type	V (mag)	Amp. (mag)	Period (days)	VSX info	VSX period (days)
NGC 7654	80	TYC 4279-218-1	23:24:37.6	+61:40:22	-	-	11.396	0.176	-	-	-
NGC 7654	172	V842 Cas	23:24:52.2	+61:36:30	-	-	11.927	0.215	-	SPB	-
NGC 869/884	46	HD 14604	02:23:37.8	+56:52:46	-	G0V	9.601	0.094	-	-	-
NGC 869/884	49	BD+56 556	02:21:11.6	+56:51:14	NGC 869	OB-	9.491	0.079	-	-	-
NGC 869/884	80	V619 Per	02:22:02.8	+57:08:25	-	B2III	9.910	0.109	-	BCEP	-
NGC 869/884	174	BD+56 509C	02:18:47.7	+57:14:23	-	G0IV	9.697	0.149	-	-	-
NGC 957	101	TYC 3695-992-1	02:33:08.2	+57:28:11	-	B2V	12.094	0.150	-	EB	0.4719
NGC 957	108	TYC 3695-728-1	02:33:30.9	+57:29:04	-	-	12.031	0.303	-	-	-
NGC 957	114	2MASS J02313244+5800022	02:31:32.5	+58:00:02	-	-	12.918	0.216	-	-	-
NGC 957	120	TYC 3695-758-1	02:27:19.6	+57:35:33	-	-	12.343	0.232	-	-	-
NGC 957	173	2MASS J02333778+5740241	02:33:37.8	+57:40:24	-	-	13.206	0.234	0.5077	-	-
PZ Cas	18	TYC 4284-117-1	23:42:42.8	+62:02:55	-	-	9.598	0.044	-	-	-
PZ Cas	19	BD+61 2508	23:43:41.9	+61:56:15	-	A0	9.320	0.038	-	-	-
PZ Cas	34	TYC 4281-1268-1	23:49:02.4	+61:40:59	-	-	10.905	0.070	-	-	-
PZ Cas	54	2MASS J23480174+6214074	23:48:01.7	+62:14:07	-	-	11.508	0.112	-	-	-
PZ Cas	99	TYC 4280-100-1	23:42:09.1	+61:46:41	-	-	11.730	0.170	-	-	-
PZ Cas	127	2MASS J23421700+6212376	23:42:17.0	+62:12:38	Stock 17	-	11.921	0.104	-	-	-
PZ Cas	151	2MASS J23441671+6153312	23:44:16.7	+61:53:31	-	-	12.169	0.129	-	-	-
PZ Cas	155	2MASS J23471857+6204011	23:47:18.6	+62:04:01	-	-	12.369	0.196	25.5706	-	-
PZ Cas	408	2MASS J23475095+6206318	23:47:51.0	+62:06:32	-	-	13.144	0.196	91.7307	-	-

Table 11: Variable stars not in VSX.

Field	ID	Designation	RA J2000	DEC J2000	Cluster membership	Spectral type	V (mag)	Amp. (mag)	Period (days)	Variability type
Berkeley 86	7	HD 228898	20:19:17.2	+38:25:50	-	K5	9.169	0.085	-	-
Berkeley 86	18	HD 228689	20:16:23.2	+38:48:16	-	M4	9.792	0.142	-	SR

Table 11: continued.

Field	ID	Designation	RA J2000	DEC J2000	Cluster membership	Spectral type	V (mag)	Amp. (mag)	Period (days)	Variability type
Berkeley 86	22	HD 228989	20:20:21.4	+38:42:00	-	O8.5V:+O9.7V:	9.686	0.091	1.7734	E
Berkeley 86	28	LS II +38 39	20:18:59.4	+38:57:14	-	B1III	10.057	0.179	0.2286	BCEP
Berkeley 86	36	HD 228905	20:19:21.3	+38:24:41	Berkeley 86	OB-	10.229	0.125	-	-
Berkeley 86	52	LS II +38 43	20:19:36.8	+38:35:21	Berkeley 86	B1V	10.676	0.148	1.9102	E
Berkeley 86	323	2MASS J20194609+3851325	20:19:46.1	+38:51:32	-	-	12.855	0.372	0.1381	BCEP
Berkeley 86	381	2MASS J20190590+3853009	20:19:05.9	+38:53:01	-	-	12.808	0.569	4.3262	E
Berkeley 87	4	HD 194709	20:25:42.1	+37:08:43	-	K2	8.387	0.036	-	-
Berkeley 87	23	HD 229105	20:21:56.2	+37:21:29	-	K2II	9.955	0.037	-	SR
Berkeley 87	24	BD+37 3927	20:25:06.9	+37:27:56	-	O8.5I	10.177	0.051	-	ACYG
Berkeley 87	26	LS II +37 83	20:22:58.3	+37:14:05	-	OB	10.169	0.036	-	-
Berkeley 87	35	LS II +36 66	20:21:37.9	+37:08:15	-	OB	10.621	0.042	-	-
Berkeley 87	41	TYC 2684-1267-1	20:20:56.3	+37:07:32	-	K5V*	11.189	0.071	-	-
Berkeley 87	49	HD 229142	20:22:32.2	+36:55:55	-	A	10.603	0.040	-	-
Berkeley 87	55	LS II +36 70	20:22:53.3	+37:06:46	-	OB-	11.093	0.063	0.2158	BCEP
Berkeley 87	71	TYC 2697-169-1	20:25:02.9	+37:26:36	-	OB:	11.526	0.094	3.7068	-
Berkeley 87	92	2MASS J20222298+3712557	20:22:23.0	+37:12:56	-	-	11.796	0.077	0.6094	-
Berkeley 87	118	TYC 2684-312-1	20:23:24.7	+37:13:54	-	-	11.973	0.084	0.8602	SPB
Berkeley 87	124	TYC 2684-476-1	20:21:54.5	+37:00:00	-	em	12.226	0.133	-	Be
Berkeley 87	128	2MASS J20254911+3732182	20:25:49.1	+37:32:18	MWSC 3336	-	12.912	0.354	29.5716	SR
Berkeley 87	131	TYC 2697-883-1	20:25:38.3	+37:03:11	-	-	12.188	0.183	1.8632	E
Berkeley 87	171	2MASS J20225899+3705131	20:22:59.0	+37:05:13	-	-	13.156	0.132	-	SR
Berkeley 87	203	2MASS J2022399+3658020	20:22:24.0	+36:58:02	Berkeley 87	-	12.940	0.198	20.3009	E
Berkeley 87	240	2MASS J20234453+3713410	20:23:44.5	+37:13:41	Berkeley 87	-	13.048	0.146	3.0662	SPB
Berkeley 87	251	2MASS J20215480+3654426	20:21:54.8	+36:54:43	-	-	13.324	0.376	6.4827	E
Berkeley 87	262	IRAS 20236+3725	20:25:30.9	+37:35:35	-	-	14.011	0.447	41.6787	SR
Berkeley 87	338	UCAC3 255-208501	20:24:26.8	+37:19:33	-	-	13.468	0.333	0.1986	BCEP
Berkeley 87	462	AS 407	20:21:28.4	+37:26:20	-	B2e	14.228	0.356	-	Be
Cygnus OB2	10	BD+40 4241	20:35:06.9	+41:20:01	-	-	9.718	0.040	-	-
Cygnus OB2	14	Schulte 8C	20:33:18.0	+41:18:31	Cygnus OB2	O5III	10.115	0.039	-	-

Table 11: continued.

Field	ID	Designation	RA J2000	DEC J2000	Cluster membership	Spectral type	V (mag)	Amp. (mag)	Period (days)	Variability type
Cygnus OB2	34	TYC 3161-1060-1	20:33:03.5	+41:27:15	-	-	10.761	0.041	34.7074	-
Cygnus OB2	42	Schulte 1	20:31:10.5	+41:31:54	Cygnus OB2	O8V	11.072	0.089	4.8523	E
Cygnus OB2	43	[CPR2002] A23	20:30:39.7	+41:08:49	-	B0.7Ib	11.296	0.085	-	ACYG
Cygnus OB2	81	[MT91] 615	20:33:42.1	+41:07:54	-	B2V	11.405	0.079	0.8139	SPB
Cygnus OB2	94	Schulte 8D	20:33:16.3	+41:19:02	-	O8.5V	11.920	0.099	-	-
Cygnus OB2	121	Schulte 30	20:34:43.6	+41:29:05	-	B2IIIe	12.240	0.220	-	Be
Cygnus OB2	126	TYC 3161-1170-1	20:30:01.9	+41:28:21	-	-	11.850	0.084	-	-
Cygnus OB2	173	TYC 3157-779-1	20:31:57.0	+41:12:34	-	-	12.529	0.073	-	E
Cygnus OB2	190	[MT91] 626	20:33:45.0	+41:22:32	-	-	12.541	0.108	1.1100	SPB
Cygnus OB2	197	[MT91] 152	20:31:51.3	+41:23:23	-	G3V	12.674	0.144	-	-
Cygnus OB2	212	[MT91] 115	20:31:37.3	+41:23:36	FSR 0236	G6V	12.951	0.127	-	-
Cygnus OB2	224	[MT91] 720	20:34:06.0	+41:08:09	-	B0.5V+B1.5V	13.415	0.241	4.3620	E
Cygnus OB2	229	[MT91] 29	20:30:53.5	+41:27:01	-	-	12.813	0.120	1.3136	SPB
Cygnus OB2	1498	2MASS J20304696+4106392	20:30:47.0	+41:06:39	-	-	13.781	0.379	8.6462	E
Cygnus OB2	1512	Schulte 18	20:33:30.8	+41:15:23	-	B1Ib	10.860	0.093	-	ACYG
EO Per	7	BD+56 733	02:52:40.7	+57:27:52	-	B1II-III*	9.711	0.048	-	ACYG
EO Per	8	BD+56 739	02:54:50.8	+57:26:36	-	B2III	9.704	0.054	-	-
EO Per	17	TYC 3709-420-1	02:53:28.5	+57:48:41	-	A1V*	10.590	0.064	-	-
EO Per	62	2MASS J02505003+5752025	02:50:50.0	+57:52:03	-	-	12.676	0.120	-	-
EO Per	98	2MASS J02504641+5734517	02:50:46.4	+57:34:52	-	-	12.438	0.115	-	E
EO Per	140	UCAC4 738-028961	02:53:00.5	+57:32:34	-	-	13.025	0.275	2.2368	E
EO Per	158	2MASS J02522011+5717211	02:52:20.1	+57:17:21	-	-	13.062	0.162	-	E
EO Per	161	2MASS J02532561+5734465	02:53:25.6	+57:34:46	-	-	13.567	0.167	-	-
EO Per	193	2MASS J02505080+5746415	02:50:50.8	+57:46:42	-	-	13.835	0.211	22.7993	-
EO Per	201	2MASS J02554267+5721199	02:55:42.7	+57:21:20	-	-	13.571	0.206	51.5116	-
EO Per	432	2MASS J02550398+5750425	02:55:04.0	+57:50:42	-	-	14.793	0.554	-	SR
Gemini OB1	7	HD 253017	06:11:45.5	+23:01:49	-	M0Ib	9.230	0.116	-	SR
Gemini OB1	44	HD 252944	06:11:27.7	+23:13:53	-	B9	10.869	0.228	0.3852	SPB
IC 1805	33	IRAS 02254+6112	02:29:14.0	+61:25:54	-	M5	11.428	0.237	29.8360	SR

Table 11: continued.

Field	ID	Designation	RA J2000	DEC J2000	Cluster membership	Spectral type	V (mag)	Amp. (mag)	Period (days)	Variability type
IC 1805	41	LSI +61 297	02:34:15.0	+61:24:40	-	B1V	10.937	0.244	3.3674	E
IC 1805	160	IC 1805 39	02:30:07.2	+61:31:08	-	A3V	12.864	0.438	1.7626	E
IC 1805	164	2MASS J02334807+6142036	02:33:48.1	+61:42:04	-	-	13.601	0.378	74.5100	SR
NGC 581	20	HD 236763	01:31:31.8	+60:33:36	NGC 581	B5	9.507	0.116	4.1740	E
NGC 581	36	TYC 4031-1368-1	01:33:33.9	+60:42:59	-	M4lab:	10.905	0.236	22.5632	SR
NGC 581	46	TYC 4031-754-1	01:39:19.3	+60:39:38	-	-	11.178	0.512	122.3000	SR
NGC 581	2935	BD+59 288	01:37:29.0	+60:34:57	-	F2	10.231	0.101	-	-
NGC 663	3	BD+60 327	01:45:38.8	+61:02:23	-	K0:III:	8.277	0.138	63.3533	SR
NGC 663	4	BD+60 321	01:44:21.1	+61:17:51	-	K0:III:	8.256	0.026	-	SR
NGC 663	5	LSI +61 232	01:46:23.8	+61:15:30	NGC 663	B5Ib	8.472	0.055	-	ACYG
NGC 663	8	MLR 106	01:43:10.1	+60:55:54	-	G2III	8.977	0.078	-	SR
NGC 663	13	LSI +60 183	01:45:56.1	+61:14:05	-	B8Iab	8.928	0.054	-	ACYG
NGC 663	15	LSI +60 191	01:47:20.2	+61:07:55	NGC 663	B2V	9.068	0.045	-	-
NGC 663	18	BD+60 358	01:49:38.6	+61:03:02	-	B1Ve*	9.231	0.098	-	Be
NGC 663	26	BD+60 344	01:46:34.0	+61:09:02	-	B2V	10.043	0.226	-	Be
NGC 663	41	TYC 4032-2137-1	01:46:07.0	+61:11:51	-	B3	10.471	0.066	-	-
NGC 663	46	BD+60 307	01:41:46.5	+61:19:30	-	B2Ve	10.657	0.106	-	Be
NGC 663	56	LSI +61 238	01:48:23.1	+61:15:53	-	B2Ve	10.867	0.158	-	Be
NGC 663	86	TYC 4032-3085-1	01:49:43.6	+61:25:40	-	G0	11.468	0.090	-	-
NGC 663	90	TYC 4032-1627-1	01:49:07.2	+61:05:21	NGC 663	B3	11.445	0.066	-	-
NGC 663	91	TYC 4032-2513-1	01:47:38.9	+61:01:04	-	B3	11.481	0.203	1.4957	E
NGC 663	96	LSI +60 188	01:46:57.6	+61:01:40	-	B(e)	11.525	0.102	-	Be
NGC 663	104	LSI +61 220	01:43:40.8	+61:19:47	-	OBe:	11.914	0.298	-	Be
NGC 663	105	TYC 4031-1261-1	01:41:59.4	+61:21:23	-	-	11.732	0.094	-	-
NGC 663	172	TYC 4032-2601-1	01:47:39.4	+61:18:21	-	B1Ve	12.383	0.168	-	E
NGC 663	173	TYC 4032-1819-1	01:46:35.6	+61:13:39	-	B1Ve	12.311	0.149	-	Be
NGC 663	200	2MASS J01441735+6116503	01:44:17.4	+61:16:50	-	-	12.541	0.295	1.5974	E
NGC 663	524	2MASS J01471474+6127387	01:47:14.7	+61:27:39	-	-	14.110	0.373	47.7310	-
NGC 663	565	2MASS J01430579+6053307	01:43:05.8	+60:53:31	-	-	13.352	0.310	-	E

Table 11: continued.

Field	ID	Designation	RA J2000	DEC J2000	Cluster membership	Spectral type	V (mag)	Amp. (mag)	Period (days)	Variability type
NGC 6913	2	HD 194153	20:22:35.6	+38:07:46	-	B1Ia	8.542	0.061	-	ACYG
NGC 6913	6	HD 229153	20:22:45.3	+37:57:41	-	O9.7III	9.132	0.040	-	-
NGC 6913	8	HD 194356	20:23:47.1	+37:58:58	-	B9.5V	8.625	0.031	-	-
NGC 6913	17	HD 229171	20:23:02.9	+38:27:21	-	B2IV	9.380	0.057	0.2855	BCEP
NGC 6913	20	HD 229152	20:22:43.0	+38:28:17	-	K2III	9.773	0.037	-	SR
NGC 6913	24	TYC 3152-196-1	20:25:02.9	+38:02:35	-	k0.5III	10.222	0.037	-	-
NGC 6913	30	HD 229253	20:24:25.2	+38:29:07	-	B5IV	10.155	0.033	1.5719	SPB
NGC 6913	36	LS II +38 67	20:22:41.8	+38:10:38	NGC 6913	B3III	10.642	0.064	0.7952	SPB
NGC 6913	41	LS II +37 93	20:25:58.8	+38:08:46	-	OB-	10.811	0.046	-	-
NGC 6913	48	LS II +38 62	20:22:07.6	+38:23:51	-	B5III	10.745	0.053	-	-
NGC 6913	76	TYC 3152-1235-1	20:24:55.2	+38:33:27	-	F5	11.352	0.053	-	-
NGC 6913	91	TYC 3152-1008-1	20:22:19.0	+38:01:48	-	em	11.871	0.160	-	Be
NGC 6913	108	2MASS J20223358+3804105	20:22:33.6	+38:04:11	-	f2IV	11.703	0.056	-	-
NGC 6913	150	TYC 3152-340-1	20:25:08.7	+38:29:23	-	A6IV	12.149	0.110	0.5274	-
NGC 6913	164	IRAS 20238+3746	20:25:44.0	+37:56:50	-	m4III	13.168	0.220	-	SR
NGC 6913	167	TYC 3152-944-1	20:22:57.2	+38:18:25	-	b3	12.554	0.137	9.7214	E
NGC 6913	300	2MASS J20242110+3810010	20:24:21.1	+38:10:01	-	g:	13.272	0.145	4.8150	-
NGC 6913	309	NGC 6913 36	20:23:41.2	+38:27:00	-	f	14.032	0.535	3.4379	CEP
NGC 6913	384	2MASS J20244750+3810584	20:24:47.5	+38:10:58	-	b5V	13.826	0.434	1.9103	E
NGC 6913	396	2MASS J20255147+3802425	20:25:51.5	+38:02:43	-	-	13.775	0.481	1.8187	E
NGC 6913	444	2MASS J20221996+3812386	20:22:20.0	+38:12:39	-	-	13.998	0.265	2.3788	E
NGC 6913	1148	HD 229271	20:24:45.9	+37:59:34	-	B9	10.623	0.061	1.3757	SPB
NGC 7510	5	HD 240254	23:18:19.2	+60:16:22	-	M2	9.105	0.139	-	SR
NGC 7510	7	HD 240221	23:12:12.2	+60:39:59	-	B5III	8.765	0.043	-	-
NGC 7510	8	BD+59 2678	23:14:51.3	+60:44:57	FSR 0422	M2Iab	9.506	0.132	-	SR
NGC 7510	12	TYC 4279-711-1	23:11:30.2	+60:47:02	-	-	9.720	0.075	-	-
NGC 7510	14	TYC 4279-334-1	23:16:00.9	+60:18:41	-	G5IV	9.638	0.028	-	-
NGC 7510	16	HD 218941	23:11:14.8	+60:34:22	NGC 7510	OB+e:	9.678	0.052	-	Be
NGC 7510	22	LS III +60 53	23:13:11.0	+60:42:20	-	B	10.392	0.088	-	-

Table 11: continued.

Field	ID	Designation	RA J2000	DEC J2000	Cluster membership	Spectral type	V (mag)	Amp. (mag)	Period (days)	Variability type
NGC 7510	25	BD+59 2692	23:17:27.3	+60:15:00	-	B7II	9.849	0.058	1.3032	SPB
NGC 7510	26	HD 240218	23:11:22.6	+60:15:10	-	A2	9.850	0.075	3.3628	E
NGC 7510	35	TYC 4279-2213-1	23:17:48.0	+60:26:49	-	-	10.415	0.040	0.8982	SPB
NGC 7510	40	LS III +60 58	23:16:12.3	+60:27:24	Markarian 50	OB	10.663	0.053	0.2138	BCEP
NGC 7510	42	LS III +60 42	23:11:02.9	+60:33:33	-	B0.5V	10.808	0.073	8.4064	E
NGC 7510	44	LS III +59 52	23:14:02.9	+60:14:34	-	OB-	10.681	0.031	-	-
NGC 7510	45	TYC 4279-2508-1	23:17:52.2	+60:32:19	-	A3III	10.696	0.040	-	-
NGC 7510	48	2MASS J23175940+6047486	23:17:59.4	+60:47:49	-	-	11.402	0.108	101.6920	-
NGC 7510	57	TYC 4279-2336-1	23:13:49.0	+60:23:59	-	-	11.111	0.043	-	-
NGC 7510	75	2MASS J23181916+6019065	23:18:19.2	+60:19:07	-	-	11.859	0.102	-	-
NGC 7510	77	TYC 4279-1959-1	23:18:18.0	+60:36:43	-	-	11.326	0.055	-	-
NGC 7510	84	LS III +60 59	23:16:33.1	+60:28:48	-	OB	11.629	0.050	0.1928	BCEP
NGC 7510	85	TYC 4279-2067-1	23:10:47.5	+60:31:53	-	B0Ve	11.766	0.108	0.5820	Be
NGC 7510	95	GSC 04279-02000	23:10:27.6	+60:31:07	-	K0	12.067	0.068	-	-
NGC 7510	116	TYC 4279-877-1	23:16:01.9	+60:11:48	-	-	11.806	0.052	-	-
NGC 7510	161	2MASS J23180979+6045083	23:18:09.8	+60:45:08	FSR 0422	-	12.282	0.092	-	-
NGC 7510	224	2MASS J23112618+6040222	23:11:26.2	+60:40:22	-	-	12.749	0.196	-	-
NGC 7510	232	2MASS J23175230+6025022	23:17:52.3	+60:25:02	-	-	12.725	0.111	0.1651	BCEP
NGC 7510	375	2MASS J23165008+6018047	23:16:50.1	+60:18:05	-	-	13.273	0.155	0.3798	-
NGC 7510	477	2MASS J23152566+6048592	23:15:25.7	+60:48:59	-	-	13.502	0.489	0.5832	E
NGC 7510	482	WRAM 37	23:17:00.7	+60:31:03	-	-	13.547	0.171	3.0937	SPB
NGC 7510	854	2MASS J23140953+6050335	23:14:09.5	+60:50:34	-	-	15.233	0.488	-	SR
NGC 7510	912	2MASS J23102945+6029168	23:10:29.4	+60:29:17	-	-	14.741	0.479	6.0826	E
NGC 7510	1099	2MASS J23144017+6013054	23:14:40.2	+60:13:05	-	-	14.666	0.711	0.5702	E
NGC 7510	1337	2MASS J23163318+6031477	23:16:33.2	+60:31:48	-	-	15.188	0.489	0.1520	BCEP
NGC 7510	2356	2MASS J23173196+6041026	23:17:32.0	+60:41:03	-	-	13.017	0.131	-	-
NGC 7654	5	BD+60 2537	23:25:09.3	+61:22:00	NGC 7654	K2	8.919	0.113	-	-
NGC 7654	6	BD+60 2524	23:21:29.1	+61:06:43	-	G8III	8.824	0.072	-	SR
NGC 7654	14	BD+60 2549	23:28:10.0	+61:09:06	-	B7V	9.433	0.072	1.2710	SPB

Table 11: continued.

Field	ID	Designation	RA J2000	DEC J2000	Cluster membership	Spectral type	V (mag)	Amp. (mag)	Period (days)	Variability type
NGC 7654	16	TYC 4279-1821-1	23:22:40.0	+61:13:33	-	G0V	9.817	0.089	30.9760	E
NGC 7654	17	TYC 4279-1503-1	23:23:46.1	+61:05:55	-	M4	10.461	0.144	24.0044	SR
NGC 7654	26	TYC 4280-1353-1	23:27:39.0	+61:17:28	Czernik 43	M6	10.828	0.257	40.4007	SR
NGC 7654	46	LS III +61 27	23:21:11.4	+61:31:33	-	OB:e:	11.419	0.230	-	Be
NGC 7654	56	TYC 4279-785-1	23:22:14.6	+61:41:31	-	F2	10.938	0.097	-	-
NGC 7654	80	TYC 4279-218-1	23:24:37.6	+61:40:22	-	-	11.396	0.176	-	-
NGC 7654	116	IRAS 23260+6106	23:28:20.4	+61:23:19	-	-	12.393	0.537	253.7790	SR
NGC 7654	136	IRAS 23269+6105	23:29:10.2	+61:22:16	-	-	12.673	0.305	38.4499	SR
NGC 7654	686	2MASS J23212953+6121441	23:21:29.5	+61:21:44	-	-	14.854	1.104	172.8580	SR
NGC 7654	1340	IRAS 23260+6101	23:28:22.0	+61:18:03	-	-	15.012	1.197	-	SR
NGC 7654	1509	2MASS J23282926+6105510	23:28:29.3	+61:05:51	-	-	14.467	0.755	1.1681	E
NGC 869/884	16	RS Per	02:22:24.0	+57:06:33	-	M4I	8.555	0.932	-	SR
NGC 869/884	35	HD 14321	02:20:52.9	+56:55:33	NGC 884	B2III	9.287	0.099	-	E
NGC 869/884	46	HD 14604	02:23:37.8	+56:52:46	-	G0V	9.601	0.094	-	-
NGC 869/884	49	BD+56 556	02:21:11.6	+56:51:14	NGC 869	OB-	9.491	0.079	-	-
NGC 869/884	55	BD+56 534	02:19:26.5	+57:04:42	-	B0Ve	9.649	0.124	-	Be
NGC 869/884	63	BD+56 493	02:18:18.4	+56:51:02	-	B1IV/Ve	9.686	0.145	-	Be
NGC 869/884	83	BD+56 586	02:22:36.3	+57:04:54	-	B1V	9.986	0.070	0.1621	BCEP
NGC 869/884	88	BD+56 489	02:18:15.1	+57:10:16	-	B3e	10.219	0.147	-	E
NGC 869/884	102	NGC 884 2649	02:23:04.2	+57:07:39	-	B2e	10.428	0.141	-	Be
NGC 869/884	104	NGC 884 2804	02:23:33.1	+57:04:33	-	OBe	10.435	0.219	-	Be
NGC 869/884	106	BD+56 516	02:18:54.3	+57:09:30	-	B2V	10.386	0.143	-	Be
NGC 869/884	107	MWC 448	02:23:24.9	+57:19:03	-	B2IIIe	10.763	0.257	78.5370	Be
NGC 869/884	112	MWC 447	02:22:47.0	+56:58:06	-	B0e	10.593	0.106	-	Be
NGC 869/884	130	MWC 711	02:22:48.1	+57:12:01	-	B0/IVe	10.443	0.204	-	Be
NGC 869/884	174	BD+56 509C	02:18:47.7	+57:14:23	-	G0IV	9.697	0.149	-	-
NGC 869/884	203	NGC 869 1438	02:19:47.8	+57:06:40	-	B2e	11.362	0.317	-	Be
NGC 869/884	212	NGC 884 2085	02:21:42.9	+57:05:31	-	B3	11.368	0.162	-	Be
NGC 869/884	232	2MASS J02163833+5705124	02:16:38.3	+57:05:13	-	M2:*	12.081	0.732	-	SR

Table 11: continued.

Field	ID	Designation	RA J2000	DEC J2000	Cluster membership	Spectral type	V (mag)	Amp. (mag)	Period (days)	Variability type
NGC 869/884	354	NGC 884 2646	02:23:04.1	+57:10:09	NGC 869	B2V	12.136	0.356	8.2006	E
NGC 869/884	405	IRAS 02133+5644	02:16:56.4	+56:58:18	-	-	13.129	0.468	-	SR
NGC 869/884	4167	NGC 884 1772	02:20:52.8	+57:13:28	-	B2e	11.443	0.211	-	Be
NGC 957	7	HD 15571	02:32:24.8	+57:25:44	-	BIII	8.425	0.065	-	ACYG
NGC 957	13	BD+56 640	02:31:08.4	+57:31:37	NGC 957	B2III:	9.607	0.100	1.7070	SPB
NGC 957	38	TYC 3695-212-1	02:30:34.3	+57:36:34	NGC 957	-	10.819	0.072	0.1904	BCEP
NGC 957	46	LS V +57 46	02:33:10.6	+57:32:54	-	B0/IVe	11.218	0.322	-	Be
NGC 957	108	TYC 3695-728-1	02:33:30.9	+57:29:04	-	-	12.031	0.303	-	-
NGC 957	114	2MASS J02313244+5800022	02:31:32.5	+58:00:02	-	-	12.918	0.216	-	-
NGC 957	120	TYC 3695-758-1	02:27:19.6	+57:35:33	-	-	12.343	0.232	-	-
NGC 957	173	2MASS J02333778+5740241	02:33:37.8	+57:40:24	-	-	13.206	0.234	0.5077	-
P Cygni	61	LS II +37 47	20:17:30.2	+38:05:56	-	B5III	10.970	0.210	-	Be
P Cygni	132	2MASS J20195689+3750073	20:19:56.9	+37:50:07	-	-	12.099	0.348	3.1640	E
P Cygni	170	IRAS 20150+3808	20:16:51.9	+38:18:21	-	-	12.807	0.511	-	SR
P Cygni	249	SI * 642	20:16:58.1	+38:07:26	-	S	13.183	0.659	-	SR
P Cygni	320	2MASS J20170807+3758584	20:17:08.1	+37:58:58	-	-	13.028	0.583	2.7104	E
P Cygni	405	2MASS J20173903+3804143	20:17:39.0	+38:04:14	-	-	13.591	0.506	5.0511	CEP
PZ Cas	8	HD 223044	23:46:00.4	+61:59:28	-	em	8.466	0.089	-	Be
PZ Cas	14	BD+60 2615	23:44:42.1	+61:40:05	-	B0.2(I)	9.142	0.061	-	ACYG
PZ Cas	18	TYC 4284-117-1	23:42:42.8	+62:02:55	-	-	9.598	0.044	-	-
PZ Cas	19	BD+61 2508	23:43:41.9	+61:56:15	-	A0	9.320	0.038	-	-
PZ Cas	20	BD+61 2531	23:48:35.9	+62:14:46	-	B1.2(II)	9.421	0.045	-	ACYG
PZ Cas	21	BD+61 2536	23:49:19.0	+61:57:46	-	OB-	9.602	0.091	1.1047	E
PZ Cas	30	2MASS J23461792+6201334	23:46:17.9	+62:01:33	Stock 17	-	10.077	0.177	9.0030	E
PZ Cas	34	TYC 4281-1268-1	23:49:02.4	+61:40:59	-	-	10.905	0.070	-	-
PZ Cas	37	TYC 4281-1792-1	23:44:32.8	+61:45:00	-	-	10.428	0.229	-	E
PZ Cas	51	LS I +61 34	23:44:31.2	+61:59:13	-	OB-	10.716	0.068	3.2740	E
PZ Cas	54	2MASS J23480174+6214074	23:48:01.7	+62:14:07	-	-	11.508	0.112	-	-
PZ Cas	66	WR 158	23:43:30.6	+61:55:48	-	WN7	11.282	0.073	-	WR

Table 11: continued.

Field	ID	Designation	RA J2000	DEC J2000	Cluster membership	Spectral type	V (mag)	Amp. (mag)	Period (days)	Variability type
PZ Cas	97	LS1 +61 51	23:46:08.6	+62:03:01	-	OB-	11.433	0.567	3.3005	E
PZ Cas	98	2MASS J23465305+6155290	23:46:53.1	+61:55:29	-	-	12.189	0.575	-	SR
PZ Cas	99	TYC 4280-100-1	23:42:09.1	+61:46:41	-	-	11.730	0.170	-	-
PZ Cas	127	2MASS J23421700+6212376	23:42:17.0	+62:12:38	Stock 17	-	11.921	0.104	-	-
PZ Cas	151	2MASS J23441671+6153312	23:44:16.7	+61:53:31	-	-	12.169	0.129	-	-
PZ Cas	155	2MASS J23471857+6204011	23:47:18.6	+62:04:01	-	-	12.369	0.196	25.5706	-
PZ Cas	171	2MASS J23443377+6207168	23:44:33.8	+62:07:17	-	-	12.372	0.201	4.4177	E
PZ Cas	190	GSC 04284-00313	23:41:45.7	+62:04:34	-	em	12.549	0.216	-	Be
PZ Cas	217	TYC 4281-1348-1	23:43:44.4	+61:36:55	-	-	12.526	0.173	0.4334	E
PZ Cas	250	2MASS J23461052+6137333	23:46:10.5	+61:37:33	-	-	12.731	0.226	1.3156	E
PZ Cas	404	2MASS J23493339+6157236	23:49:33.4	+61:57:24	-	-	13.245	0.194	1.0504	SPB
PZ Cas	408	2MASS J23475095+6206318	23:47:51.0	+62:06:32	-	-	13.144	0.196	91.7307	-
PZ Cas	516	2MASS J23483201+6216474	23:48:32.0	+62:16:48	-	-	13.536	0.418	5.4486	E
PZ Cas	583	2MASS J23485763+6200549	23:48:57.6	+62:00:55	-	-	14.385	0.683	-	SR
PZ Cas	930	2MASS J23465248+6141157	23:46:52.5	+61:41:16	-	-	14.289	0.634	2.1354	E
PZ Cas	1287	2MASS J23444605+6144316	23:44:46.1	+61:44:32	-	-	14.062	0.706	-	E

Notes. Variability types: E - Eclipsing binary; BE - Be star; BCEP - β Cephei type star; SPB - Slowly pulsating B star; ACYG - α Cygni type star; CEP - Cepheid; WR - Wolf-Rayet star; SR - late-type star; "-" - unclassified.

CURRICULUM VITAE

Personal data

Name	Jaan Laur
Date and place of birth	21 st of May 1986, Tallinn, Estonia
Citizenship	Estonian
Current employment	Tartu Observatory
Address	Tartu Observatory 61602 Tõravere Tartumaa, Estonia
Phone	(+372) 55 582 825
E-mail	jaanlaur@ut.ee

Education

1993 – 2005	Tallinna Mustamäe Gümnaasium
2005 – 2009	University of Tartu, Bachelor in Physics, BSc 2009 (physics)
2009 – 2011	University of Tartu, Master in Astrophysics, MSc 2011 (astrophysics)
2011 – 2017	University of Tartu, PhD in Astrophysics

Employment

2012 – ...	Tartu Observatory, Junior Researcher
------------	--------------------------------------

Professional training

28.07 – 11.08 2012	The NordForsk school “Observational Astrophysics in the Era of Gaia and Kepler Space Missions”, Moletai, Lithuania.
14.07 – 27.07 2013	“The 2013 NEON school in LaPalma”, La Palma, Spain.
24.08 – 28.08 2014	Summer school “Scientific Writing for Young Astronomers”, Tihany, Hungary.
12.09 – 16.09 2016	11th Heidelberg Summer School on “Astrostatistics & Data Mining”, Heidelberg, Germany.

Conference presentations

- 21.09 – 22.09 2011 Conference “Tartu - Tuorla annual meeting 2011: Remote sensing of the Universe”
Tartu, Estonia.
Oral presentation: “Remote observing of luminous stars in OB associations”
- 06.05 – 09.05 2012 Conference “Baltic Applied Astroinformatics and Space data Processing”,
Ventspils, Latvia.
Oral presentation: “Variability survey of massive stars in northern OB-associations: Results on CygOB2”
- 10.06 – 14.06 2013 Conference “Massive Stars: From α to Ω ”,
Rhodes, Greece.
Poster presentation: “Variability time-scales and amplitudes of massive stars in selected OB associations”
- 22.09 – 25.09 2015 Conference “Tartu – Tuorla annual meeting 2015: (Always Look on) The Bright Side of Space”,
Kubija, Estonia.
Oral presentation: “Looking for period change in massive binaries”

Language skills

Estonian	native speaker
English	excellent command

Honours and Awards

2009 Ernst Julius Öpik scholarship (Tartu Observatory)
2011 Ernst Julius Öpik scholarship (Tartu Observatory)

Fields of research

Binary star interactions.
Stellar variability and asteroseismology.

Publications

- J. Laur, T. Tuvikene, T. Eenmäe, I. Kolka and L. Leedjärv. Variability Survey of Massive Stars in OB-Associations: Preliminary Results on the Cygnus Region. *Baltic Astronomy*, 21,531–536, 2012.
- S. Tamburri, B. Hendricks, M. Smailagic, J. Laur, T. Pursimo and R. Ojha. Optical Activity of the Flaring Gamma-ray Blazar TXS 1100+122. *The Astronomer's Telegram*, 5221, 2013.
- J. Laur, E. Tempel, T. Tuvikene, T. Eenmäe and I. Kolka. Period change of massive binaries from combined photometric and spectroscopic data in Cygnus OB2. *A&A*, 581,A37, 2015.
- J. Laur, I. Kolka, T. Eenmäe, T. Tuvikene and L. Leedjärv. Variability survey of brightest stars in selected OB associations. *A&A*, 598,A108, 2017.

ELULOOKIRJELDUS

Isikuandmed

Nimi	Jaan Laur
Sünniaeg ja -koht	21. mai 1986, Tallinn, Eesti
Kodakondsus	Eesti
Prægune töökoht	Tartu Observatoorium
Aadress	Observatooriumi 1, 61602 Tõravere Tartumaa, Eesti
Telefon	(+372) 55 582 825
E-post	jaanlaur@ut.ee

Haridustee

1993 – 2005	Tallinna Mustamäe Gümnaasium
2005 – 2009	Tartu Ülikool, füüsika eriala
2009 – 2011	Tartu Ülikool, magistriõpe (astrofüüsika)
2011 – 2017	Tartu Ülikool, doktoriõpe (astrofüüsika)

Teenistuskäik

2012 – ...	Tartu Observatoorium, nooremteadur
------------	------------------------------------

Täiendkoolitus

28.07 – 11.08 2012	NordForski suvekool “Observational Astrophysics in the Era of Gaia and Kepler Space Missions”, Moletai, Leedu.
14.07 – 27.07 2013	suvekool “The 2013 NEON school in LaPalma”, La Palma, Hispaania.
24.08 – 28.08 2014	suvekool “Scientific Writing for Young Astronomers”, Tihany, Ungari.
12.09 – 16.09 2016	11. Heidelbergi suvekool “Astrostatistics & Data Mining”, Heidelberg, Saksamaa.

Konverentside ettekanded

- 21.09 – 22.09 2011 Konverents “Tartu - Tuorla annual meeting 2011: Remote sensing of the Universe”
Tartu, Eesti.
Suuline ettekanne: “Remote observing of luminous stars in OB associations”
- 06.05 – 09.05 2012 Konverents “Baltic Applied Astroinformatics and Space data Processing”,
Ventspils, Läti.
Suuline ettekanne: “Variability survey of massive stars in northern OB-associations: Results on CygOB2”
- 10.06 – 14.06 2013 Konverents “Massive Stars: From α to Ω ”,
Rhodos, Kreeka.
Poster: “Variability time-scales and amplitudes of massive stars in selected OB associations”
- 22.09 – 25.09 2015 Konverents “Tartu – Tuorla annual meeting 2015: (Always Look on) The Bright Side of Space”,
Kubija, Eesti.
Suuline ettekanne: “Looking for period change in massive binaries”

Keelteoskus

eesti keel	emakeel
inglise keel	väga hea

Uurimistoetused ja stipendiumid

2009	Ernst Julius Öpiku nimeline stipendium (Tartu Observatoorium)
2011	Ernst Julius Öpiku nimeline stipendium (Tartu Observatoorium)

Peamised uurimissuunad

Kaksiktähtede vahelised interaktsioonid.
Tähtede muutlikkus ja asteroseismoloogia.

Publikatsioonid

J. Laur, T. Tuvikene, T. Eenmäe, I. Kolka and L. Leedjärv. Variability Survey of Massive Stars in OB-Associations: Preliminary Results on the Cygnus Region. *Baltic Astronomy*, 21,531–536, 2012.

S. Tamburri, B. Hendricks, M. Smailagic, J. Laur, T. Pursimo and R. Ojha. Optical Activity of the Flaring Gamma-ray Blazar TXS 1100+122. *The Astronomer's Telegram*, 5221, 2013.

J. Laur, E. Tempel, T. Tuvikene, T. Eenmäe and I. Kolka. Period change of massive binaries from combined photometric and spectroscopic data in Cygnus OB2. *A&A*, 581,A37, 2015.

J. Laur, I. Kolka, T. Eenmäe, T. Tuvikene and L. Leedjärv. Variability survey of brightest stars in selected OB associations. *A&A*, 598,A108, 2017.

DISSERTATIONES ASTRONOMIAE UNIVERSITATIS TARTUENSIS

1. **Tõnu Viik.** Numerical realizations of analytical methods in theory of radiative transfer. Tartu, 1991.
2. **Enn Saar.** Geometry of the large scale structure of the Universe. Tartu, 1991.
3. **Maret Einasto.** Morphological and luminosity segregation of galaxies. Tartu, 1991.
4. **Urmas Haud.** Dark Matter in galaxies. Tartu, 1991.
5. **Eugene A. Ustinov.** Inverse problems of radiative transfer in sounding of planetary atmospheres. Tartu, 1992.
6. **Peeter Tenjes.** Models of regular galaxies. Tartu, 1993.
7. **Ivar Suisalu.** Simulation of the evolution of large scale structure elements with adaptive multigrid method. Tartu, 1995.
8. **Teimuraz Shvelidze.** Automated quantitative spectral classification of stars by means of objective prism spectra: the method and applications. Tartu, 1999.
9. **Jelena Gerškevič.** Formation and evolution of binary systems with compact objects. Tartu, 2002.
10. **Ivan Suhhonenko.** Large-scale motions in the universe. Tartu, 2003.
11. **Antti Tamm.** Structure of distant disk galaxies. Tartu, 2006.
12. **Vladislav-Veniamin Pustynski.** Modeling the reflection effect in pre-cataclysmic binary systems. Tartu, 2007.
13. **Anna Aret.** Evolutionary separation of mercury isotopes in atmospheres of chemically peculiar stars. Tartu, 2009.
14. **Mari Burmeister.** Characteristics of the hot components of symbiotic stars. Tartu, 2010.
15. **Elmo Tempel.** Tracing galaxy evolution by their present-day luminosity function. Tartu, 2011.
16. **Anti Hirv.** Estimation of time delays from light curves of gravitationally lensed quasars. Tartu, 2011.
17. **Rain Kipper.** Galaxy modelling: dynamical methods and applications. Tartu, 2016, 134 p.
18. **Lauri Juhan Liivamägi.** Properties and spatial distribution of galaxy superclusters. Tartu, 2017, 185 p.